

**THE METAL TRIGGERED SELF ASSEMBLY OF CELL-ADHESIVE  
AND FLUORINATED COLLAGEN MIMETIC PEPTIDES**

by

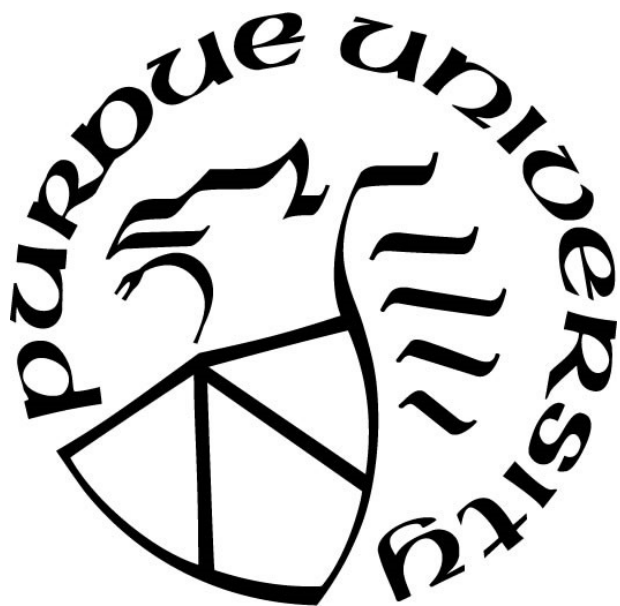
**Vallabh Suresh**

**A Dissertation**

*Submitted to the Faculty of Purdue University*

*In Partial Fulfillment of the Requirements for the degree of*

**Doctor of Philosophy**



Department of Chemistry

West Lafayette, Indiana

August 2020

**THE PURDUE UNIVERSITY GRADUATE SCHOOL  
STATEMENT OF COMMITTEE APPROVAL**

**Dr. Jean Chmielewski, Chair**

Department of Chemistry

**Dr. Jeffrey Youngblood**

School of Materials Engineering

**Dr. Christopher Uyeda**

Department of Chemistry

**Dr. David Thompson**

Department of Chemistry

**Approved by:**

Dr. Christine Hrycyna

*Dedicated to Amma and Appa*

## ACKNOWLEDGMENTS

No one is an island. We are all a product of the people who teach us what we know, push us to do difficult things, and believe in us when we don't believe in ourselves. I have always been a person who follows my gut instincts but I never really know where I'm going. The reason I didn't get lost is because of the army of people who showed me the way. My achievements were only possible because of all of you. I am humbled and forever in your debt.

Firstly, I would like to thank Prof. Jean Chmielewski, my current advisor and the latest in a line of teachers who've shaped my thinking. Before working with Jean, I was competent but not always confident in my abilities. As a result of Jean's support, guidance, and constructive criticism, I am now more confident in my abilities as a scientist than ever. In difficult situations, I used to give up quickly but today, I am relentless until I achieve what I set out to do. After my experience in Jean's research group, I am now feeling like nothing can stop me from achieving my goals as long as I put my mind to it. Similarly, I would like to thank my committee: Prof. Jeffrey Youngblood, Prof. Chris Uyeda, and Prof. David Thompson. Prof. Youngblood and Prof. Uyeda taught me in classes during my first few years in grad schools. In my final semester, Prof. Thompson served as my supervisor when I taught organic chemistry lab. All three have always been there to answer my questions when I sent emails. I am grateful for your support and feedback. I would also like to thank Prof. Mark Lipton: when I had no idea how to purify a compound, you suggested to triturate it with ether and that changed everything!

Getting a PhD would have been impossible without my lab-mates. Thank you to Dr. Manish Nepal for knocking me down just enough to make me stronger and for all the good times where we played soccer together. Thank you to Dr. Neha Agrawal for coaching me through the tough times and watching Game of Thrones with me. Thank you to Dr. Monesha Nambiar and Kevin Strauss for teaching me all the skills that I needed to study peptide self-assembly. Thank you to Dr. Reena Blade for being someone I look up to as an example of how to be calm no matter how crazy things got. Thank you to Dr. Jenny Rowe, who was my mentor when I first got to Purdue and who even now continues to be my mentor and answer my texts when I need help in figuring out what to do in life. Thank you to Vinay Menon, who reminded of how good I have it when I needed to realize this. Thank you to Paulo Pitasse for the excellent conversation when we both worked late at night in lab. Thank you to Moises Morales-Padilla, Samantha Zeiders, Ryan Curtis

(who ran DLS for me), Corey Johnson, Tad Dietsche, Michael Jorgenson, Ambar Rosario, Nosa Idahagabon, Megan Willoughby, and Colin Caine for making me feel like I belonged in the research group. Thank you to Travis Beamon and Jessica Pham, two of the most excellent undergraduate researchers I've ever had the pleasure of mentoring! And lastly, thank you to Jason Goebel for answering all of my biochemistry questions!

Next, I would like to thank those who trained me on instruments. Without you all, my work could not have been carried out. Thank you to Dr. Patricia Bishop and Hartmut Hedderich who trained me on many different instruments at the Amy Instrumentation Facility. Thank you to Dr. Andy Schaber for training me in confocal microscopy. Thank you to Dr. Chris Gilpin, Laurie Mueller, and Robert Seiler who helped me become an expert in electron microscopy. Thank you to Courtney Rupert, who ran ion mobility spectrometry for me. Thank you to Dr. Julia Beck, who ran analytical ultracentrifugation for me!

Outside of the lab, I met some amazingly interesting people who have become lifelong friends. Thank you to Miranda Belcher and Matthew Hewitt, my core friends during my my time at Purdue. Thank you to Dr. Emilio Cardenas, Dr. Luke Kassekert, Dr. Annie Veitschegger, Dr. Matthew Hostetler, Charlie Bupp, Abriti Pokhrel, Wes Salameh, Andrea Chambers, Zack Struzik, and Brandon Martin. All of you have taught me different things about life and I'll always cherish the good times. Thank you to Brian Hanley, Catherine Ingram, Bill Arnold, Prof. Matthew Lynall, Mont Handley Ashley Bryan, Joey Woodyard, and Wade Lange for helping understand how businesses work. It had always been my dream to start my own company and for the first time ever, I know what I have to do to reach this goal because of what you all taught me.

Before I came to Purdue, the foundations of my learning were set by my teachers at Florida Atlantic University. Thank you to Prof. Salvatore Lepore and Prof. Charles Carraher! I chose to go to graduate school because I looked up to you two as role models and wanted to emulate your success. Thank you to Dr. Susovan Jana, who taught me everything I know about organic synthesis. Thank you to Dr. Mohammed Alhuniti, Prof. Bilal Bhat, Dr. Edith Nagy, Dr. Animesh Roy, and Krishna Yadavalli. Even though I was just an undergraduate, you all made me treated me like a full-fledged researcher and this is why I became one in time. Thank you to Carlos Salas, Paul Scesa, Ryan Crichton, Ben Chen, Dyllan To, Arianna Gagnon, and Alexander Ruiz. I was not always academically inclined and didn't like school. You've seen me during the lowest points in life. But I learned about my weaknesses from my experiences with you all. Today, I am a vastly different

person than I was back then and I am indebted to you for showing me a better path. Lastly, thank you to Dr. David Kelly, Dr. Terri Watson, Dr. Shevrin Jones, Dr. Agnes Nemeth, and the rest of the FAU High School Program. I did not realize it back then but joining this program was perhaps the most pivotal moment in my journey thus far. You allowed me to attend university without spending a dime.

Finally, I dedicate this thesis to Hemavathi Iyengar and Suresh Srinivasamurthy, my amma and appa. When I was little, I didn't understand the value of discipline, which you always pointed out to me. Today, I realize what you were talking about. You always taught me about life in an encouraging and positive way, never authoritarian. I couldn't have asked for better parents and for a better foundation in my life. Thank you!

## TABLE OF CONTENTS

LIST OF TABLES .....	9
LIST OF FIGURES .....	10
ABSTRACT .....	13
CHAPTER 1. CELL-BIOMATERIALS INTERACTIONS AND THEIR USE IN BIOMATERIALS DESIGN .....	14
1.1 Introduction.....	14
1.2 The Extracellular Matrix.....	14
1.3 Natural and Synthetic Biomaterials .....	16
1.4 Interactions of Cells with Biomaterials.....	17
1.4.1 Cell Adhesion to Biomaterials.....	18
1.4.2 Cell Migration on Biomaterials .....	19
1.4.3 Collagen Induced Endothelial Network Formation.....	20
1.5 Collagen Structure and Processing .....	23
1.6 Peptide Mimetics .....	25
1.7 Collagen Mimetic Peptides: Triple Helical Stability .....	25
1.8 Collagen Mimetic Peptides: Self-Assembly Strategies .....	27
1.9 Metal Ion Promoted Self Assembly of Collagen Mimetic Peptides.....	30
1.10 Conclusions .....	37
1.11 References .....	38
CHAPTER 2. THE SELF ASSEMBLY OF A CELL ADHESIVE COLLAGEN MIMETIC PEPTIDE .....	48
2.1 Introduction.....	48
2.2 NCoH-FOGER.....	50
2.3 Results and Discussion .....	51
2.3.1 Synthesis of Protected Nitrilotriacetate 3 .....	51
2.3.2 Synthesis of NCoH-FOGER.....	51
2.3.3 Confirmation of the Triple Helicity of NCoH-FOGER.....	52
2.3.4 Metal Mediated Self Assembly of NCoH-FOGER .....	56
2.3.5 Stabilization of NCoH-FOGER-Co(II) Particles.....	64

2.3.6	Adherence of Cobalt(III)-NCoH-FOGER Particles to Endothelial Cells.....	65
2.3.7	HUVEC Network Formation Induced By Cobalt(III)-NCoH-FOGER Particles .....	66
2.3.8	Actin Staining in Endothelial Cells .....	69
2.3.9	Experiments with a More Stable Peptide, NCoH-FOGER-8 .....	70
2.4	Conclusion .....	74
2.5	Materials and Methods.....	74
2.6	References.....	79
CHAPTER 3. THE SELF ASSEMBLY OF A FLUORINATED COLLAGEN MIMETIC		
PEPTIDE .....		
		82
3.1	Introduction.....	82
3.2	NCoH7 and NCoH7F.....	84
3.3	Results and Discussion .....	84
3.3.1	Synthesis of Fmoc-Seg-OH .....	84
3.3.2	Solid Phase Synthesis of NCoH7F .....	85
3.3.3	Confirming the Triple Helicity of NCoH7 and NCoH7F .....	86
3.3.4	Metal-Triggered Self Assembly .....	87
3.3.5	A Discussion of Nucleation and Growth.....	91
3.3.6	Oxidation and Stabilization of Peptide-Cobalt Particles .....	92
3.4	Conclusion .....	93
3.5	Materials and Methods.....	93
3.6	References.....	99
PUBLICATION.....		
		101

## LIST OF TABLES

Table 2-1. Measurements of particle lengths and widths of assemblies made from 300  $\mu\text{M}$   $\text{Co}(\text{NO}_3)_2$  and different NCoH-FOGER concentrations in 20 mM MOPS buffer overnight. .... 62

Table 2-2. Measurements of particle lengths and widths of assemblies made from 1 mM NCoH-FOGER and different  $\text{Co}(\text{NO}_3)_2$  peptide concentrations in 20 mM MOPS buffer overnight. .... 63

## LIST OF FIGURES

Figure 1.1. The extracellular matrix is made up of structural proteins, proteoglycans, glycosaminoglycans, vesicles, and growth factors. ....	16
Figure 1.2. In cell migration, (a.) lamellopodia extend from the cell with polymerization of actin (red), (b.) an adhesion is formed at the destination site, (c.) lamellopodia retract and pull the cell towards the destination, and (d.) the cell moves and adheres to the new site. (Adapted from 60.) .....	20
Figure 1.3. It is hypothesized that formation of endothelial cell networks on a collagen gel requires clustering of Integrin $\alpha 2\beta 1$ ; simple binding with antibodies or peptides, in the absence of clustering, has been shown to inhibit network formation. (Adapted from Ref. 65.) .....	22
Figure 1.4. The structure of the collagen triple helix (a) showing glycine hydrogen bonds (b, c). (Adapted from Ref. 62).....	24
Figure 1.5. Trans-4-fluoroproline residues preferentially adopt an exo pucker due to favorable orbital overlaps.....	27
Figure 1.6. The self-assembly of blunt ended triple helices (a., b.) was used to form d-periodic fibers. (Adapted from Ref. 112.).....	28
Figure 1.7. Sticky-Ended CMP self-assembly involves off-register triple helices (a.) which condense in a lengthwise manner (b.) into fibrous matrices (c.). (Adapted from Ref. 117) .....	29
Figure 1.8. Chirality driven assembly of oppositely handed triple helices. Adopted from Ref. 125. .....	30
Figure 1.9. The metal-mediated self-assembly of HByp3 into curved disks and hollow spheres. Adopted from Ref. 127. ....	32
Figure 1.10. The linear design of NCoH. Adopted from Ref. 134. ....	33
Figure 1.11. NCoH Microflorettes labelled with two different fluorescent proteins. Adopted from reference 135.....	33
Figure 1.12. Banded particles from the tandem co-assembly of HisCol and IdaCol. Adopted from Ref. 138.....	35
Figure 1.13. HeLa Cells in NHBipy Meshes. a.) Cells stained with DAPI (Blue) and Meshes stained green; b.) CryoSEM of HeLa cells in meshes; c.) Cells stained with calcein AM (Green) to show viability. Adopted from Ref. 140. ....	36
Figure 2.1. The design of NCoH-FOGER; yellow circles are metal ions. ....	50
Figure 2.2. Synthesis of protected nitrilotriacetate 3 .....	51
Figure 2.3. Circular dichroism of NCoH-FOGER in water and aqueous methanol .....	53

Figure 2.4. Temperature dependent circular dichroism of NCoH-FOGER in water and aqueous methanol.....	53
Figure 2.5. Analytical ultracentrifugation of NCoH-FOGER shows a dimer and trimer.....	54
Figure 2.6. Ion mobility mass spectroscopy shows a trimer with a charge of 5.....	55
Figure 2.7. Ion mobility mass spectroscopy shows a dimer with a charge of 3.....	55
Figure 2.8. Relative abundances of dimer and trimer peaks by ion-mobility spectrometry.....	56
Figure 2.9. Solution turbidity due to precipitation of NCoH-FOGER (1 mM) assemblies with metal ions (300 $\mu$ M) in 20 mM MOPS overnight. ....	57
Figure 2.10. EDTA (10 mM) eliminates assembly associated turbidity.....	57
Figure 2.11. Dynamic Light Scattering of NCoH-FOGER (1 mM) with metal ions (300 $\mu$ M) in 20 mM MOPS overnight.....	58
Figure 2.12. SEM Images of Assemblies formed from NCoH-FOGER (1 mM) in 20 mM MOPS Buffer (pH 7.4) overnight with 300 $\mu$ M (a) $\text{Co}(\text{NO}_3)_2$ , (b) $\text{CuSO}_4$ , and (c) $\text{ZnCl}_2$ . ....	59
Figure 2.13. TEM Images of Assemblies formed from NCoH-FOGER (1 mM) with $\text{ZnCl}_2$ (300 $\mu$ M) in 20 mM MOPS Buffer overnight. ....	60
Figure 2.14. Phase diagram of NCoH-FOGER concentration and zinc chloride concentration showing morphologies achieved at different conditions. ....	61
Figure 2.15. (a.) Layered particles from the assembly of 1.5 mM NCoH-FOGER and 300 $\mu$ M $\text{ZnCl}_2$ in MOPS buffer; (b.) Fibrillar particles from the assembly of 1 mM NCoH-FOGER and 300 $\mu$ M $\text{ZnCl}_2$ in 20 mM MOPS. ....	61
Figure 2.16. For all assemblies, 300 $\mu$ M $\text{Co}(\text{NO}_3)_2$ and 20 mM MOPS was used. NCoH-FOGER was varied: (a.) 300 $\mu$ M, (b.) 600 $\mu$ M, (c.) 1 mM, (d.) 1.2 mM.....	62
Figure 2.17. For all assemblies, 1 mM NCoH-FOGER and 20 mM MOPS was used. $\text{Co}(\text{NO}_3)_2$ was varied: a) 200 $\mu$ M, b) 300 $\mu$ M, c) 600 $\mu$ M, d) 1 mM, e) 1.5 mM. ....	63
Figure 2.18. $\text{H}_2\text{O}_2$ oxidized and His <sub>6</sub> -rhodamine tagged Cobalt(III)-NCoH-FOGER (Each 1 mM during preparation) imaged by (a) SEM after being resuspended in DMEM media for 24 h. (b) Fluorescence Microscopy of His <sub>6</sub> -rhodamine tagged Cobalt(III)-NCoH-FOGER particles resuspended in DMEM media for 24h.....	65
Figure 2.19. His <sub>6</sub> Rhodamine tagged NCoH-FOGER Co(III) Assembly (red channel) adhered to 200,000 Calcein AM stained HUVEC Cells (Green Channel) in DMEM with 10% FBS.....	66
Figure 2.20. HUVEC network formation in serum free DMEM induced by a.) NCoH-FOGER-Co(III) assemblies and (b.) His <sub>6</sub> -rhodamine labelled assemblies; A sample without any material, (c.), did not form networks. ....	68
Figure 2.21. HUVEC network formation in serum free DMEM was not induced by controls: a.) 200 $\mu$ M NCoH-FOGER, (b.) 200 $\mu$ M $\text{Co}(\text{NO}_3)_2$ , c.) non-oxidized NCoH-FOGER-Co(II) assemblies.....	68

Figure 2.22. Cells stained with actin stained with FITC Phalloidin (Green) and nuclei stained with Hoescht 33342 dye (blue). (a.) Cells treated with NCoH-FOGER-Cobalt(III) assemblies in serum free DMEM show actin networks stained green with FITC-phalloidin. (b.) Untreated cells in serum free DMEM show green fluorescence only around nuclei. ....	70
Figure 2.23. NCoH-FOGER-8, a longer analog of NCoH-FOGER.....	71
Figure 2.24. CD spectrum and melting curve for 100 $\mu$ M NCoH-FOGER-8 in 20 mM MOPS buffer shows a $T_m$ of 35 $^{\circ}$ C.....	71
Figure 2.25. NCoH-FOGER-8 (1 mM) assembled with 1 mM (a) $ZnCl_2$ , (b) $CuSO_4$ , and (c) $Co(NO_3)_2$ in 20 mM MOPS buffer. The cobalt (II) assemblies were oxidized with $H_2O_2$ to cobalt (III), resuspended in DMEM media overnight, and then imaged (d.). ....	72
Figure 2.26. TEM of NCoH-FOGER-8 (1 mM) assembled with 1 mM (a) $Co(NO_3)_2$ , (b) $CuSO_4$ , and (c) $ZnCl_2$ in 20 mM MOPS Buffer.....	73
Figure 2.27. Endothelial Cells in serum free DMEM treated with a.) NCoH-FOGER-8 Cobalt(III) assemblies and b) not treated. ....	74
Figure 3.1. Stability of Collagen Triple Helix .....	83
Figure 3.2. The design of NCoH7 and NCoH7F; yellow circles represent metal ions.....	84
Figure 3.3. The Synthesis of Fmoc-Seg-OH.....	85
Figure 3.4. a.) MALDI-TOF spectrum showing NCoH7F as well as sodium and potassium adducts. b.) Purified NCoH7F boiled with EDTA prior to HPLC analysis shows 2 peaks, tentatively a random coil and a triple helix. ....	86
Figure 3.5. Circular Dichroism of 100 $\mu$ M NCoH7 and 100 $\mu$ M NCoH7F in 20 mM MOPS. ...	87
Figure 3.6. Structures formed with 1 mM NCoH7 and 700 $\mu$ M $Co(NO_3)_2$ (a. and b.), 700 $\mu$ M $ZnCl_2$ (c.), and $CuSO_4$ (d.) in 20 mM MOPS overnight.....	88
Figure 3.7. Side by side comparison of 1 mM NCoH7 and 1 mM NCoH7F assembly with 700 $\mu$ M $Co(NO_3)_2$ (a. and b., respectively); c.) Assembly of 500 $\mu$ M NCoH7F and 500 $\mu$ M $Co(NO_3)_2$ ; d.) assembly of 1 mM NCoH7F without any metal over 2h. All assemblies done overnight in 20 mM MOPS.....	89
Figure 3.8. Side-by-side comparison of NCoH7 and NCoH7F cobalt(II) assemblies using TEM. Samples are stained with 1% uranyl acetate. All assemblies were prepared in 20 mM MOPS overnight. ....	90
Figure 3.9. Close up of TEM images of NCoH7 assemblies reveals a banding pattern which could be the result of a linear assembly of triple helices. ....	90
Figure 3.10. A Nucleation and Growth Mechanism May Explain the Particle Sizes Observed in NCoH7 and NCoH7F assemblies .....	92
Figure 3.11. Oxidized cobalt assemblies of NCoH7 (a.) and NCoH7F (b.) after suspension in PBS for 24 h.....	93

## **ABSTRACT**

Collagen I, a natural protein found in animal tissues, can self-assemble into fibrous matrices that support cell and tissue growth. Peptide mimics of collagen are able to recapitulate this self-assembly process towards the development of biomaterials for tissue engineering. In recent years, the metal mediated self-assembly of collagen mimetic peptides (CMPs) has allowed access to various particle morphologies. Herein, two studies are presented. In the first, NCOH-FOGER, a cell adhesive CMP capable of metal-triggered self-assembly, was utilized to develop a model system to mimic natural collagen's interactions with endothelial cells. Notably, a cobalt(III)-NCoH-FOGER assembly was able to induce endothelial cells to form network-like structures. In the second, a CMP was modified to include an unnatural amino acid, L-4-trans-fluoroproline, which increased the thermostability of its folded state. The effect of this substitution on the morphology of self-assembled particles was evaluated.

# **CHAPTER 1. CELL-BIOMATERIALS INTERACTIONS AND THEIR USE IN BIOMATERIALS DESIGN**

## **1.1 Introduction**

The demand for organ transplant surgeries remains an unmet need in the healthcare sector. Since the beginning of the 21st century, the wait list has continued to be greater than the number of surgeries performed. As of March 2020, more than 112,200 patients require organ transplants.<sup>1</sup> It is estimated that a new patient joins the wait list every 10 minutes.<sup>1</sup> A lack of organ donors is the bottleneck in addressing medical demand. To address this, attempts are being made to utilize isolated cells instead of donated organs. Since cells can be grown in large amounts in vitro, these could potentially be assembled into tissues, which can be used to create a supply of new organs.

In the rapidly growing field of tissue engineering, material scaffolds are used to promote cellular organization and growth.<sup>2,4</sup> Scaffolds can either be directly implanted or cultured with cells in vitro. They will then guide regeneration in vivo or the formation of implantable organoid constructs in vitro. This promising method and its variations has yielded approved prostheses for cartilage<sup>7</sup>, bone<sup>8</sup> and skin<sup>9</sup>. Towards larger or more complex tissues, several major challenges have been studied: reliable sourcing of cells, host responses, and vascularization.<sup>5</sup> The latter is especially towards creating thicker constructs, where nutrients cannot easily diffuse throughout.<sup>10</sup> In natural tissues, blood vessels ensure that nutrients and oxygen are able to penetrate into all areas regardless of tissue thickness. As such, methods to integrate blood vessel networks into synthetic tissues may be valuable for optimal vascularization in future.<sup>11</sup>

## **1.2 The Extracellular Matrix**

To develop tissue engineering further, inspiration and guiding principles can be derived by studying the extracellular matrix (ECM). The ECM, a conglomerate of proteins, carbohydrates, lipids, interstitial fluid, and various nutrients, forms the structure and environment in which cells grow within complex organisms (Fig. 1.1).<sup>13</sup> This milieu contains structural proteins (various collagens, elastin, laminin, fibronectin, etc.), glycans (aggrecan, heparin sulfate, chondroitin sulfate, keratan sulfate, hyaluronic acid), growth factors, and vesicles excreted by cells.<sup>14</sup> Tissues,

and ultimately organs, are comprised of cells and ECM. ECM components, like collagen protein, can be used in the construction of scaffolds for tissue engineering as well as to inform the development of bio-mimetics.<sup>13</sup>

In vivo, one of the main functions of the extracellular matrix is to provide support for cell adhesion.<sup>15,16</sup> When cells are not adhered to a surface, they undergo apoptosis and release factors that cause inflammation.<sup>16</sup> Inflammatory markers often drive detrimental host responses in tissue engineering.<sup>17</sup> Integration of tissue constructs often resembles the process of wound healing, which involves the interaction of cells with extracellular matrix components like collagen and fibronectin.<sup>18</sup> As such, understanding how the ECM directs cell attachment can allow for better host responses in tissue engineering.

Secondly, the physical properties, especially stiffness, of the ECM control the differentiation behavior of stem cells. Adipose derived stromal cells differentiate into adipose cells when grown on softer matrices. On much stiffer constructs, however, they take on an osteogenic phenotype and behave like bone cells.<sup>19</sup> The differentiation of stem cells can provide a reliable process for producing other cell types. This can address the problem of cell sourcing in tissue engineering.

Lastly, chemical cues, like cell adhesive ligands found in ECM proteins, play a role in angiogenesis, the sprouting of blood vessels.<sup>20,21</sup> Understanding the mechanisms of how this works can provide an avenue for tissue construct vascularization. The cell adhesive protein sequence, glycine-phenylalanine-hydroxyproline-glycine-glutamate-arginine (GFOGER), directs endothelial cells to form network-like structures, reminiscent of blood vessels, on surfaces comprising the ECM protein, collagen, in vitro.<sup>20</sup> This process is thought to be similar to how collagen directs angiogenesis in vivo.<sup>21</sup> Other components, like laminin and proteoglycans, can also direct cells to sprout into blood vessels.<sup>22</sup> Understanding the properties of the ECM will allow for the production of vascularized tissues, an important step towards the ultimate goal of organ production and regeneration.

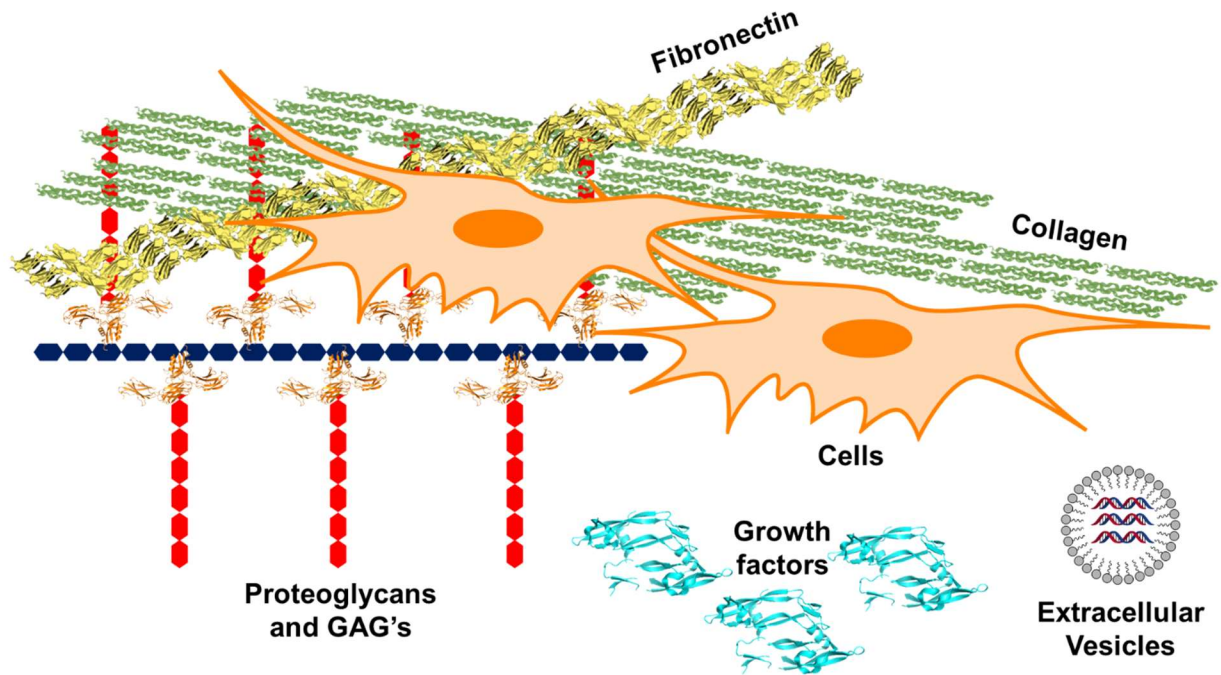


Figure 1.1. The extracellular matrix is made up of structural proteins, proteoglycans, glycosaminoglycans, vesicles, and growth factors.

### 1.3 Natural and Synthetic Biomaterials

Biomaterials are defined as “materials exploited in contact with living tissues, organisms, or microorganisms”.<sup>23</sup> Various biomaterials are used to construct scaffolds for tissue engineering. The chemical functionality of these materials must allow for compatibility with cells, stability in biological milieu, and sterilizability in processing. A variety of physical properties, like stiffness, porosity, and morphology must also be optimized to achieve successful tissue engineering.

Natural ECM components, like collagen, hyaluronic acid, laminin, fibronectin, proteoglycans, and elastin are used widely to create scaffolds.<sup>24,25,26,13</sup> Collagen is especially popular in scaffolds for cartilage and skin regeneration.<sup>7</sup> The advantage of natural materials is an inherent biocompatibility and controlled biodegradation.<sup>17,18,19</sup> Natural materials have disadvantages in their processability, however. Thermal processing and chemical crosslinking can ruin protein structure and degrade biochemical function.<sup>29,30</sup> Furthermore, sterilization of natural materials is often very costly and difficult.<sup>31</sup>

Synthetic biomaterials, like metals, polymers, and ceramics, are often cheaper to produce, easier to sterilize, and wider in their space of accessible materials properties. However, each type comes with disadvantages and all synthetic materials run the risk of foreign body response.<sup>32,33</sup> Biocompatible metals, like cobalt and stainless steel, and ceramics, like bio-glass, can be molded into various shapes for use as implants.<sup>34</sup> The hardness and stability of these classes of materials makes them especially suited for use in bone related conditions. Their stability becomes a disadvantage, however, for use in tissue engineering, where it is optimal for an implanted scaffold to degrade after organ regeneration is achieved. Polymers, like polylactic-co-glycolic acid (PLGA) and polyethylene glycol (PEG), offer an alternative with tunable mechanical and degradative properties.<sup>2,35</sup> Degradable PEG scaffolds were used to grow neural tissues.<sup>35</sup> In another work, photocrosslinking was used to tune the stiffness of polyethylene glycol gels that were used to study cancer cell migration.<sup>36</sup> Due to this high level of control, polymers are currently the most commonly used for the purposes of tissue engineering. The disadvantages of polymers are a lack of bio-functionality. Natural materials contain a variety of cell and growth factor binding sites as a result of evolutionary optimization for their biological roles.<sup>37,38</sup> This lack of bio-functionality may underlie the foreign body responses sometimes seen with synthetic polymer implants.<sup>33</sup>

To capture the richness of natural ECM, cell and protein binding sites are being introduced into synthetic polymers to create the next generation of scaffold materials.<sup>39</sup> Osteogenesis was increased when cell adhesive peptides were incorporated into diacrylate hydrogels.<sup>40</sup> Covalently immobilizing growth factors in polyethylene glycol gels allowed for increased vascularization.<sup>41</sup> In creating hybrid materials such as these, new best practices may emerge. One newly discovered principle is that the density of cell binding sites displayed on materials modulates receptor clustering.<sup>42</sup> Optimizing receptor clustering is crucial for processes like blood vessel formation and stem cell differentiation.<sup>43,44</sup> Explorations towards these ends may reveal novel biochemistry as well as achieve better tissue engineering.

#### **1.4 Interactions of Cells with Biomaterials**

Understanding the interactions of cells with biomaterials is an important step towards improved tissue scaffolds. Cells are capable of adhering to, migrating on, degrading, and remodeling biomaterial matrices. The properties of scaffolds determine the proliferation and response of

seeded cells. To engineer more complex tissue architectures, scaffolds must be optimized to prime cells for crucial functions, such as the formation of blood vessel networks.

#### 1.4.1 Cell Adhesion to Biomaterials

To explain how cells adhere to biomaterials, mechanisms, based on electrostatic charge and specific protein/proteoglycan mediation, are invoked.<sup>45,46</sup> The former, considered as a non-specific mechanism, is most commonly used to explain binding to surfaces coated with charged polymers.<sup>46</sup> Made up of anionic phospholipids, cell membranes are negatively charged. As a result, non-specific cell adhesion can be thought of as charge pairing with cationic polymers, like poly-lysine. Several studies have shown higher cell adhesion on positively charged materials.<sup>45,46,47,48</sup> However, further exploration has shown that this type of adhesion may not be due to non-specific interactions with cell membranes.<sup>47</sup> Instead, the attachment may be mediated by specific proteoglycans, cell surface proteins attached to negatively charged polysaccharides. When treated with chondroitinase ABC, an enzyme that degrades proteoglycans, the ability of cells to adhere to positively charged surfaces is abrogated.<sup>47</sup> The hypothesis that cell adhesion may be mostly mediated by specific proteins may inform future biomaterials design.

Integrins, a family of cell-surface proteins, are the best studied players invoked in specific cell adhesion mechanisms.<sup>43</sup> Made up of  $\alpha$  and  $\beta$  subunits that wrap around each other, integrins are primed for binding to various ECM proteins.<sup>49</sup> Two of the most well studied integrins are  $\alpha 2\beta 1$  and  $\alpha 5\beta 3$ . These bind to the ECM derived protein sequences GFOGER, from collagen, and RGD, from fibronectin, respectively. In a process known as outside-in signaling, integrins transmit structural information from the ECM to the cytoskeleton.<sup>50,51</sup> When bound to their targets in the ECM, integrins undergo conformational changes that allow their intracellular domain to bind to the protein, talin, which subsequently nucleates actin fibers, a major component of the cytoskeleton.<sup>52</sup> When binding sites in the ECM are located in close proximity to each other, multiple copies of integrins are clustered together as these receptors bind their targets.<sup>44</sup> Integrin clusters are known to template actin fibers to a greater extent and the increased outside-in signaling causes the formation of the membrane protrusions known as focal adhesions.<sup>53,54,55</sup> The presence of actin fibers and focal adhesions are a hallmark of protein mediated cell adhesion to surfaces. The understanding of integrin clustering and focal adhesions has prompted the development of

biomaterials displaying nanoscopic patterns of adhesion sequences.<sup>55,42</sup> These offer enhanced cell adhesion and integrin signalling due to increased ability to cluster adhesion receptors.

#### **1.4.2 Cell Migration on Biomaterials**

Multicellular behaviors, like network formation by endothelial cells during blood vessel formation, often require a balance of cell adhesion and migration.<sup>56</sup> An understanding of cell migration may lead to materials scaffolds that promote these processes. The mechanism of cell migration on biomaterial surfaces is debated but like adhesion, it is associated with the formation of actin fibers.<sup>57,58,59,60</sup>

When a cell migrates, actin fibers form at protrusions, called lamellipodia, on its leading edge (Fig. 1.2).<sup>60</sup> Lamellipodia extend and adhere to the ECM at the destination of the cell's movement. The rest of the cell is pulled towards the direction of the protrusion as it deconstructs. Integrins are known to play a role in the formation and adhesion of lamellipodia, suggesting mechanisms of actin polymerization that are similar to cell adhesion and spreading.<sup>61</sup> On gradients of RGD in polyethylene glycol gels, which binds integrin  $\alpha5\beta3$ , cells migrate in the direction of increasing ligand density.<sup>62</sup>

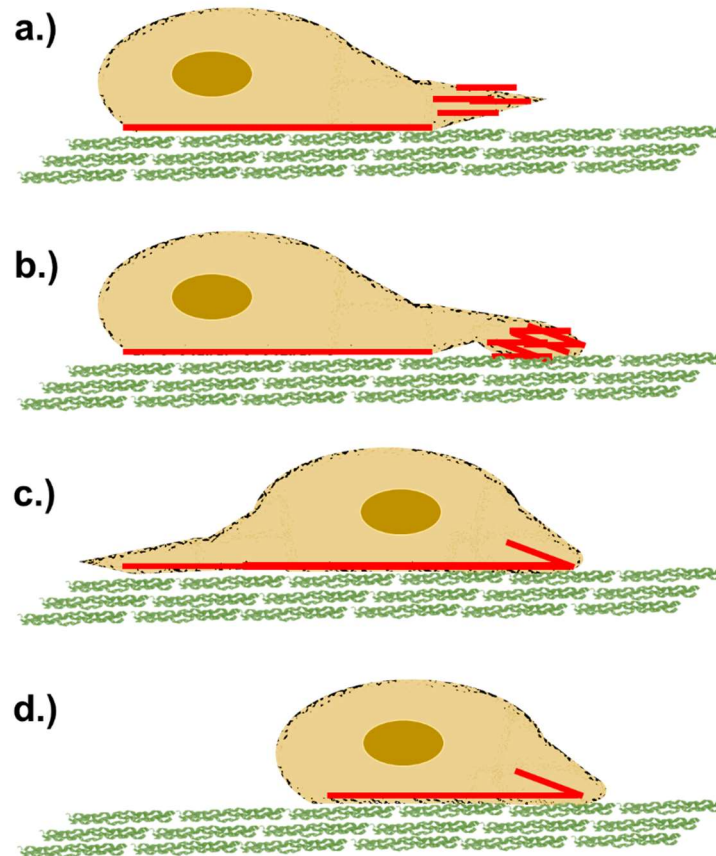


Figure 1.2. In cell migration, (a.) lamellopodia extend from the cell with polymerization of actin (red), (b.) an adhesion is formed at the destination site, (c.) lamellopodia retract and pull the cell towards the destination, and (d.) the cell moves and adheres to the new site. (Adapted from 60.)

### 1.4.3 Collagen Induced Endothelial Network Formation

In 1988, Kubota et al reported that endothelial cells plated on basement membrane gels formed capillary-like networks.<sup>63</sup> This process of endothelial cell network formation is related to angiogenesis, the process in which new blood vessels are sprouted. Basement membrane gels are derived from the natural ECM and contain collagen, laminin, and various other proteins. Kubota et al, thus, demonstrated that angiogenesis-related processes can be activated by constituents of the ECM. Endothelial cell tube formation on purified type I collagen gels has also been shown (Fig. 1.3.).<sup>64,65,66,67,20</sup> This process highlights the ability of natural biomaterials to activate complex multicellular behaviors. Uncovering the mechanism of action will lead to advanced synthetic biomaterials for tissue engineering.

Various studies have highlighted the importance of integrin  $\alpha 2\beta 1$  in collagen induced endothelial cell network formation.<sup>20,65,66,67,68</sup> On type I collagen gels, growth factors, like VEGF, are known to accelerate the network formation process.<sup>64</sup> VEGF was shown to increase the expression of integrin  $\alpha 2\beta 1$  subunits.<sup>66</sup> When cells are treated with antibodies or peptides that bind to the integrin  $\alpha 2\beta 1$  subunits, network formation ceases.<sup>20,65</sup> While integrin binding, with peptides or antibodies, is generally shown to be inhibitory, integrin clustering seems activate the process. Whelan and Senger used a system of two antibodies to cluster integrin  $\alpha 2\beta 1$  in microvascular endothelial cells.<sup>20</sup> This promoted the formation of actin fibers, a feature also observed with network formation. Using a polyvalent antibody preparation, Turner et al showed that clustering integrins accelerates tube formation on collagen gels.<sup>68</sup> The involvement of integrin clustering, actin formation, and a biomaterial surface suggests similarities to cell adhesion. The activation of the process by growth factors, which are known to increase cell migration, suggest a more dynamic scenario, however.<sup>69</sup> The true mechanism may be somewhere between adhesion and migration.

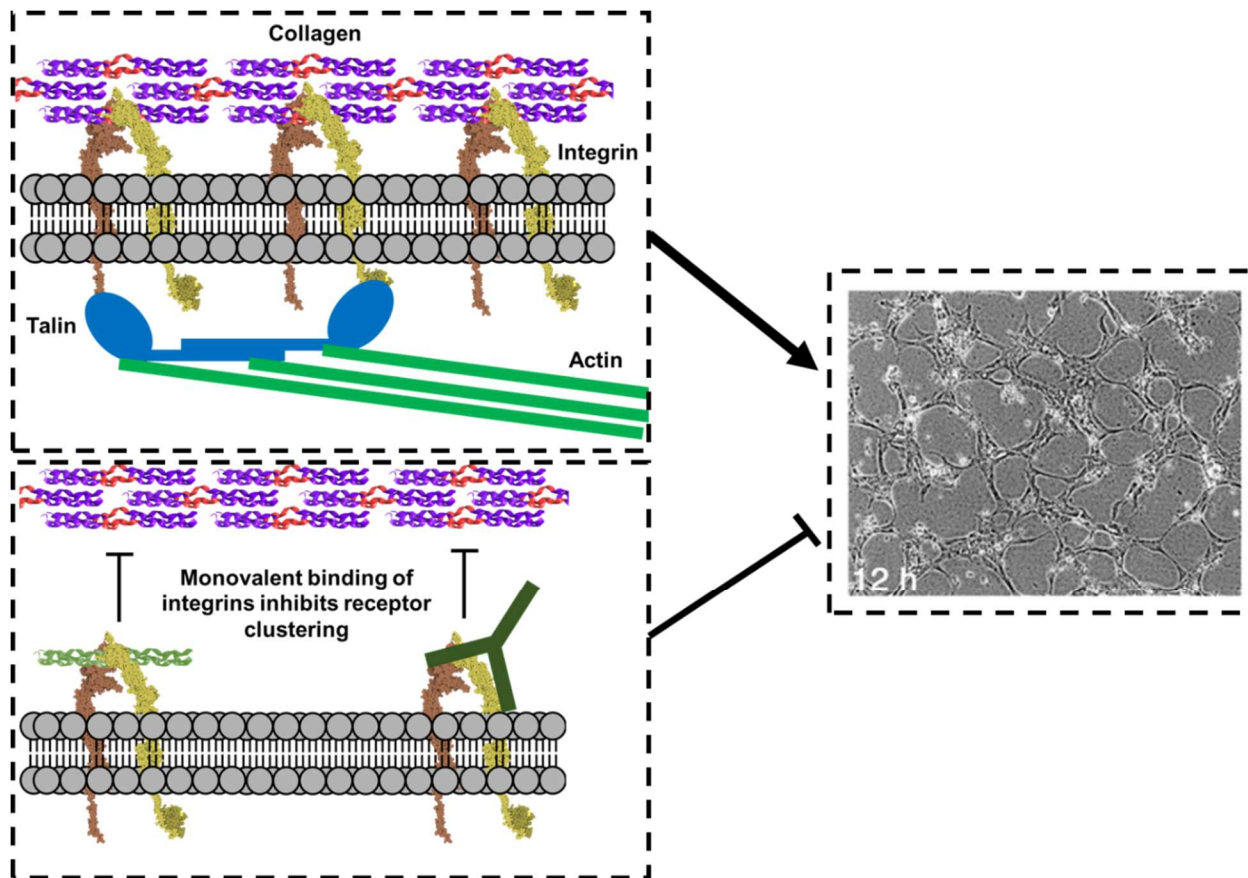


Figure 1.3. It is hypothesized that formation of endothelial cell networks on a collagen gel requires clustering of Integrin  $\alpha2\beta1$ ; simple binding with antibodies or peptides, in the absence of clustering, has been shown to inhibit network formation. (Adapted from Ref. 65.)

Taken together, the studies suggest that type I collagen presents the GFOGER in a polyvalent manner capable of clustering integrin  $\alpha2\beta1$ . Subsequently, actin fiber polymerization and network formation are observed. This principle was used to develop biomaterials: GFOGER laden polyethylene glycol gels are shown to support growth factor induced endothelial tube formation.<sup>70</sup> Here, the monovalent peptide sequence was distributed homogeneously throughout the gel and it is unlikely that two copies of the sequence would be located close enough to induce a clustering event. The growth factor likely enhanced cell migration and integrin expression. As a result of the pulling force generated by cell migration and integrin binding, copies of the GFOGER sequence were likely pulled together towards the cells in the gel to induce an indirect form of receptor clustering. Once this occurred, endothelial cell tube formation would commence. A direct demonstration of network formation with a well-defined polyvalent construct of GFOGER peptide is lacking.

## 1.5 Collagen Structure and Processing

Collagen has found a plethora of applications in tissue engineering and has also served as inspiration for a variety of synthetic materials. At 30% of the mass of the ECM, collagen (discuss types) is the most abundant protein found in animal tissues. Yao et al. have used type I collagen microspheres to promote the full differentiation of oligodendrocyte progenitor cells into neuronal micro-tissues.<sup>71</sup> Matsunga et. al. showed that type I collagen beads, loaded with fibroblasts, could be used to prepare millimeter thick tissues in pre-formed molds.<sup>72</sup> Understanding the structure of collagens will allow for the design of collagen-like biomaterials.

On microscopic scale, type I collagen proteins consist of interwoven fibrous networks.<sup>73</sup> The sturdy fibers are made up of smaller fibrils that intertwine around each other.<sup>74</sup> The fibrils, when stained for viewing by electron microscopy, display a regular pattern of stripes occurring at every 67 nm. These are believed to result from a staggered packing of triple helices, the secondary structural elements of most collagen proteins. A triple helix is made up of three individual chains of collagen wrapped around each other almost like a braid. Within a triple helix, each individual chain adopts a left handed polyproline type II helix, characterized by  $(\phi, \psi)$  backbone dihedral angles of approximately  $(-75^\circ, 150^\circ)$ . These properties result from type I collagen's sequence which contains many copies of the three-amino acid repeat, proline-trans-4-hydroxyproline-glycine (POG).<sup>74</sup> The high content of proline and hydroxy-proline causes steric repulsion between pyrrolidine rings, enforcing the geometries of the polyproline type II helix. Every third residue in the triple helical regions of most collagens is glycine; hydrogen-bonding between glycine amides and the carbonyl groups of adjacent chains helps to stabilize and tighten the triple helical secondary structure (Fig. 1.4). Intermittently between POG repeats, many functional sequences, such as GFOGER, are found. From the molecular structure, all the way to its macroscopic properties, collagen has evolved to act like a strong rope which is interwoven to form the structure of the ECM.

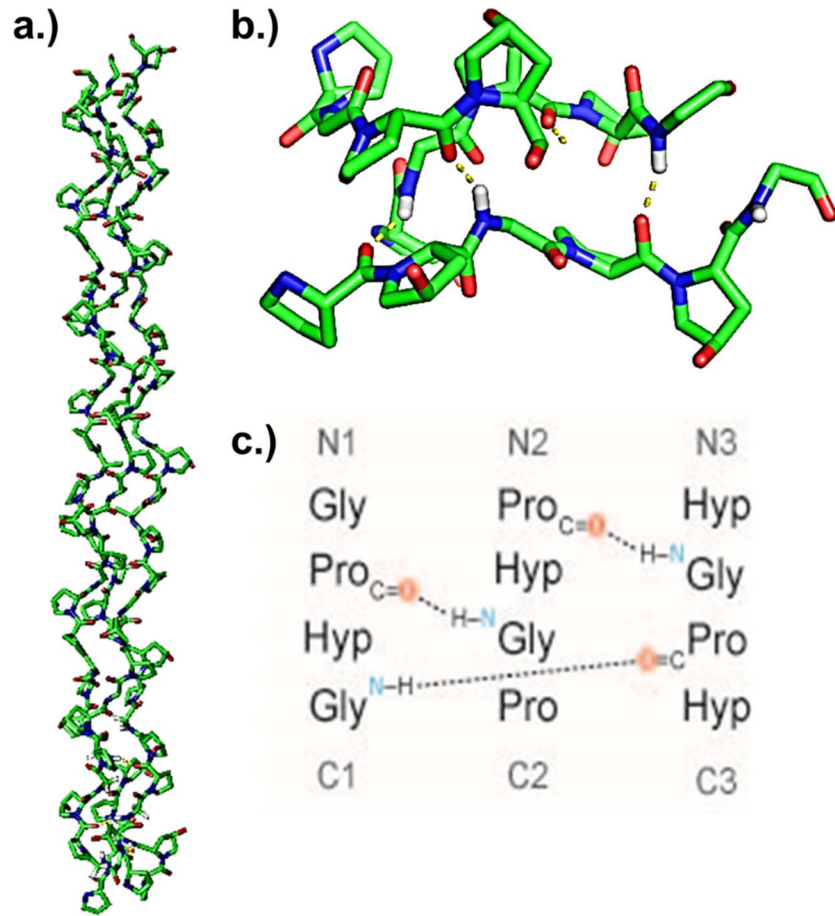


Figure 1.4. The structure of the collagen triple helix (a) showing glycine hydrogen bonds (b, c). (Adapted from Ref. 62)

The processing, sourcing, and cost present disadvantages for the use of type I collagen in tissue engineering. Collagen proteins are extracted from animal tissues using acidic conditions.<sup>75</sup> To promote formation of fibers from soluble type I collagen in acidic solution, the solution is neutralized with base or buffer.<sup>76</sup> Various techniques, including freeze-drying, molding, and coating, can be used to fabricate or include the protein into tissue scaffolds.<sup>72,77,78</sup> Unfortunately, these methods often produce collagen materials with poor thermal stability.<sup>79</sup> The triple helix of full length type I collagen proteins unfolds in an irreversible manner.<sup>80</sup> This type of degradation ruins the mechanical properties of tissue scaffolds. In a natural setting, the enzyme, lysyl oxidase, promotes the crosslinking of type I collagen fibers, rendering them fully insoluble.<sup>81</sup> When extracted with acidic solution, the soluble collagen has not been stabilized via crosslinking and remains thermally unstable at physiological temperatures.<sup>80</sup> The production of recombinant lysyl

oxidase is expensive and its use in crosslinking collagen scaffolds in vitro yields poor results.<sup>82</sup> Chemical crosslinkers offer an alternative, but can destroy important bioactive sequences like GFOGER.<sup>83</sup> In an effort to circumvent the limitations of natural collagen, peptide-based synthetic materials are currently being studied.

## **1.6 Peptide Mimetics**

Peptides are attractive candidates for the construction of tissue scaffolds with diverse and even unnatural functionality.<sup>84</sup> The short size of peptides enables the possibility of chemical synthesis. This offers distinct advantages over proteins, which must be expressed recombinantly or extracted from tissues. Peptide synthesis also allows the easy introduction of unnatural or post-translationally modified amino acids into a sequence. As such, peptides based on ECM components, like fibronectin, laminin, and collagen have been synthesized and explored.<sup>85,86,87,88</sup>

Collagen mimetic peptides (CMP) are a particularly interesting class because they can be designed to avoid the difficulties of natural collagen processing while maintaining many of its advantages.<sup>88</sup> The bulk of CMP research has focused on understanding the triple helical structure of natural type I collagen.<sup>74,89,90</sup> Importantly, recent explorations have developed methods of constructing CMPs into biomaterials.<sup>88</sup> These ventures will yield structurally-tunable model systems for understanding the function of the ECM in complex cellular behaviors. Eventually, CMP based systems may even replace natural collagen as a biomaterial of choice for scaffolding in tissue engineering.

## **1.7 Collagen Mimetic Peptides: Triple Helical Stability**

The sequence of collagen mimetic peptides most commonly contains a repeating motif, Xaa-Yaa-Gly.<sup>74</sup> Like natural collagen, the most common residue found in the Xaa position is proline (Pro; P) and in the Yaa position is 4-trans-hydroxyproline (Hyp; O). Analysis by circular dichroism (CD) spectroscopy, nuclear magnetic resonance (NMR), X-ray diffraction (XRD), and various other techniques have shown that these peptides adopt the triple helical structure just like natural collagen.<sup>89,90,91,92,93,94</sup> As such, CMPs have provided easily accessible model systems for studying collagen's structure and the principles behind its thermal stability. Because natural collagen must

be crosslinked to achieve stability, stabilized CMPs may offer a better alternative for biomaterials applications.

As with natural collagen, having a glycine at every third residue is of paramount importance for triple helix folding. Glycine forms inter-chain hydrogen bonds that hold a triple helical structure together. Brodsky and coworkers have shown that mutating the glycine residue results in CMPs with an interrupted ability to form triple helices.<sup>95,96</sup> These non-triple helical CMPs are characterized by sub-ambient transition melting temperatures ( $T_m$ ), the point at which half the population of peptide molecules exists in an unfolded state. Glycine mutations underlie the most fatal etiologies in collagen related diseases.<sup>97,98</sup>

Hyp increases the thermal stability of the triple helical conformation.<sup>74</sup> Analogous peptides, containing proline instead of Hyp at the Xaa position, have a significantly lower  $T_m$ .<sup>99</sup> Originally, the hydroxyl group was thought to stabilize triple helices by forming hydrogen bonds with water molecules.<sup>100</sup> The resulting water bridges would lock the peptides into their folded triple helical state. Brodsky and coworkers demonstrated the existence of these water bridges in crystal structures.<sup>100</sup> However, this water bridge hypothesis had deficiencies. Firstly, CMP triple helices were found to be more stable in aqueous alcohol solutions than in pure aqueous solutions; Water bridges would be more likely in pure aqueous solutions.<sup>101</sup> Secondly, CMPs containing cis-4-hydroxyproline, instead of the usual trans isomer, had significantly lower  $T_m$  even though both isomers should have been capable of forming water bridges.<sup>102</sup>

Studies by Raines and coworkers offered a much better explanation based on the stereo-electronics of proline ring conformations. In crystal structures, hydroxyproline was observed to take on a trans ring conformation.<sup>99</sup> This allowed a favorable  $n-\pi^*$  interaction between a C-H sigma bond and the C-O antibonding orbital.<sup>103</sup> Based on a hypothesis that the interaction was responsible for the stabilization of triple helices, Raines and coworkers synthesized analogous CMPs where trans-4-hydroxyproline was replaced with trans-4-fluoroproline.<sup>99</sup> The C-F antibonding orbital, being a better acceptor, was hypothesized to allow for a stronger  $\sigma-\sigma^*$  interaction (Fig. 1.5).<sup>104</sup> The fluorinated CMP chains, due to the stronger orbital overlap, would be pre-organized into a structure favoring triple helix formation. Using CD spectroscopy, it was shown that this resulted

in a  $T_m$  almost 30 degrees higher than that of CMP's with trans-4-hydroxyproline. In addition, a variety of control experiments showed that this remarkable stabilization was not due to hydrophobic effect.<sup>105,106,107</sup> The pre-organization hypothesis is currently the most agreed upon explanation for the effect of the Xaa position in collagen stability.

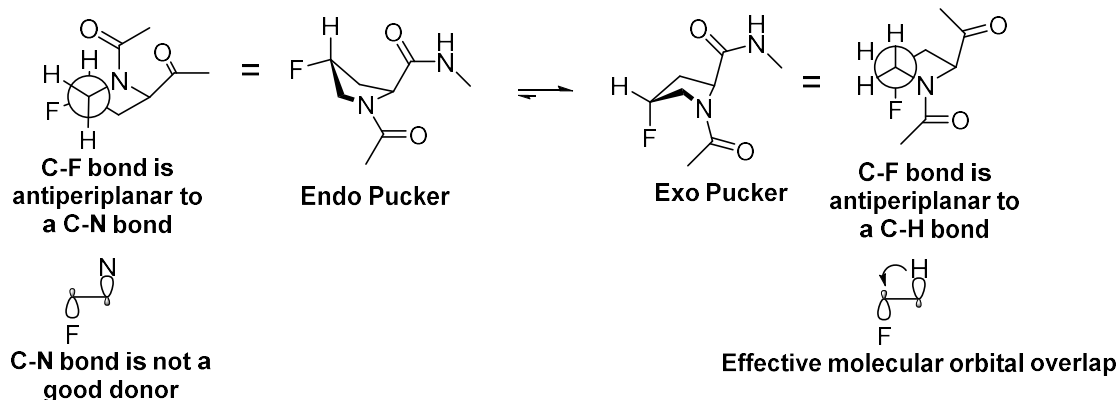


Figure 1.5. Trans-4-fluoroproline residues preferentially adopt an exo pucker due to favorable orbital overlaps.

Finally, other methods have been found for increasing CMP stability, highlighting the role of unnatural amino acids. Chenoweth and coworkers have shown that using the aza-glycine, in place of glycine, endowed a triple helical CMP with a  $T_m$  higher than the boiling point of water.<sup>108</sup> Crystal structures revealed that this was a consequence of the enhanced hydrogen bonding ability of aza-glycine.<sup>109</sup> Wennemers and coworkers showed that peptides with appended hydrophobic groups are also stabilized as compared to control molecules.<sup>110</sup> This is thought to occur because the hydrophobic group folds on top of the triple helix, preventing it from unravelling.

## 1.8 Collagen Mimetic Peptides: Self-Assembly Strategies

The use of natural collagen as a biomaterial is made possible by its ability to form fibers. This process highlights the ability of collagen molecules to self-assemble into structures on much larger size scales. Self-assembly is a process in which disordered systems, like a solution of protein molecules, can form large ordered structures, like collagen fibers, without external manipulation.<sup>111</sup> To fabricate advanced synthetic biomaterials, recent research has used a wide variety of chemistries to promote the self-assembly of CMP's into nano- and microscale



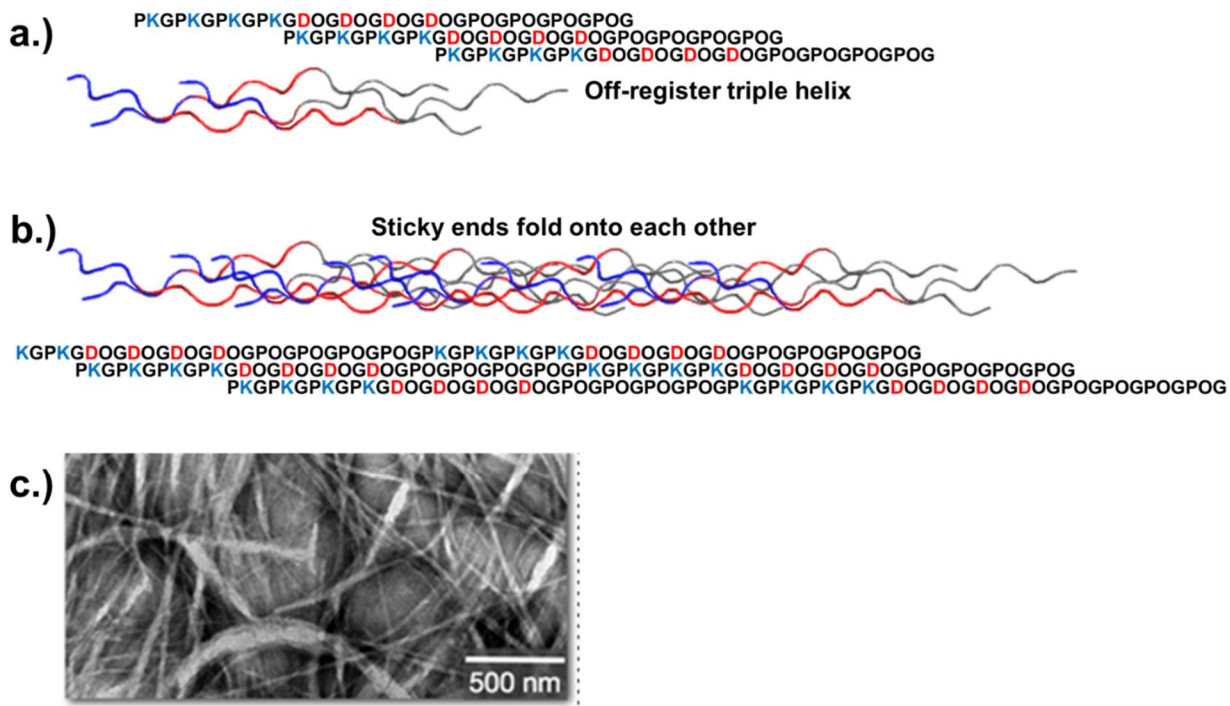


Figure 1.7. Sticky-Ended CMP self-assembly involves off-register triple helices (a.) which condense in a lengthwise manner (b.) into fibrous matrices (c.). (Adapted from Ref. 117)

Hydrophobic interactions, of various types, have been used to promote CMP self-assembly. Many studies have utilized collagen mimetic peptide amphiphiles. Containing large aliphatic hydrophobic tails, these molecules behave like surfactants while also being able to form triple helices.<sup>121,122</sup> This allows for a combination of micelle-like self-assembly and triple helix packing. The mechanism most commonly yields a fiber-like morphology and has been extended to make cell adhesive fiber matrices.<sup>121</sup> Cejas et al utilized a different approach involving aromatic-based hydrophobic interactions.<sup>123</sup> The best self-assembly results were obtained when pentafluorophenyl and phenyl groups were displayed on the N- and C-termini, respectively. The resulting peptide formed a dynamic noodle-like fiber structure with domains that resembled d-periodic banding. This peptide assembly promoted platelet aggregation, a bio-property also displayed by natural collagen. The authors suggested that hydrophobic interactions were the main driver for self-assembly. However, this may not be a traditional entropy derived hydrophobic effect. The pair of an electron poor arene, pentafluorophenyl, and a phenyl group suggests that pi-pi stacking is involved. Brodsky and coworkers have also shown that aromatic stacking interactions play a role in CMP self-association under heated conditions.<sup>124</sup>

The designs described until this point utilize end-on self-assembly signals at peptide termini and end-on linear propagation. Lateral designs, though less common, have also yielded many significant results in CMP self-assembly. Through chirality driven interactions, Xu et al added a twist the concept of hydrophobic self-assembly: while pure solutions of individual CMP enantiomers were stable, a 1:1 mixture of each isomer had significantly decreased solubility.<sup>125</sup> The resulting solid was made up of extended sheetlike structures (Fig. 1.8). The packing of the triple helices was explained with an analogy to two screws. Screws of opposite handedness pack more closely together than two of the same handedness. As such, the mixture of enantiomers also packs more closely together in a manner driven by the hydrophobic effect. The same group also reported CMPs with hydrophobic amino acids at radial positions.<sup>126</sup> These peptides packed laterally to form discs. A similar result was also reported by Przybyla et al: Hbyp3, a CMP designed to display radial bipyridine moieties, self-assembled into disks.<sup>127</sup> Hydrophobic and aromatic interactions between the bipyridine units may be the driving force for this process.

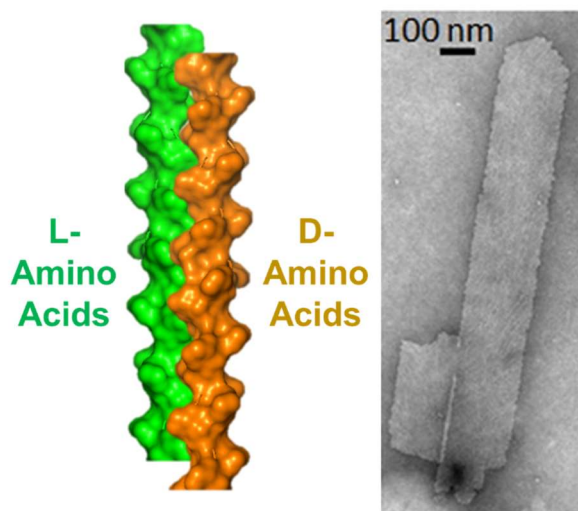


Figure 1.8. Chirality driven assembly of oppositely handed triple helices. Adopted from Ref. 125.

### 1.9 Metal Ion Promoted Self Assembly of Collagen Mimetic Peptides

While electrostatic interactions and the hydrophobic effect are the most commonly used strategies for CMP self-assembly, metal chelation offers a different avenue. The overall strategy involves

the use of CMPs equipped with metal binding ligands at either terminal or radial positions.<sup>88</sup> Upon addition of metal salts, the chelation interaction will promote the association and assembly of the peptide. This method offers a unique advantage: the chelation interaction can be tuned by simply varying the metal ion. For applications where reversibility may be advantageous, weakly binding metal-ligand pairs, like nitrilotriacetic acid (NTA) and iron (II), can be utilized.<sup>128</sup> Without having to change the ligand and synthesize a new CMP, the interaction can be made almost as strong as a covalent bond through the use of exchange inert metals, like cobalt (III) or chromium (III).<sup>129,130</sup> Any intermediate strength interactions can be achieved by using other metal ions. By contrast, electrostatic and hydrophobic interactions are much more difficult to tune and require a new peptide to be synthesized for each change.

Metal triggered radial assembly has been used to fabricate particles of diverse morphology. In 2008, Przybyla and Chmielewski designed a peptide, H-byp, containing repeating POG units and a radial bipyridine appendage.<sup>131</sup> When incubated with Fe(II) ions, H-byp formed nanofibers as seen by transmission electron microscopy (TEM). Complexation of iron ions by the bipyridine ligands was confirmed by absorbance spectroscopy of the pink colored complex. Furthermore, the fibers were dissolved when treated with ethylenediamine tetra-acetic acid (EDTA), which competes for complexation. These observations suggested a metal chelation based radial self-assembly mechanism. This concept was extended by Przybyla and coworkers with CMPs, Hbyp2 and Hbyp3, containing 2 and 3 radial bipyridine appendages, respectively.<sup>132, 127</sup> Hbyp2 was found to form EDTA-reversible disks in a metal ion dependent manner. Hbyp3 formed disks even without metal, indicating a possible aromatic or hydrophobic interaction, as described above. When metal ions were added, HByp3 disks assembled in a quilt-like manner into hollow sphere-like structures (Fig. 1.9). Addition of EDTA reverted the spheres into disks, suggesting that metal ions were important in the mechanism. In each of these cases, the identity of the metal ion did not seem to affect the assembly; The only criteria appeared to be divalency, giving these ions a charge of 2<sup>+</sup>. To further validate the use of metal triggered assembly, Hbyp3 hollow spheres were loaded with various cargos and showed release rates dependent on temperature.<sup>133</sup> As such, this type of self-assembly can allow access to the next generation of timed release drug delivery devices.

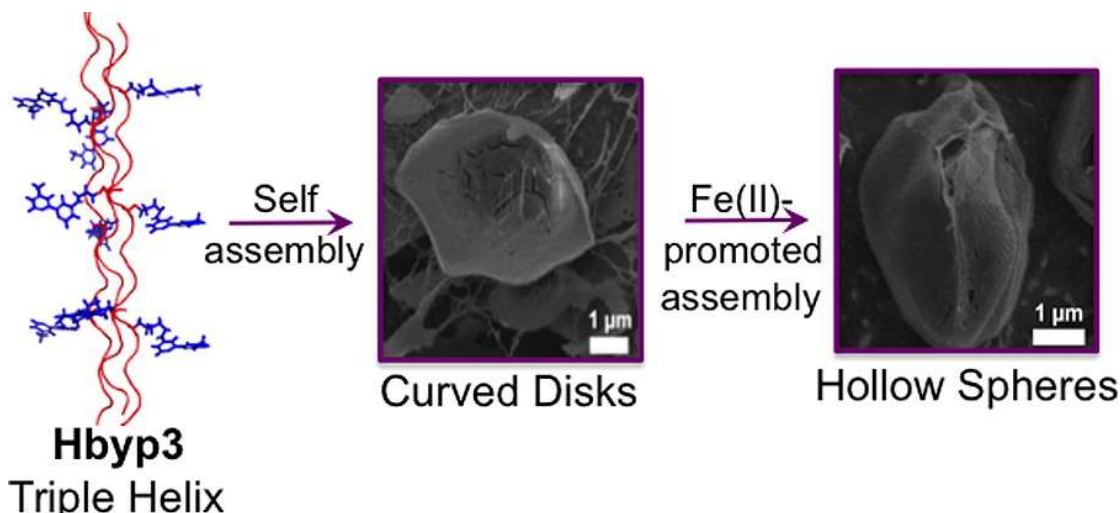


Figure 1.9. The metal-mediated self-assembly of HByp3 into curved disks and hollow spheres. Adopted from Ref. 127.

Metal ions are also able to promote linear assembly in designed CMPs. Pires and Chmielewski showed that a linearly designed CMP, NCoH, formed ruffled spherical particles called microflorettes.<sup>134</sup> NCoH's design had three elements: a core of 9 POG repeats, two histidine residues at the C-terminus, and a nitrilotriacetic acid moiety on the N-terminus (Fig. 1.10). The ligands were chosen to add directionality to the linear assembly: metal ions would link NTA ends only to di-histidine ends. Impressively, microflorettes, derived from NCoH self-assembly, could be simultaneously loaded with two different protein cargos, (Fig. 1.11).<sup>135</sup> If the cargo was included during the CMP self-assembly process, it would be loaded into the particle core. Afterwards, a second cargo could be attached to the particle surfaces using metal ions and non-metallated ligands on the particle surface. These cargos could then be slowly released as the particles dissolved.

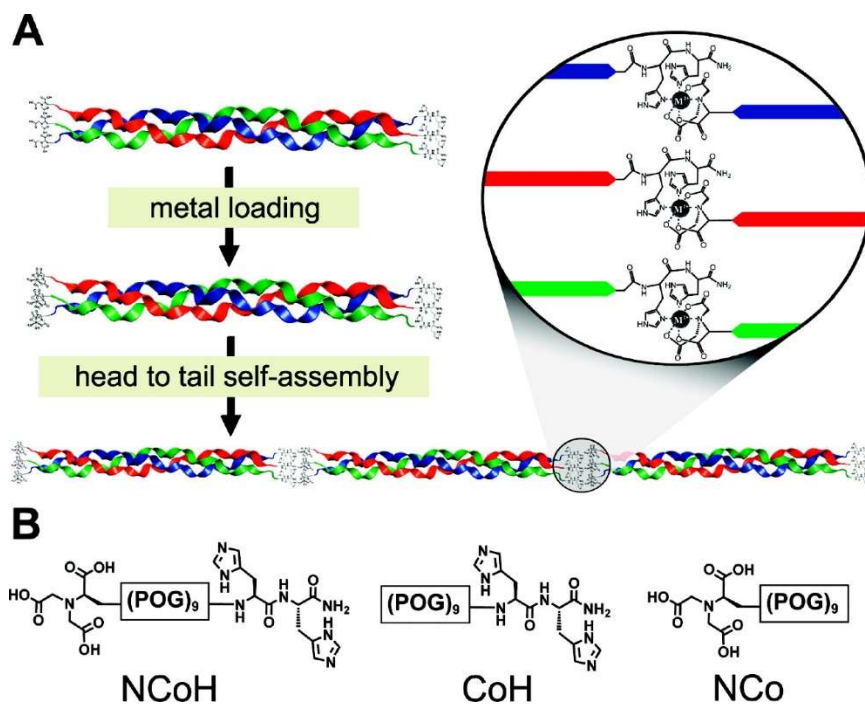


Figure 1.10. The linear design of NCoH. Adopted from Ref. 134.

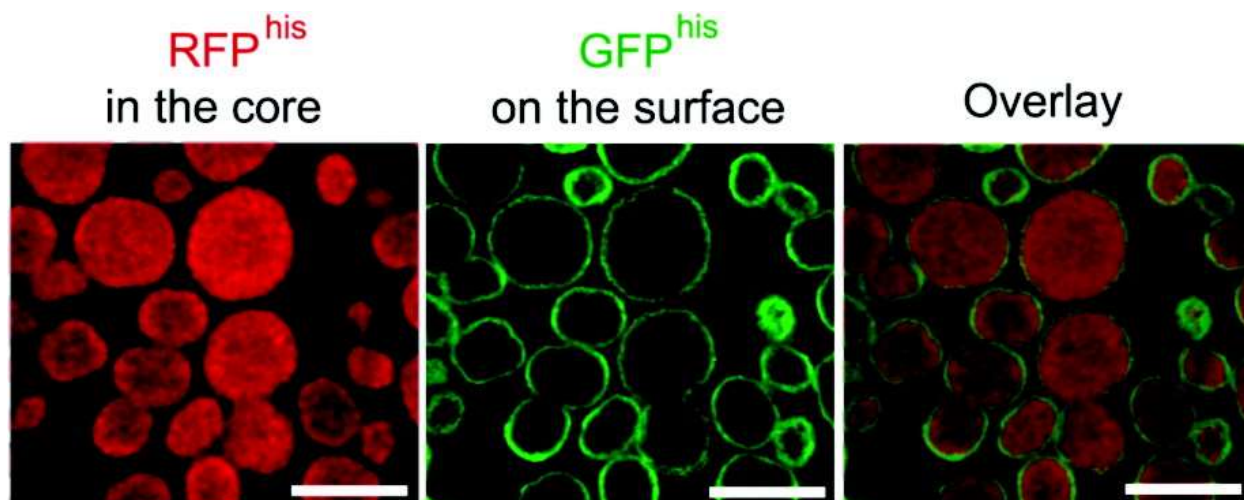


Figure 1.11. NCoH Microflorettes labelled with two different fluorescent proteins. Adopted from reference 135

The metal promoted linear self-assembly was explored further in a series of studies. In the first, the morphology of the assembled particles was studied as a function of the number of core POG units.<sup>136</sup> The number of POG repeats determined the thermal stability of the resulting triple helices. The lesser the number of repeats, the lower the  $T_m$  measured. With less stable triple helices containing 5 and 7 repeats, the metal mediated self-assembly process did not proceed using the

same conditions as NCoH (9 repeats). At 11 and 13 repeats, the process formed saddle-like structures. The authors, here, concluded that triple helical stability was of paramount importance for achieving self-assembly. In a second study, the ligand NTA was replaced with iminodiacetic acid (IDA), which contained one less chelating carboxylic acid.<sup>137</sup> The loss of one carboxylate had a profound effect on the observed morphology. While NCoH, which contains NTA, formed microflorettes, ICoH, which contained IDA, formed nanofibril stacks. Furthermore, these stacks displayed a periodic banding pattern, indicating similarity to natural collagen. In the third study, two CMPs with 9 POG repeats, namely HisCol and IdaCol, were designed to contain only one type of ligand at their termini.<sup>138</sup> HisCol contained four total histidine residues with two at each termini. IdaCol contained an IDA ligand at each termini. When the two were mixed and metal ions were added, petal-like structures were observed. These also displayed a clear banding pattern as observed by transmission electron microscopy (Fig. 1.12). The periodicity of the pattern was 10 nm, about the length of the triple helices used. This suggested a linear arrangement of these structural elements, as intended in their design. A fourth study also explored mixed peptide assemblies.<sup>139</sup> When NCoH and HisCol were mixed and metal ions were added, micron scale spiraled horns were formed. These structures displayed a binding affinity for HeLa cells. All the studies, taken together, demonstrate that each aspect of the designed CMPS, namely the core and ligands, can greatly affect the result of metal triggered assembly.

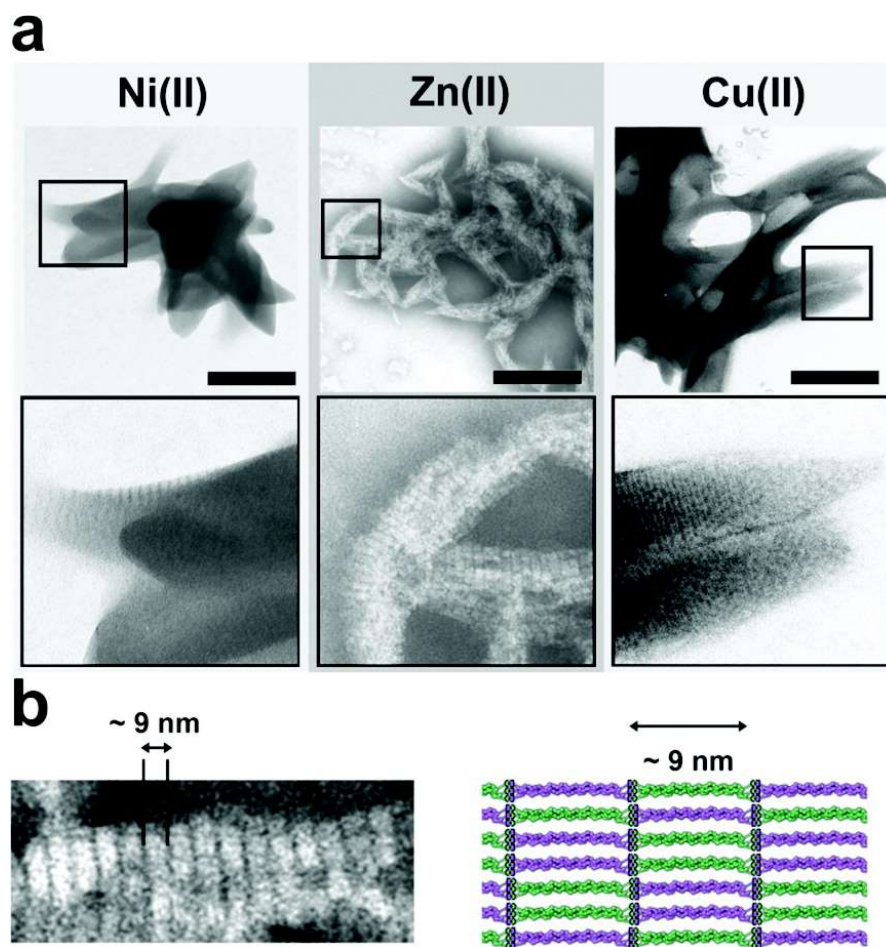


Figure 1.12. Banded particles from the tandem co-assembly of HisCol and IdaCol. Adopted from Ref. 138.

Metal mediated self-assembly has allowed the fabrication of crosslinked CMP-based biomaterials. Crosslinking enables materials to have the stability and strength to be used as tissue scaffolds. Most natural collagen scaffolds are crosslinked before they are seeded with cells. To achieve crosslinked materials with CMPs, the linear and radial designs were combined. This combination was brought to life in the design of NHBipy, a CMP with a radial bipyridine moiety as well as terminal NTA and dihistidine units.<sup>140</sup> Upon addition of metal salts to solutions of NHBipy, Pires and coworkers observed the formation of highly crosslinked meshes. This morphology has similarities to the crosslinked fiber networks of natural collagen. These meshes were easily solubilized by the addition of EDTA as in previous metal-based systems. The NHBipy assembly process allowed the inclusion of other ligand containing CMPs, as seen in the successful production of fluorescent and biotin labelled biomaterials. The ultimate test of NHBipy meshes

was in their ability to successfully support cell culture. In their first cell culture experiment, Pires and coworkers showed that HeLa cells could be encapsulated when meshes were triggered to form in their presence (Fig. 1.13). The encapsulated cells remained viable even after 5 days of culture. The ability of the scaffold to be rendered fluorescent allowed selective visualization of the scaffold and cells by confocal microscopy. After this period of culture, the cells could easily be retrieved by treatment with EDTA and re-cultured.

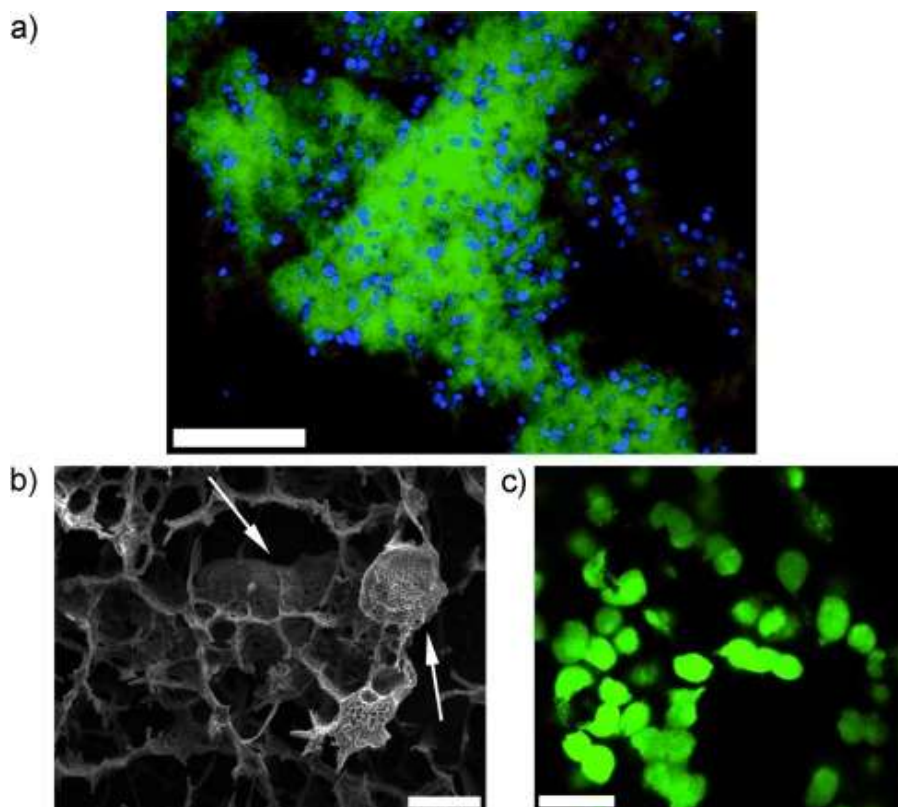


Figure 1.13. HeLa Cells in NHBipy Meshes. a.) Cells stained with DAPI (Blue) and Meshes stained green; b.) CryoSEM of HeLa cells in meshes; c.) Cells stained with calcein AM (Green) to show viability. Adopted from Ref. 140.

The crosslinked design, for metal-mediated CMP self-assembly, was next used to develop more complex extracellular matrix mimics.<sup>141</sup> CMPs containing the integrin  $\alpha 5 \beta 3$  binding sequence, arginine-glycine-aspartate-serine (RGDS), were co-assembled with NHBipy and  $\text{Ni}^{2+}$  ions. The resulting mesh scaffold was able to support the growth of a non-tumor breast epithelial cell line, MCF10A. In vivo, epithelial cells form tissue-like structures in the presence of ECM growth factors. To recapitulate this phenomenon, octahistidine tagged human epidermal growth factor

(hEGF-His<sub>8</sub>) was immobilized onto from the metal-peptide scaffold. This allowed for the slow and controlled release of hEGF-His<sub>8</sub>. The growth factor releasing RGDS-laden mesh was found to promote the organization of MCF10A cells into spheroid structures. This study highlighted an important step towards translating CMP-based meshes into scaffolds for tissue engineering. While macroscopic CMP-derived tissues are still out of reach, these biomaterials are poised as well defined model systems for studying the effect of ECM on complex cellular behaviors.

## 1.10 Conclusions

The field of tissue engineering arose in response to the supply-demand imbalance for organ donations. A common approach in this field is to use scaffolds to direct the growth of cells into tissue and organoid structures. The choice of materials for the construction of scaffolds is paramount for tissue engineering. Various materials classes, like natural proteins, synthetic polymers, biocompatible metals, and ceramics have been used. Impressively, tissues like cartilage, bone, and skin have been achieved and products for each have found their way into clinical practice. These successes validate the approach of scaffold-based tissue engineering. However, important challenges must be solved for continued innovation. To construct larger tissues and whole organs, scaffolds need to either have a blood supply or some other method to promote nutrient distribution. The extracellular matrix plays a key role in promoting the formation of the complex cellular networks that make up the blood supply. As such, understanding the natural ECM can allow us to design biomaterials for complex tissue engineering. Peptide based biomaterials can capture the complexity of the ECM while maintaining simplicity in their synthesis. Peptides mimicking collagen, the major component of the ECM, are especially suited for this purpose. The self-assembly of collagen mimetic peptides (CMPs) is an elegant way to produce biomaterials containing bioactive sequences and secondary structures. Of the known self-assembly processes, metal ion mediated approaches has been successfully used to construct CMP-based materials for use in cell culture. This method is thus an excellent choice for constructing model systems to study complex cellular behavior like the organization of endothelial networks during blood supply formation. Understanding the factors controlling metal ion promoted CMP assembly and testing the bioactivity of the resultant materials will open the door for complex tissue engineering. The age of synthetic organs awaits!

## 1.11 References

- [1] "Organ Donation Statistics." Organ Donor, 10 Apr. 2020, [www.organdonor.gov/statistics-stories/statistics.html#waiting-list](http://www.organdonor.gov/statistics-stories/statistics.html#waiting-list).
- [2] Vacanti, Joseph P., and Robert Langer. "Tissue engineering: the design and fabrication of living replacement devices for surgical reconstruction and transplantation." *The lancet* 354 (1999): S32-S34.
- [3] Badylak, Stephen F., Doris Taylor, and Korkut Uygun. "Whole-organ tissue engineering: decellularization and recellularization of three-dimensional matrix scaffolds." *Annual review of biomedical engineering* 13 (2011): 27-53.
- [4] Lanza, Robert, Robert Langer, Joseph P. Vacanti, eds. *Principles of tissue engineering*. Academic press, 2020.
- [5] Khademhosseini, Ali, and Robert Langer. "A decade of progress in tissue engineering." *Nature protocols* 11.10 (2016): 1775.
- [6] Langer, Robert. "Chemical and Biological Approaches to Regenerative Medicine and Tissue Engineering." *Molecular Frontiers Journal* (2019): 1-7.
- [7] "A Step-by-Step Guide to the MACI Procedure." *The MACI Procedure, Step-by-Step*, [www.maci.com/healthcare-professionals/about-the-procedure/the-maci-procedure.html](http://www.maci.com/healthcare-professionals/about-the-procedure/the-maci-procedure.html).
- [8] RMS Regenerative Medical System, [www.rmsbio.net/html/Stem\\_Cell\\_System/Ossron.asp](http://www.rmsbio.net/html/Stem_Cell_System/Ossron.asp).
- [9] "Vericel Corporation: Advanced Cell Therapies." Vericel Corporation | Advanced Cell Therapies, [www.vcel.com/](http://www.vcel.com/).
- [10] McMurtrey, Richard J. "Analytic models of oxygen and nutrient diffusion, metabolism dynamics, and architecture optimization in three-dimensional tissue constructs with applications and insights in cerebral organoids." *Tissue Engineering Part C: Methods* 22.3 (2016): 221-249.
- [11] Rouwkema, Jeroen, Nicolas C. Rivron, and Clemens A. van Blitterswijk. "Vascularization in tissue engineering." *Trends in biotechnology* 26.8 (2008): 434-441.
- [12] Buranawat, B., P. Kalia, and L. Di Silvio. "Vascularisation of tissue-engineered constructs." *Standardisation in Cell and Tissue Engineering*. Woodhead Publishing, 2013. 77-103a.
- [13] Hussey, George S., Jenna L. Dziki, and Stephen F. Badylak. "Extracellular matrix-based materials for regenerative medicine." *Nature Reviews Materials* 3.7 (2018): 159-173.
- [14] Bosman, Fred T., and Ivan Stamenkovic. "Functional structure and composition of the extracellular matrix." *The Journal of Pathology: A Journal of the Pathological Society of Great Britain and Ireland* 200.4 (2003): 423-428.
- [15] Dai, R., A. Iwama, S. Wang, and Y. L. Kapila. "Disease-associated fibronectin matrix fragments trigger anoikis of human primary ligament cells: p53 and c-myc are suppressed." *Apoptosis* 10.3 (2005): 503-512.
- [16] Rock, Kenneth L., and Hajime Kono. "The inflammatory response to cell death." *Annu. Rev. Pathol. Mech. Dis.* 3 (2008): 99-126.
- [17] Ji, Ye, Gong ping Xu, Zhi peng Zhang, Jing jun Xia, Jing long Yan, and Shang ha Pan. "BMP-2/PLGA delayed-release microspheres composite graft, selection of bone particulate diameters, and prevention of aseptic inflammation for bone tissue engineering." *Annals of biomedical engineering* 38.3 (2010): 632-639.
- [18] Buser, Daniel, H-P. Weber, and Nikolaus P. Lang. "Tissue integration of non-submerged implants. 1-year results of a prospective study with 100 ITI hollow-cylinder and hollow-screw implants." *Clinical oral implants research* 1.1 (1990): 33-40.

- [19] Xie, Jing, Demao Zhang, Chenchen Zhou, Quan Yuan, Ling Ye, and Xuedong Zhou. "Substrate elasticity regulates adipose-derived stromal cell differentiation towards osteogenesis and adipogenesis through  $\beta$ -catenin transduction." *Acta biomaterialia* 79 (2018): 83-95.
- [20] Whelan, Mary C., and Donald R. Senger. "Collagen I initiates endothelial cell morphogenesis by inducing actin polymerization through suppression of cyclic AMP and protein kinase A." *Journal of Biological Chemistry* 278.1 (2003): 327-334.
- [21] Kamei, Makoto, et al. "Endothelial tubes assemble from intracellular vacuoles in vivo." *Nature* 442.7101 (2006): 453-456.
- [22] Shakado, Satoshi, Shotaro Sakisaka, Kazunori Noguchi, Masao Yoshitake, Masaru Harada, Yoshihiro Mimura, Michio Sata, and Kyuichi Tanikawa. "Effects of extracellular matrices on tube formation of cultured rat hepatic sinusoidal endothelial cells." *Hepatology* 22.3 (1995): 969-973.
- [23] Vert, Michel, Yoshiharu Doi, Karl-Heinz Hellwich, Michael Hess, Philip Hodge, Przemyslaw Kubisa, Marguerite Rinaudo, and François Schué. "Terminology for biorelated polymers and applications (IUPAC Recommendations 2012)." *Pure and Applied Chemistry* 84.2 (2012): 377-410.
- [24] Glowacki, Julie, and Shuichi Mizuno. "Collagen scaffolds for tissue engineering." *Biopolymers: Original Research on Biomolecules* 89.5 (2008): 338-344.
- [25] Monteiro, I. P., Shukla, A., Marques, A. P., Reis, R. L., & Hammond, P. T. "Spray-assisted layer-by-layer assembly on hyaluronic acid scaffolds for skin tissue engineering." *Journal of Biomedical Materials Research Part A* 103.1 (2015): 330-340.
- [26] Dong, Chanjuan, and Yonggang Lv. "Application of collagen scaffold in tissue engineering: recent advances and new perspectives." *Polymers* 8.2 (2016): 42.
- [27] Patterson, J., Siew, R., Herring, S. W., Lin, A. S., Guldborg, R., & Stayton, P. S. "Hyaluronic acid hydrogels with controlled degradation properties for oriented bone regeneration." *Biomaterials* 31.26 (2010): 6772-6781.
- [28] Hussein, Kamal Hany, Kyung-Mee Park, Kyung-Sun Kang, and Heung-Myong Woo. "Biocompatibility evaluation of tissue-engineered decellularized scaffolds for biomedical application." *Materials Science and Engineering: C* 67 (2016): 766-778.
- [29] Sun, Yen, Wei-Liang Chen, Sung-Jan Lin, Shiou-Hwa Jee, Yang-Fang Chen, Ling-Chih Lin, Peter TC So, and Chen-Yuan Dong. "Investigating mechanisms of collagen thermal denaturation by high resolution second-harmonic generation imaging." *Biophysical journal* 91.7 (2006): 2620-2625.
- [30] Nong, Lu-Ming, Dong Zhou, Dong Zheng, Yu-Qing Jiang, Nan-Wei Xu, Gong-Yin Zhao, Hui Wei, Si-Yuan Zhou, Hui Han, and Long Han. "The effect of different cross-linking conditions of EDC/NHS on type II collagen scaffolds: an in vitro evaluation." *Cell and tissue banking* 20.4 (2019): 557-568.
- [31] Matuska, Andrea M., and Peter S. McFetridge. "The effect of terminal sterilization on structural and biophysical properties of a decellularized collagen-based scaffold; implications for stem cell adhesion." *Journal of Biomedical Materials Research Part B: Applied Biomaterials* 103.2 (2015): 397-406.
- [32] Cobb WS, Kercher KW, Heniford BT. The argument for lightweight polypropylene mesh in hernia repair. *Surg Innov* 2005;12:63-69.

- [33] Vegas, Arturo J., Omid Veisoh, Joshua C. Doloff, Minglin Ma, Hok Hei Tam, Kaitlin Bratlie, Jie Li, Andrew R Bader, Erin Langan, Karsten Olejnik, Patrick Fenton, Jeon Woong Kang, Jennifer Hollister-Locke, Matthew A Bochenek, Alan Chiu, Sean Siebert, Katherine Tang, Siddharth Jhunjhunwala, Stephanie Aresta-Dasilva, Nimit Dholakia, Raj Thakrar, Thema Vietti, Michael Chen, Josh Cohen, Karolina Siniakowicz, Meirigeng Qi, James McGarrigle, Adam C Graham, Stephen Lyle, David M Harlan, Dale L Greiner, Jose Oberholzer, Gordon C Weir, Robert Langer & Daniel G Anderson. "Combinatorial hydrogel library enables identification of materials that mitigate the foreign body response in primates." *Nature biotechnology* 34.3 (2016): 345.
- [34] Ratner, Buddy D., Allan S. Hoffman, Frederick J. Schoen, and Jack E. Lemons. *Biomaterials science: an introduction to materials in medicine*. Elsevier, 2004.
- [35] Mahoney, Melissa J., and Kristi S. Anseth. "Three-dimensional growth and function of neural tissue in degradable polyethylene glycol hydrogels." *Biomaterials* 27.10 (2006): 2265-2274.
- [36] Soman, Pranav, Jonathan A. Kelber, Jin Woo Lee, Tracy N. Wright, Kenneth S. Vecchio, Richard L. Klemke, and Shaochen Chen. "Cancer cell migration within 3D layer-by-layer microfabricated photocrosslinked PEG scaffolds with tunable stiffness." *Biomaterials* 33.29 (2012): 7064-7070.
- [37] Özbek, Suat, Prakash G. Balasubramanian, Ruth Chiquet-Ehrismann, Richard P. Tucker, and Josephine C. Adams. "The evolution of extracellular matrix." *Molecular biology of the cell* 21.24 (2010): 4300-4305.
- [38] Hubbell, Jeffrey A. "Matrix-bound growth factors in tissue repair." *Swiss medical weekly* 136.2526 (2006).
- [39] Zheng, Wenting, Zhihong Wang, Lijie Song, Qiang Zhao, Jun Zhang, Dong Li, Shufang Wang, Jihong Hana, Xi-Long Zheng, Zhimou Yanga, Deling Kong. "Endothelialization and patency of RGD-functionalized vascular grafts in a rabbit carotid artery model." *Biomaterials* 33.10 (2012): 2880-2891.
- [40] Yang, Fan, Christopher G. Williams, Dong-an Wang, Hyukjin Lee, Paul N. Manson, and Jennifer Elisseeff. "The effect of incorporating RGD adhesive peptide in polyethylene glycol diacrylate hydrogel on osteogenesis of bone marrow stromal cells." *Biomaterials* 26.30 (2005): 5991-5998.
- [41] Saik, Jennifer E., Daniel J. Gould, Emily M. Watkins, Mary E. Dickinson, and Jennifer L. West. "Covalently immobilized platelet-derived growth factor-BB promotes angiogenesis in biomimetic poly (ethylene glycol) hydrogels." *Acta biomaterialia* 7.1 (2011): 133-143
- [42] Maheshwari, Gargi, Gillian Brown, Douglas A. Lauffenburger, Alan Wells, and Linda G. Griffith. "Cell adhesion and motility depend on nanoscale RGD clustering." *J Cell Sci* 113.10 (2000): 1677-1686.
- [43] García, Andrés J. "Get a grip: integrins in cell–biomaterial interactions." *Biomaterials* 26.36 (2005): 7525-7529.
- [44] Karimi, Fatemeh, Andrea J. O'Connor, Greg G. Qiao, and Daniel E. Heath. "Integrin clustering matters: a review of biomaterials functionalized with multivalent integrin-binding ligands to improve cell adhesion, migration, differentiation, angiogenesis, and biomedical device integration." *Advanced healthcare materials* 7.12 (2018): 1701324.
- [45] Bodhak, Subhadip, Susmita Bose, and Amit Bandyopadhyay. "Role of surface charge and wettability on early stage mineralization and bone cell–materials interactions of polarized hydroxyapatite." *Acta Biomaterialia* 5.6 (2009): 2178-2188.

- [46] Hoshiba, Takashi, Chiaki Yoshikawa, and Keita Sakakibara. "Characterization of initial cell adhesion on charged polymer substrates in serum-containing and serum-free media." *Langmuir* 34.13 (2018): 4043-4051.
- [47] Massia, Stephen P., and Jeffrey A. Hubbell. "Immobilized amines and basic amino acids as mimetic heparin-binding domains for cell surface proteoglycan-mediated adhesion." *Journal of Biological Chemistry* 267.14 (1992): 10133-10141.
- [48] Van Wachem, P. B., A. H. Hogt, T. Beugeling, J. Feijen, A. Bantjes, J. P. Detmers, and W. G. Van Aken. "Adhesion of cultured human endothelial cells onto methacrylate polymers with varying surface wettability and charge." *Biomaterials* 8.5 (1987): 323-328.
- [49] Emsley, Jonas, C. Graham Knight, Richard W. Farndale, and Michael J. Barnes. "Structure of the integrin  $\alpha 2\beta 1$ -binding collagen peptide." *Journal of molecular biology* 335.4 (2004): 1019-1028.
- [50] Khurana, Satish, Sarah Schoutedden, Javed K. Manesia, Albert Santamaria-Martínez, Joerg Huelsken, Adam Lacy-Hulbert, and Catherine M. Verfaillie. "Outside-in integrin signalling regulates haematopoietic stem cell function via Periostin-Itgav axis." *Nature communications* 7.1 (2016): 1-14.
- [51] Calderwood, David A., and Mark H. Ginsberg. "Talin forges the links between integrins and actin." *Nature cell biology* 5.8 (2003): 694-696.
- [52] Butler, Boyd, Chunlei Gao, Akos T. Mersich, and Scott D. Blystone. "Purified integrin adhesion complexes exhibit actin-polymerization activity." *Current Biology* 16.3 (2006): 242-251.
- [53] DeMali, Kris A., Krister Wennerberg, and Keith Burridge. "Integrin signaling to the actin cytoskeleton." *Current opinion in cell biology* 15.5 (2003): 572-582.
- [54] Mostafavi-Pour, Zohreh, Janet A. Askari, Scott J. Parkinson, Peter J. Parker, Tony TC Ng, and Martin J. Humphries. "Integrin-specific signaling pathways controlling focal adhesion formation and cell migration." *The Journal of cell biology* 161.1 (2003): 155-167.
- [55] Cavalcanti-Adam, Elisabetta Ada, Tova Volberg, Alexandre Micoulet, Horst Kessler, Benjamin Geiger, and Joachim Pius Spatz. "Cell spreading and focal adhesion dynamics are regulated by spacing of integrin ligands." *Biophysical journal* 92.8 (2007): 2964-2974.
- [56] Reinhart-King, Cynthia A. "Endothelial cell adhesion and migration." *Methods in enzymology* 443 (2008): 45-64.
- [57] Wang, Yu-Li. "Exchange of actin subunits at the leading edge of living fibroblasts: possible role of treadmilling." *The Journal of cell biology* 101.2 (1985): 597-602.
- [58] Theriot, Julie A., and Timothy J. Mitchison. "Actin microfilament dynamics in locomoting cells." *Nature* 352.6331 (1991): 126-131.
- [59] Haeger, Anna, Katarina Wolf, Mirjam M. Zegers, and Peter Friedl. "Collective cell migration: guidance principles and hierarchies." *Trends in cell biology* 25.9 (2015): 556-566.
- [60] Mattila, Pieta K., and Pekka Lappalainen. "Filopodia: molecular architecture and cellular functions." *Nature reviews Molecular cell biology* 9.6 (2008): 446-454.
- [61] Kiosses, William B., Sanford J. Shattil, Nisar Pampori, and Martin Alexander Schwartz. "Rac recruits high-affinity integrin  $\alpha \beta 3$  to lamellipodia in endothelial cell migration." *Nature cell biology* 3.3 (2001): 316-320.
- [62] DeLong, Solitaire A., Andrea S. Gobin, and Jennifer L. West. "Covalent immobilization of RGDS on hydrogel surfaces to direct cell alignment and migration." *Journal of Controlled Release* 109.1-3 (2005): 139-148.

- [63] Kubota, Yasuo, Hynda K. Kleinman, George R. Martin, and Thomas J. Lawley. "Role of laminin and basement membrane in the morphological differentiation of human endothelial cells into capillary-like structures." *The Journal of cell biology* 107.4 (1988): 1589-1598.
- [64] Bauer, Stephen M., Richard J. Bauer, Zhao-Jun Liu, Haiying Chen, Lee Goldstein, and Omaid C. Velazquez. "Vascular endothelial growth factor-C promotes vasculogenesis, angiogenesis, and collagen constriction in three-dimensional collagen gels." *Journal of vascular surgery* 41.4 (2005): 699-707.
- [65] Sweeney, Shawn M., Gloria DiLullo, Simon J. Slater, José Martinez, Renato V. Iozzo, Janelle L. Lauer-Fields, Gregg B. Fields, and James D. San Antonio. "Angiogenesis in collagen I requires  $\alpha 2\beta 1$  ligation of a GFP\* GER sequence and possibly p38 MAPK activation and focal adhesion disassembly." *Journal of Biological Chemistry* 278.33 (2003): 30516-30524.
- [66] Senger, Donald R., Kevin P. Claffey, Julie E. Benes, Carole A. Perruzzi, Ageliki P. Sergiou, and Michael Detmar. "Angiogenesis promoted by vascular endothelial growth factor: regulation through  $\alpha 1\beta 1$  and  $\alpha 2\beta 1$  integrins." *Proceedings of the National Academy of Sciences* 94.25 (1997): 13612-13617.
- [67] Senger, Donald R., Carole A. Perruzzi, Michael Streit, Victor E. Kotliansky, Antonin R. de Fougères, and Michael Detmar. "The  $\alpha 1\beta 1$  and  $\alpha 2\beta 1$  integrins provide critical support for vascular endothelial growth factor signaling, endothelial cell migration, and tumor angiogenesis." *The American journal of pathology* 160.1 (2002): 195-204.
- [68] Turner, Kevin R., Christopher Adams, Stephanie Staelens, Hans Deckmyn, and James San Antonio. "Crucial Role for Endothelial Cell  $\alpha 2\beta 1$  Integrin Receptor Clustering in Collagen-Induced Angiogenesis." *Crucial Role for Endothelial Cell  $\alpha 2\beta 1$  Integrin Receptor Clustering in Collagen-Induced Angiogenesis.* *The Anatomical Record* (2019).
- [69] Ware, Margaret F., Alan Wells, and Douglas A. Lauffenburger. "Epidermal growth factor alters fibroblast migration speed and directional persistence reciprocally and in a matrix-dependent manner." *Journal of Cell Science* 111.16 (1998): 2423-2432.
- [70] García, José R., Amy Y. Clark, and Andrés J. García. "Integrin-specific hydrogels functionalized with VEGF for vascularization and bone regeneration of critical-size bone defects." *Journal of biomedical materials research Part A* 104.4 (2016): 889-900.
- [71] Yao, Li, Francis Phan, and Yongchao Li. "Collagen microsphere serving as a cell carrier supports oligodendrocyte progenitor cell growth and differentiation for neurite myelination in vitro." *Stem cell research & therapy* 4.5 (2013): 109.
- [72] Matsunaga, Yukiko T., Yuya Morimoto, and Shoji Takeuchi. "Molding cell beads for rapid construction of macroscopic 3D tissue architecture." *Advanced materials* 23.12 (2011): H90-H94.
- [73] Frantz, Christian, Kathleen M. Stewart, and Valerie M. Weaver. "The extracellular matrix at a glance." *Journal of cell science* 123.24 (2010): 4195-4200.
- [74] Shoulders, Matthew D., and Ronald T. Raines. "Collagen structure and stability." *Annual review of biochemistry* 78 (2009): 929-958.
- [75] Silvipriya, K. S., K. Krishna Kumar, A. R. Bhat, B. Dinesh Kumar, Anish John, and P. Lakshmanan. "Collagen: Animal sources and biomedical application." *J. Appl. Pharm. Sci* 5.3 (2015): 123-127.
- [76] Peterson, Alexander. "Protocol for Preparing Fibrillar Collagen Matrices on Untreated Polystyrene Labware (Petri)\*: A Potential Reference Extracellular Matrix With Robust and Reproducible Cell Responses." (2012).

- [77] O'Brien, Fergal J., Brendan A. Harley, Ioannis V. Yannas, and Lorna Gibson. Influence of freezing rate on pore structure in freeze-dried collagen-GAG scaffolds." *Biomaterials* 25.6 (2004): 1077-1086.
- [78] Naik, Nisarga, Jeffrey Caves, Elliot L. Chaikof, and Mark G. Allen. "Generation of spatially aligned collagen fiber networks through microtransfer molding." *Advanced healthcare materials* 3.3 (2014): 367-374.
- [79] Pietrucha, Krystyna. "Changes in denaturation and rheological properties of collagen–hyaluronic acid scaffolds as a result of temperature dependencies." *International journal of biological macromolecules* 36.5 (2005): 299-304.
- [80] a.) Leikina, E., M. V. Merts, N. Kuznetsova, and S. Leikin. "Type I collagen is thermally unstable at body temperature." *Proceedings of the National Academy of Sciences* 99.3 (2002): 1314-1318.; b.) Persikov, Anton V., and Barbara Brodsky. "Unstable molecules form stable tissues." *Proceedings of the National Academy of Sciences* 99.3 (2002): 1101-1103.
- [81] Uzel, Mehmet I., Sarah D. Shih, Howard Gross, Efrat Kessler, Louis C. Gerstenfeld, and Philip C. Trackman. "Molecular events that contribute to lysyl oxidase enzyme activity and insoluble collagen accumulation in osteosarcoma cell clones." *Journal of Bone and Mineral Research* 15.6 (2000): 1189-1197.
- [82] Siegel, ROBERT C. "Collagen cross-linking. Synthesis of collagen cross-links in vitro with highly purified lysyl oxidase." *Journal of Biological Chemistry* 251.18 (1976): 5786-5792.
- [83] Bax, Daniel V., Natalia Davidenko, Donald Gullberg, Samir W. Hamaia, Richard W. Farndale, Serena M. Best, and Ruth E. Cameron. "Fundamental insight into the effect of carbodiimide crosslinking on cellular recognition of collagen-based scaffolds." *Acta biomaterialia* 49 (2017): 218-234.
- [84] Lee, Andy Chi-Lung, Janelle Louise Harris, Kum Kum Khanna, and Ji-Hong Hong. "A comprehensive review on current advances in peptide drug development and design." *International journal of molecular sciences* 20.10 (2019): 2383.
- [85] Mammadov, Busra, Rashad Mammadov, Mustafa O. Guler, and Ayse B. Tekinay. "Cooperative effect of heparan sulfate and laminin mimetic peptide nanofibers on the promotion of neurite outgrowth." *Acta biomaterialia* 8.6 (2012): 2077-2086.
- [86] Chen, Shixuan, Min Zhang, Xuebing Shao, Xueer Wang, Lei Zhang, Pengcheng Xu, Wen Zhong, Lu Zhang, Malcolm Xing, and Lin Zhang. "A laminin mimetic peptide SIKVAV-conjugated chitosan hydrogel promoting wound healing by enhancing angiogenesis, re-epithelialization and collagen deposition." *Journal of Materials Chemistry B* 3.33 (2015): 6798-6804.
- [87] Mardilovich, Anastasia, Jennifer A. Craig, Matthew Q. McCammon, Ashish Garg, and Efrosini Kokkoli. "Design of a novel fibronectin-mimetic peptide– amphiphile for functionalized biomaterials." *Langmuir* 22.7 (2006): 3259-3264.
- [88] Strauss, Kevin, and Jean Chmielewski. "Advances in the design and higher-order assembly of collagen mimetic peptides for regenerative medicine." *Current opinion in biotechnology* 46 (2017): 34-41.
- [89] Berisio, Rita, Luigi Vitagliano, Lelio Mazzarella, and Adriana Zagari. "Crystal structure of the collagen triple helix model [(Pro-Pro-Gly) 10] 3." *Protein Science* 11.2 (2002): 262-270.

- [90] Kwak, Juliann, Elizabeth A. Jefferson, Megha Bhumralkar, and Murray Goodman. "Triple Helical Stabilities of Guest–Host Collagen Mimetic Structures." *Bioorganic & medicinal chemistry* 7.1 (1999): 153-160.
- [91] Buevich, Alexei, and Jean Baum. "Nuclear magnetic resonance characterization of peptide models of collagen–folding diseases." *Philosophical Transactions of the Royal Society of London. Series B: Biological Sciences* 356.1406 (2001): 159-168.
- [92] Prockop, Darwin J., and Andrzej Fertala. "The collagen fibril: the almost crystalline structure." *Journal of structural biology* 122.1-2 (1998): 111-118.
- [93] Fung, B. M., John Witschel Jr, and Lavon L. McAmis. "The state of water on hydrated collagen as studied by pulsed NMR." *Biopolymers: Original Research on Biomolecules* 13.9 (1974): 1767-1776.
- [94] Drzewiecki, Kathryn E., Daniel R. Grisham, Avانش S. Parmar, Vikas Nanda, and David I. Shreiber. "Circular dichroism spectroscopy of collagen fibrillogenesis: a new use for an old technique." *Biophysical journal* 111.11 (2016): 2377-2386.
- [95] Bodian, Dale L., Balaraman Madhan, Barbara Brodsky, and Teri E. Klein. "Predicting the clinical lethality of osteogenesis imperfecta from collagen glycine mutations." *Biochemistry* 47.19 (2008): 5424-5432.
- [96] Bhate, Manjiri, Xin Wang, Jean Baum, and Barbara Brodsky. "Folding and conformational consequences of glycine to alanine replacements at different positions in a collagen model peptide." *Biochemistry* 41.20 (2002): 6539-6547.
- [97] Germain, Dominique P. "Ehlers-Danlos syndrome type IV." *Orphanet Journal of Rare Diseases* 2.1 (2007): 32.
- [98] Vahedi, Katayoun, and Sonia Alamowitch. "Clinical spectrum of type IV collagen (COL4A1) mutations: a novel genetic multisystem disease." *Current opinion in neurology* 24.1 (2011): 63-68.
- [99] Holmgren, Steven K., Kimberly M. Taylor, Lynn E. Bretscher, and Ronald T. Raines. "Code for collagen's stability deciphered." *Nature* 392.6677 (1998): 666-667.
- [100] Bella, Jordi, Barbara Brodsky, and Helen M. Berman. "Hydration structure of a collagen peptide." *Structure* 3.9 (1995): 893-906.
- [101] Kotch, Frank W., and Ronald T. Raines. "Self-assembly of synthetic collagen triple helices." *Proceedings of the National Academy of Sciences* 103.9 (2006): 3028-3033.
- [102] Engel, Jürgen, and Hans Peter Bächinger. "Structure, stability and folding of the collagen triple helix." *Collagen*. Springer, Berlin, Heidelberg, 2005. 7-33.
- [103] Hodges, Jonathan A., and Ronald T. Raines. "Stereo-electronic effects on collagen stability: the dichotomy of 4-fluoroproline diastereomers." *Journal of the American Chemical Society* 125.31 (2003): 9262-9263.
- [104] Pandey, Anil K., Devan Naduthambi, Krista M. Thomas, and Neal J. Zondlo. "Proline editing: a general and practical approach to the synthesis of functionally and structurally diverse peptides. Analysis of steric versus stereo-electronic effects of 4-substituted prolines on conformation within peptides." *Journal of the American Chemical Society* 135.11 (2013): 4333-4363.
- [105] Kotch, Frank W., Ilia A. Guzei, and Ronald T. Raines. "Stabilization of the collagen triple helix by O-methylation of hydroxyproline residues." *Journal of the American Chemical Society* 130.10 (2008): 2952-2953.

- [106] Jenkins, Cara L., Alexander I. McCloskey, Ilia A. Guzei, Eric S. Eberhardt, and Ronald T. Raines. "O-acylation of hydroxyproline residues: Effect on peptide-bond isomerization and collagen stability." *Peptide Science: Original Research on Biomolecules* 80.1 (2005): 1-8.
- [107] Shoulders, Matthew D., Kimberli J. Kamer, and Ronald T. Raines. "Origin of the stability conferred upon collagen by fluorination." *Bioorganic & medicinal chemistry letters* 19.14 (2009): 3859-3862.
- [108] Zhang, Yitao, Roy M. Malamakal, and David M. Chenoweth. "Aza-glycine induces collagen hyperstability." *Journal of the American Chemical Society* 137.39 (2015): 12422-12425.
- [109] Kasznel, Alexander J., Yitao Zhang, Yang Hai, and David M. Chenoweth. "Structural basis for aza-glycine stabilization of collagen." *Journal of the American Chemical Society* 139.28 (2017): 9427-9430.
- [110] Egli, Jasmine, Christiane Siebler, Martin Köhler, Renato Zenobi, and Helma Wennemers. "Hydrophobic Moieties Bestow Fast-Folding and Hyperstability on Collagen Triple Helices." *Journal of the American Chemical Society* 141.14 (2019): 5607-5611.
- [111] Whitesides, George M., and Bartosz Grzybowski. "Self-assembly at all scales." *Science* 295.5564 (2002): 2418-2421.
- [112] Rele, Shyam, Yuhua Song, Robert P. Apkarian, Zheng Qu, Vincent P. Conticello, and Elliot L. Chaikof. "D-periodic collagen-mimetic microfibers." *Journal of the American Chemical Society* 129.47 (2007): 14780-14787.
- [113] Jiang, Tao, Chunfu Xu, Xiaobing Zuo, and Vincent P. Conticello. "Structurally homogeneous nanosheets from self-assembly of a collagen-mimetic peptide." *Angewandte Chemie International Edition* 53.32 (2014): 8367-8371.
- [114] Jiang, Tao, Owen A. Vail, Zhigang Jiang, Xiaobing Zuo, and Vincent P. Conticello. "Rational design of multilayer collagen nanosheets with compositional and structural control." *Journal of the American Chemical Society* 137.24 (2015): 7793-7802.
- [115] Merg, Andrea D., Eric van Genderen, Alisina Bazrafshan, Hanquan Su, Xiaobing Zuo, Gavin Touponse, Thorsten B. Blum, Khalid Salaita, Jan Pieter Abrahams, and Vincent P. Conticello. "Seeded Heteroepitaxial Growth of Crystallizable Collagen Triple Helices: Engineering Multifunctional Two-Dimensional Core-Shell Nanostructures." *Journal of the American Chemical Society* 141.51 (2019): 20107.
- [116] Jalan, Abhishek A., Katherine A. Jochim, and Jeffrey D. Hartgerink. "Rational design of a non-canonical "sticky-ended" collagen triple helix." *Journal of the American Chemical Society* 136.21 (2014): 7535-7538.
- [117] Sarkar, Biplab, Lesley ER O'Leary, and Jeffrey D. Hartgerink. "Self-assembly of fiber-forming collagen mimetic peptides controlled by triple-helical nucleation." *Journal of the American Chemical Society* 136.41 (2014): 14417-14424.
- [118] Jalan, Abhishek A., Katherine A. Jochim, and Jeffrey D. Hartgerink. "Rational design of a non-canonical "sticky-ended" collagen triple helix." *Journal of the American Chemical Society* 136.21 (2014): 7535-7538.
- [119] O'leary, Lesley ER, Jorge A. Fallas, Erica L. Bakota, Marci K. Kang, and Jeffrey D. Hartgerink. "Multi-hierarchical self-assembly of a collagen mimetic peptide from triple helix to nanofibre and hydrogel." *Nature chemistry* 3.10 (2011): 821.
- [120] Kumar, Vivek A., Nichole L. Taylor, Abhishek A. Jalan, Lyahn K. Hwang, Benjamin K. Wang, and Jeffrey D. Hartgerink. "A nanostructured synthetic collagen mimic for hemostasis." *Biomacromolecules* 15.4 (2014): 1484-1490.

- [121] Luo, Jingnan, and Yen Wah Tong. "Self-assembly of collagen-mimetic peptide amphiphiles into biofunctional nanofiber." *Acs Nano* 5.10 (2011): 7739-7747.
- [122] Gore, Tushar, Yoav Dori, Yeshayahu Talmon, Matthew Tirrell, and Havazelet Bianco-Peled. "Self-assembly of model collagen peptide amphiphiles." *Langmuir* 17.17 (2001): 5352-5360.
- [123] Cejas, Mabel A., William A. Kinney, Cailin Chen, Jeremy G. Vinter, Harold R. Almond, Karin M. Balss, Cynthia A. Maryanoff, Ute Schmidt, Michael Breslav, Andrew Mahan, Eilyn Lacy, and Bruce E. Maryanoff. "Thrombogenic collagen-mimetic peptides: Self-assembly of triple helix-based fibrils driven by hydrophobic interactions." *Proceedings of the National Academy of Sciences* 105.25 (2008): 8513-8518.
- [124] Kar, Karunakar, Sajjad Ibrar, Vikas Nanda, Todd M. Getz, Satya P. Kunapuli, and Barbara Brodsky. "Aromatic interactions promote self-association of collagen triple-helical peptides to higher-order structures." *Biochemistry* 48.33 (2009): 7959-7968.
- [125] Xu, Fei, I. John Khan, Kenneth McGuinness, Avanish S. Parmar, Teresita Silva, N. Sanjeeva Murthy, and Vikas Nanda. "Self-assembly of left- and right-handed molecular screws." *Journal of the American Chemical Society* 135.50 (2013): 18762-18765.
- [126] McGuinness, Kenneth, I. John Khan, and Vikas Nanda. "Morphological diversity and polymorphism of self-assembling collagen peptides controlled by length of hydrophobic domains." *ACS nano* 8.12 (2014): 12514-12523.
- [127] Przybyla, David E., Charles M. Rubert Pérez, Jeremy Gleaton, Vikas Nandwana, and Jean Chmielewski. "Hierarchical assembly of collagen peptide triple helices into curved disks and metal ion-promoted hollow spheres." *Journal of the American Chemical Society* 135.9 (2013): 3418-3422.
- [128] Motekaitis, Ramunas J., and Arthur E. Martell. "The iron (III) and iron (II) complexes of nitrilotriacetic acid." *Journal of Coordination Chemistry* 31.1 (1994): 67-78.
- [129] Wart, Harold Evan. "[10] Introduction of exchange-inert metal ions into enzymes." *Methods in enzymology*. Vol. 158. Academic Press, 1988. 95-110.
- [130] Wegner, Seraphine V., and Joachim P. Spatz. "Cobalt (III) as a Stable and Inert Mediator Ion between NTA and His6-Tagged Proteins." *Angewandte Chemie International Edition* 52.29 (2013): 7593-7596.
- [131] Przybyla, David E., and Jean Chmielewski. "Metal-triggered radial self-assembly of collagen peptide fibers." *Journal of the American Chemical Society* 130.38 (2008): 12610-12611.
- [132] Przybyla, David E., and Jean Chmielewski. "Metal-triggered collagen peptide disk formation." *Journal of the American Chemical Society* 132.23 (2010): 7866-7867.
- [133] Gleaton, Jeremy, and Jean Chmielewski. "Thermally controlled collagen peptide cages for biopolymer delivery." *ACS Biomaterials Science & Engineering* 1.10 (2015): 1002-1008.
- [134] Pires, Marcos M., and Jean Chmielewski. "Self-assembly of collagen peptides into microflorettes via metal coordination." *Journal of the American Chemical Society* 131.7 (2009): 2706-2712.
- [135] Pires, Marcos M., Dawn Ernenwein, and Jean Chmielewski. "Selective decoration and release of His-tagged proteins from metal-assembled collagen peptide microflorettes." *Biomacromolecules* 12.7 (2011): 2429-2433.
- [136] Pires, Marcos M., Jeeyeon Lee, Dawn Ernenwein, and Jean Chmielewski. "Controlling the morphology of metal-promoted higher ordered assemblies of collagen peptides with varied core lengths." *Langmuir* 28.4 (2012): 1993-1997.

- [137] Kotha, Raghavendhar R., and Jean Chmielewski. "Controlling the morphology of metal-triggered collagen peptide assemblies through ligand alteration." *Peptide Science* 104.4 (2015): 379-383.
- [138] Pires, Marcos M., David E. Przybyla, Charles M. Rubert Pérez, and Jean Chmielewski. "Metal-mediated tandem coassembly of collagen peptides into banded microstructures." *Journal of the American Chemical Society* 133.37 (2011): 14469-14471.
- [139] Strauss, Kevin, and Jean Chmielewski. "Metal-Promoted Assembly of Two Collagen Mimetic Peptides into a Biofunctional "Spiraled Horn" Scaffold." *Materials* 9.10 (2016): 838.
- [140] Pires, Marcos M., David E. Przybyla, and Jean Chmielewski. "A metal–collagen peptide framework for three-dimensional cell culture." *Angewandte Chemie International Edition* 48.42 (2009): 7813-7817.
- [141] Hernandez-Gordillo, Victor, and Jean Chmielewski. "Mimicking the extracellular matrix with functionalized, metal-assembled collagen peptide scaffolds." *Biomaterials* 35.26 (2014): 7363-7373.

## CHAPTER 2. THE SELF ASSEMBLY OF A CELL ADHESIVE COLLAGEN MIMETIC PEPTIDE

### 2.1 Introduction

Endothelial cells form the inner wall of blood vessels and capillaries.<sup>1</sup> They form a single cell thick barrier, called the endothelium, to prevent the spillage of blood and direct its flow through a vessel. Around the endothelium, a layer of extracellular matrix proteins, called the basement membrane, acts a support to give the structure a tubular shape. When a wound or other environmental cue disrupts the basement membrane, cells migrate out of the endothelium and into the newly created opening. Exposed to a higher amount of extracellular matrix proteins, these migrating endothelial cells activate the process of angiogenesis, the sprouting of new blood vessels.<sup>2</sup>

In vitro, aspects of angiogenesis can be captured in an assay called endothelial cell network/tube formation.<sup>3</sup> Here, endothelial cells are plated on a gel of basement membrane extract, most commonly matrigel or geltrex, and exposed to angiogenic cues, like vascular endothelial growth factor (VEGF). In response, the cells begin to elongate, form connections with each other, migrate along the gel surface, and adhere to the surface as needed. The result is a network of tube- or capillary-like structures which bear a resemblance to blood capillaries in vivo. Understanding the workings of this morphogenetic phenomenon can allow development of biomaterials in the field of tissue engineering. Tissue engineers seek methods for vascularization in tissue constructs to allow efficient nutrient diffusion and prevent cell death in thicker tissues.<sup>4</sup> In vivo, this is accomplished by the network of blood vessels, which carry nutrients to all tissues and organs. As such, promoting angiogenesis in synthetic tissue constructs may open the door for organ engineering.

Collagen I, the most abundant component of the basement membrane, can be formed into fibrous gels in vitro that support endothelial cell network formation through the action of VEGF and other growth factors.<sup>5</sup> Senger and co-workers found that these growth factors upregulate the expression of the collagen binding protein, integrin  $\alpha 2\beta 1$ .<sup>6,7</sup> Further experiments revealed that antibodies binding integrin  $\alpha 2\beta 1$  prevented the process of endothelial network formation.<sup>8</sup> Similarly, Fields and coworkers showed that peptides containing the sequence GFOGER, the collagenous binding

site for integrin  $\alpha 2\beta 1$ , prevented the process as well.<sup>9</sup> These studies showed that binding between the collagen gel and integrin  $\alpha 2\beta 1$  was important to promote tube formation. Since other integrin binding molecules, like antibodies and peptides, did not promote the morphogenetic process, it was hypothesized that the collagen-integrin interaction was not a scenario of simple complex formation. Instead, the process was thought to require both binding and clustering of integrin  $\alpha 2\beta 1$  on cell surfaces.<sup>10</sup> As such, collagen fibers were hypothesized to be a polyvalent ligand, containing many copies of the GFOGER sequence, to promote receptor clustering of integrin  $\alpha 2\beta 1$ . In support of this hypothesis, Whelan and Senger showed that a system of two antibodies, designed to cluster integrin  $\alpha 2\beta 1$  on cell surfaces, could trigger actin stress fiber formation, a hallmark of elongating endothelial cells.<sup>8</sup> Furthermore, Turner et al achieved endothelial network formation through the usage of polyvalent antibody presenting particles.<sup>10</sup> While each of these studies offer strong validation for the receptor clustering hypothesis, a direct demonstration of network induction by polyvalent presentation of GFOGER peptide, as would be the case with natural collagen fibers, is lacking. As an extension of exploring this avenue, biomaterials presenting polyvalent GFOGER may become the material of choice for vascularized tissue engineering.

Metal-ion promoted linear self-assembly of collagen mimetic peptides (CMPs) results in materials displaying regular polyvalent patterns.<sup>11,12,13</sup> Triple CMPs, equipped with metal binding ligands at their termini, self-associate due to a metal ion trigger. Potentially, this process, if performed with a CMP incorporating the GFOGER sequence, can produce the desired biomaterials for integrin clustering and endothelial network formation. First shown with the peptide, NCoH, this self-assembly process was used to produce microflorettes, ruffled particles which could be used to encapsulate and release proteins with spatiotemporal control.<sup>11,12</sup> Later, the co-assembly of the linearly designed peptides, HisCol and IdaCol, with metal ions resulted in petal-like materials displaying a banding pattern.<sup>13</sup> When stained with uranyl acetate for transmission electron microscopy, these particles showed thin negatively stained sections occurring every 9-10 nm. This length correlated well with that of a collagen-like triple helix formed from the peptides used. As such, the particles could truly be described as displaying the HisCol and IdaCol sequences in a polyvalent manner. Inspired by this previous result, we explored the metal-ion mediated linear assembly of a GFOGER containing CMP, NCoH-FOGER. In this chapter, we present the synthesis

of NCoH-FOGER, and its characterization, self-assembly, and evaluation for endothelial network formation.

## 2.2 NCoH-FOGER

The core of the NCoH-FOGER peptide is made up of the cell-adhesive GFOGER sequence, flanked by repeat POG sections for promoting triple helix formation (Fig. 2.1). At the C- and N-termini, respectively, NCoH-FOGER was constructed with dihistidine and nitrilotriacetic acid (NTA) motifs. These would enable metal-dependent self-assembly in a linear head-to-tail manner. Based on this, we hypothesized that the resulting assembled materials would exhibit a regular polyvalent pattern of cell adhesive ligands to promote integrin clustering.

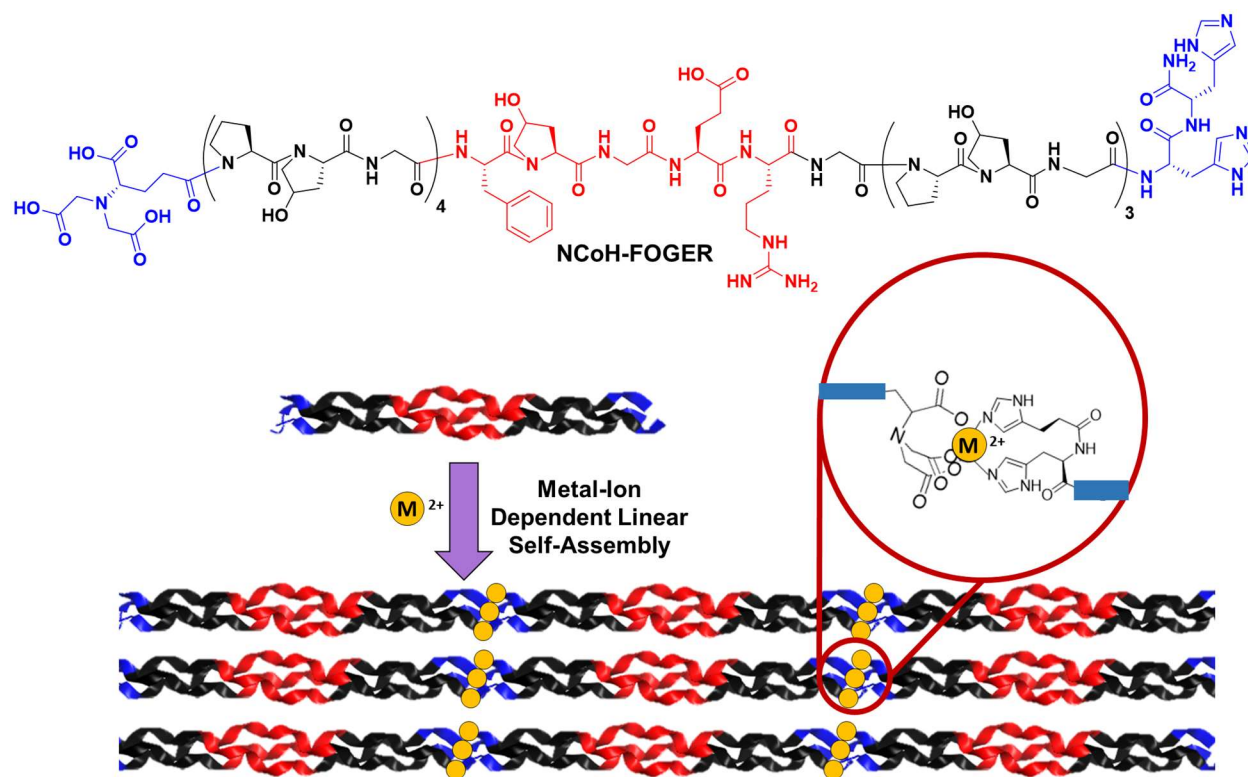


Figure 2.1. The design of NCoH-FOGER; yellow circles are metal ions.

## 2.3 Results and Discussion

### 2.3.1 Synthesis of Protected Nitrilotriacetate 3

A protected nitrilotriacetate, **3**, was synthesized for use in solid phase peptide synthesis. The two-step known procedure begins with amine alkylations with the commercially protected glutamate derivative, **1** (Fig. 2.2).<sup>14</sup> Tert-butyl bromoacetate was added dropwise to a solution of **1** in acetonitrile. The stirring reaction was then heated to 70 °C and left for 19h. Work-up and purification yielded the intermediate **2** in moderate yields. Hydrogenolysis in ethanol (EtOH) was then used to remove the benzyl protecting group to produce **3** in good yield.

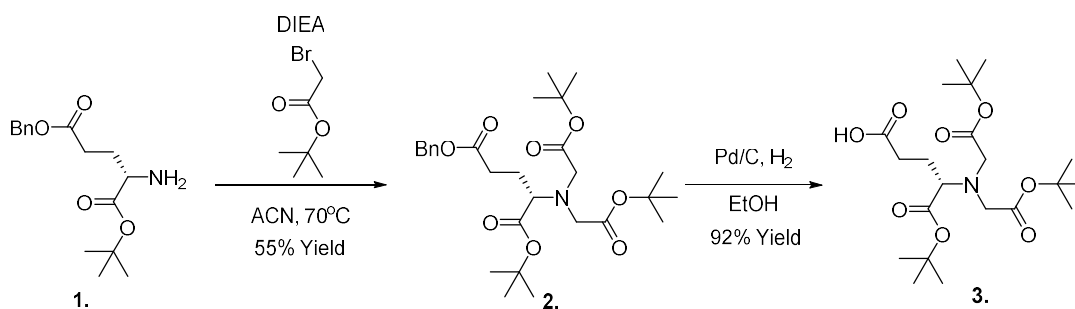


Figure 2.2. Synthesis of protected nitrilotriacetate 3

### 2.3.2 Synthesis of NCoH-FOGER

Fmoc-based solid phase peptide synthesis (SPPS) methods were used to prepare NCoH-FOGER.<sup>15</sup> Rink Amide Chem-matrix resin, made of primarily polyethylene glycol, was used due to its higher swelling capacity, a factor known to increase yield in SPPS.<sup>16</sup> The coupling reagents 1-[bis(dimethylamino)methylene]-1H-1,2,3-triazolo[4,5-b]pyridinium-3-oxide hexafluorophosphate (HATU), and 1-hydroxy-7-azabenzotriazole (HOAt) were used in the synthesis, with 2 hour couplings. Either the Kaiser-Ninhydrin test, for primary amino acid, or the chloranil method, for proline residues, was used to validate complete coupling.<sup>17,18</sup> Fmoc-protecting groups were removed with 25% piperidine in DMF for 30 minutes. After completion of the sequence, the washed resin was treated with a cocktail of 95% trifluoroacetic acid (TFA), 2.5% water, and 2.5% tri-isopropylsilane (TIPS) to release the peptide from the resin with concomitant protecting group removal. Reverse phase high performance liquid chromatography (RP-HPLC) was used to purify the peptide to homogeneity. Matrix assisted laser

desorption/ionization mass spectrometry (MALDI MS) was used to confirm the peptide structure. Analytical RP-HPLC showed that the purified NCoH-FOGER had greater than 98% purity.

### **2.3.3 Confirmation of the Triple Helicity of NCoH-FOGER**

The circular dichroism spectrum of NCoH-FOGER was determined in 3-N-morpholinopropane sulfonic acid (MOPS) buffer at pH 7.4. A strong positive ellipticity was observed at 225 nm, indicating a polyproline type II helix (Fig. 2.3).<sup>19</sup> A collagen-like triple helix consists of a trimer of polyproline type II helices. This type of a structure is known to display cooperative unfolding.<sup>19</sup> We monitored the ellipticity at 225 nm as a function of temperature. The resulting curve showed sigmoidal character, indicating cooperativity, with a transition melting temperature ( $T_m$ ) at 30 °C (Fig. 2.4). Similar studies were performed with peptide dissolved in buffered aqueous methanol. The triple helix is known to be highly stable in aqueous methanol.<sup>20</sup> This may be due to the lower competition from the solvent for the hydrogen bonds that hold the structure together.<sup>21</sup> The CD spectrum in aqueous methanol was nearly identical to that in aqueous solution (Fig. 2.3). Temperature dependent CD spectroscopy showed a cooperative transition with a  $T_m$  value of 52 °C in aqueous methanol, indicating significant stabilization of the folded structure in methanol (Fig. 2.4). These CD spectral characteristics and the thermal stabilization of NCoH-FOGER in aqueous methanol are consistent with a triple helical structure, although in aqueous buffer, the triple helix seems weakly stable.

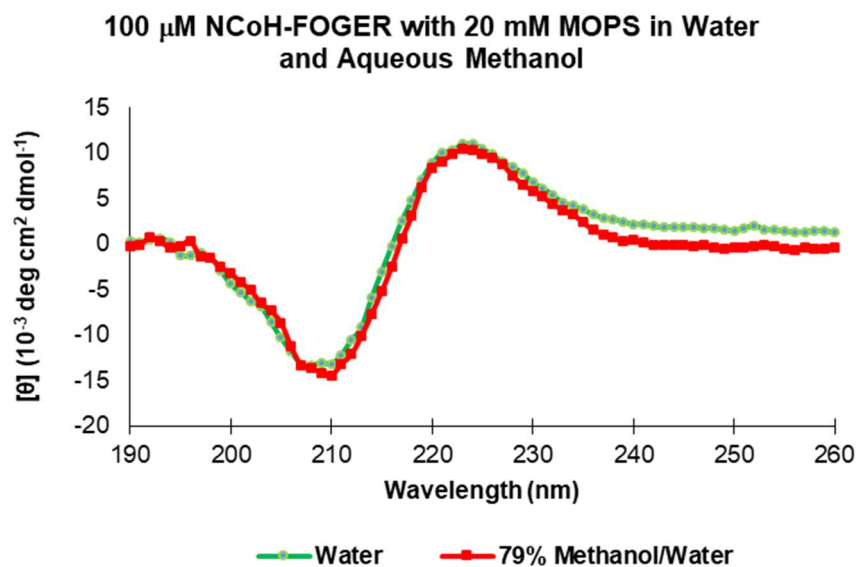


Figure 2.3. Circular dichroism of NCoH-FOGER in water and aqueous methanol

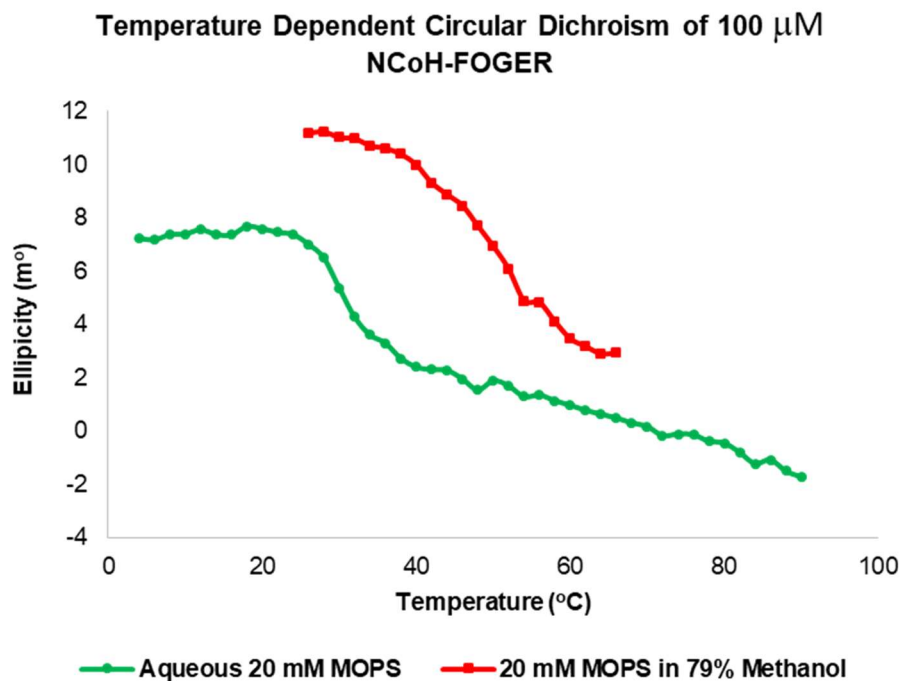


Figure 2.4. Temperature dependent circular dichroism of NCoH-FOGER in water and aqueous methanol

We next interrogated the tentative triple helical structure by a combination of analytical ultracentrifugation (AUC) and native ion-mobility spectrometry (IMS) to measure the oligomerization states of NCoH-FOGER in 20 mM MOPS and 20 mM ammonium acetate,

respectively. AUC, a technique previously used for other triple helices, revealed solution state species with masses of 9.15 and 6 kDa (Fig. 2.5).<sup>20</sup> These corresponded to the expected trimer and a dimer with a ratio of about 2 to 1 in MOPS buffer. At lower concentrations of peptide, however, only larger masses (>10 kDa) were observed and given that these could not be assigned, optical artefacts in the AUC data were suspected.<sup>22</sup> Native IMS, previously used by the groups of Wennemers and Pouilly to study triple helices, was therefore also employed and confirmed the presence of dimer and trimer across a range of concentrations (Fig. 2.6 and Fig. 2.7).<sup>23,24</sup> Relative abundance calculations agreed with the 2 to 1 ratio of trimer to dimer (Fig. 2.8). Put together, CD, AUC, and IMS suggest that NCoH-FOGER is capable of forming a triple helical structure, but, also to lesser extent, a dimeric species. Dimeric species have been detected previously by real-time NMR investigations of collagen peptide folding.<sup>25</sup> Templated collagen peptide double helices have been shown to be stable if the non-templated peptides are capable of forming a triple helix.<sup>26</sup> Perhaps, NCoH-FOGER, while predominantly triple helical, is capable of forming a double helix.

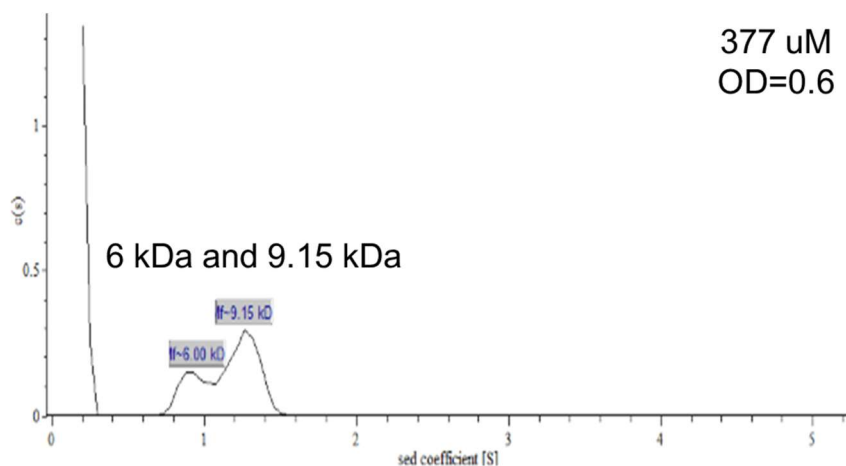


Figure 2.5. Analytical ultracentrifugation of NCoH-FOGER shows a dimer and trimer

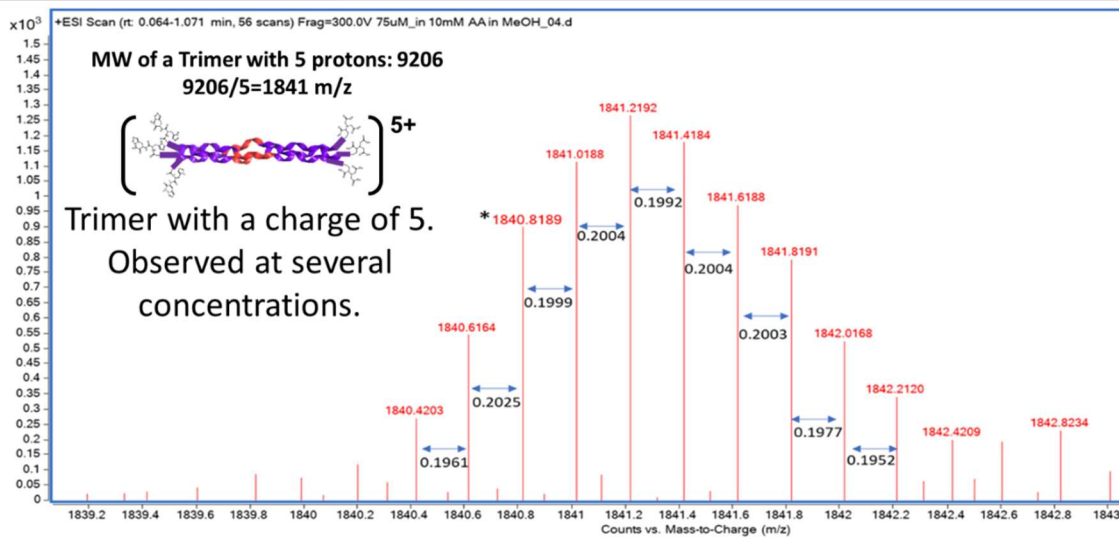


Figure 2.6. Ion mobility mass spectroscopy shows a trimer with a charge of 5

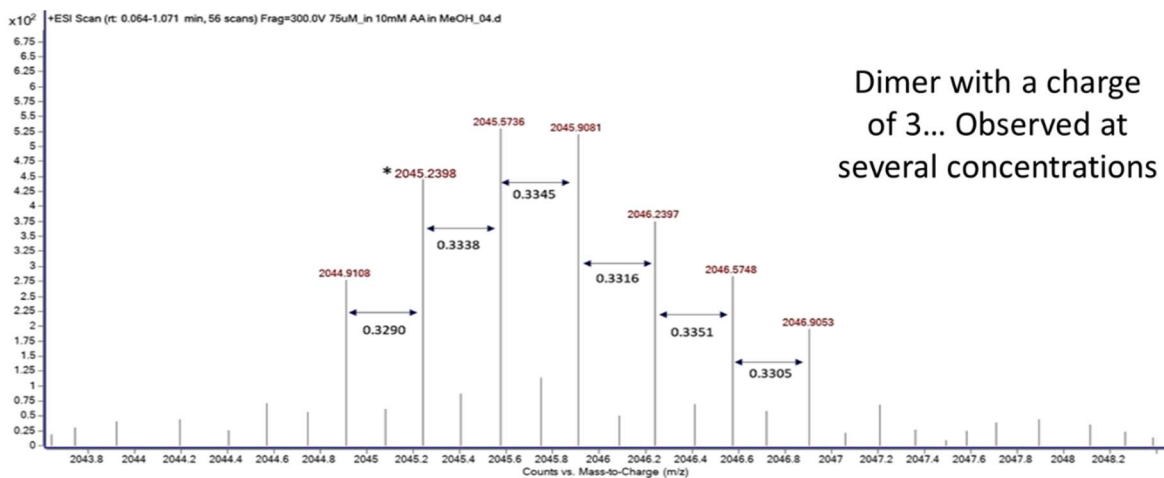


Figure 2.7. Ion mobility mass spectroscopy shows a dimer with a charge of 3

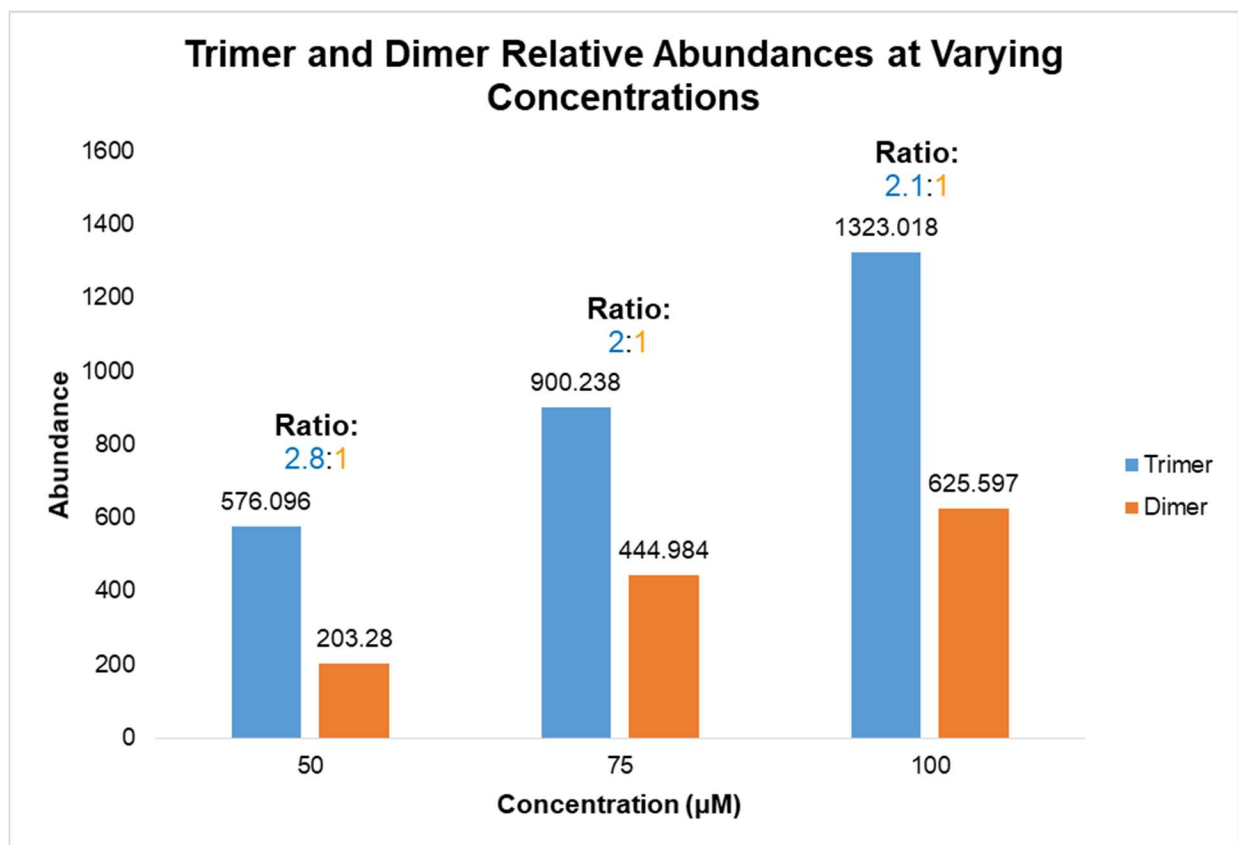


Figure 2.8. Relative abundances of dimer and trimer peaks by ion-mobility spectrometry.

### 2.3.4 Metal Mediated Self Assembly of NCoH-FOGER

To determine if NCoH-FOGER was capable of metal ion dependent self-assembly, the process was monitored with absorbance and dynamic light scattering.

Transition metal salt solutions were added to MOPS buffered solutions of NCoH-FOGER. Upon addition of Zn(II), Cu(II), or Co(II) ions, turbidity was observed within 1 min (Fig. 2.9). This behavior was not observed with the addition Ni(II) ions. To further confirm that metal ions were involved in the assembly process, ethylenediamine-tetraacetic acid (EDTA), a competing metal chelator, was added to the solution (Fig. 2.10). Upon addition of EDTA to the Zn(II) assembly was found to decrease the turbidity observed in the solution to that of the buffer, indicating that metal chelation is important in the assembly process.

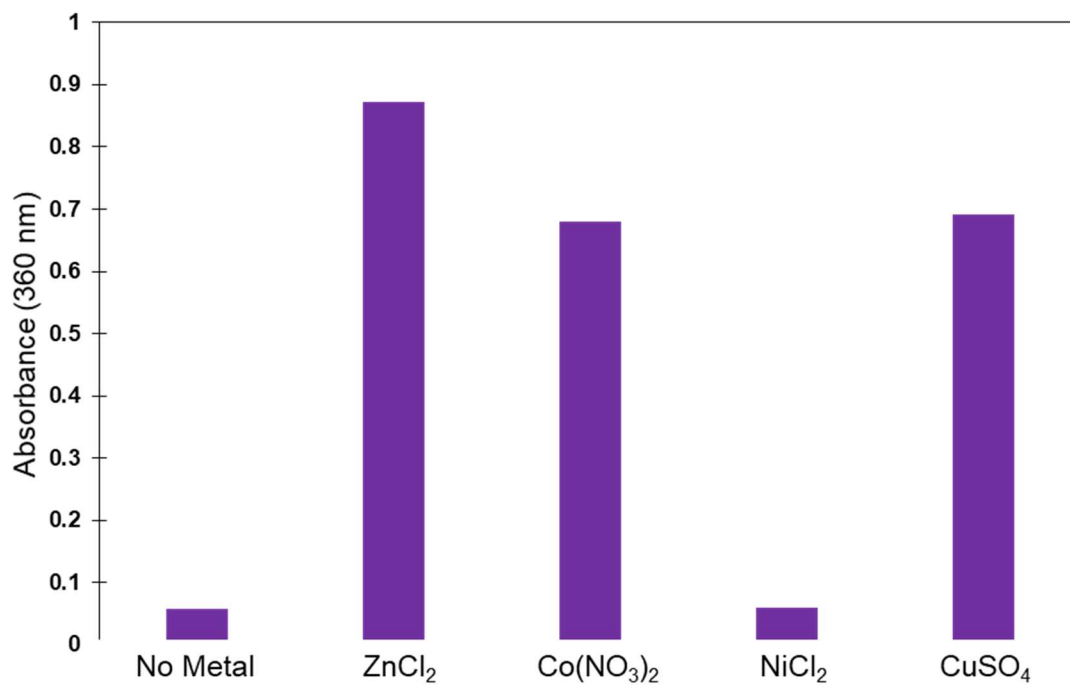


Figure 2.9. Solution turbidity due to precipitation of NCoH-FOGER (1 mM) assemblies with metal ions (300  $\mu$ M) in 20 mM MOPS overnight.

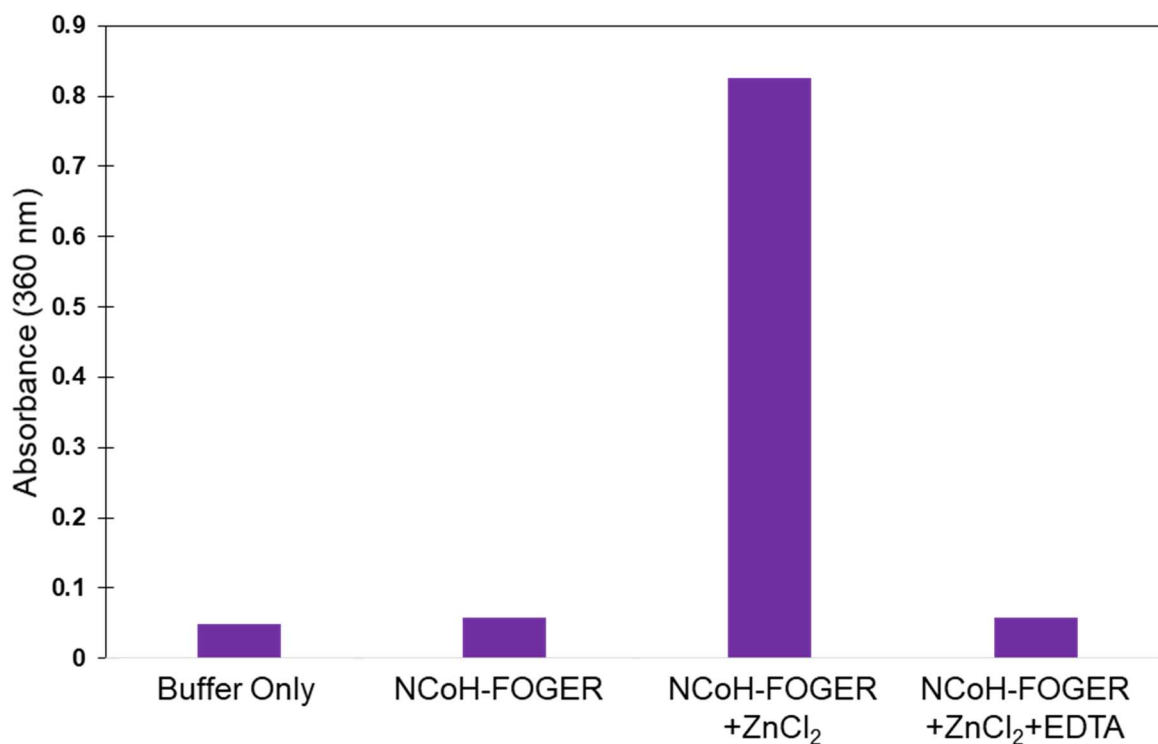


Figure 2.10. EDTA (10 mM) eliminates assembly associated turbidity.

Dynamic light scattering analysis showed that under conditions where turbidity was observed, hydrodynamic radii were found to be greater than a micron with a high polydispersity (Fig. 2.11). The sizes observed are outside the range in which this technique can be considered accurate so this data was used to qualitatively confirm that a large precipitate had, in fact, formed within the solution. The hydrodynamic radius of the unassembled peptide in solution was found to be about 4 nm, which is in agreement with previously reported peptides.<sup>11, 23</sup> Upon addition of Ni(II), we observed that the hydrodynamic radius increased to about 13 nm. This is perhaps due to a much lower level of self-assembly in solution that does not yield an isolable precipitate.

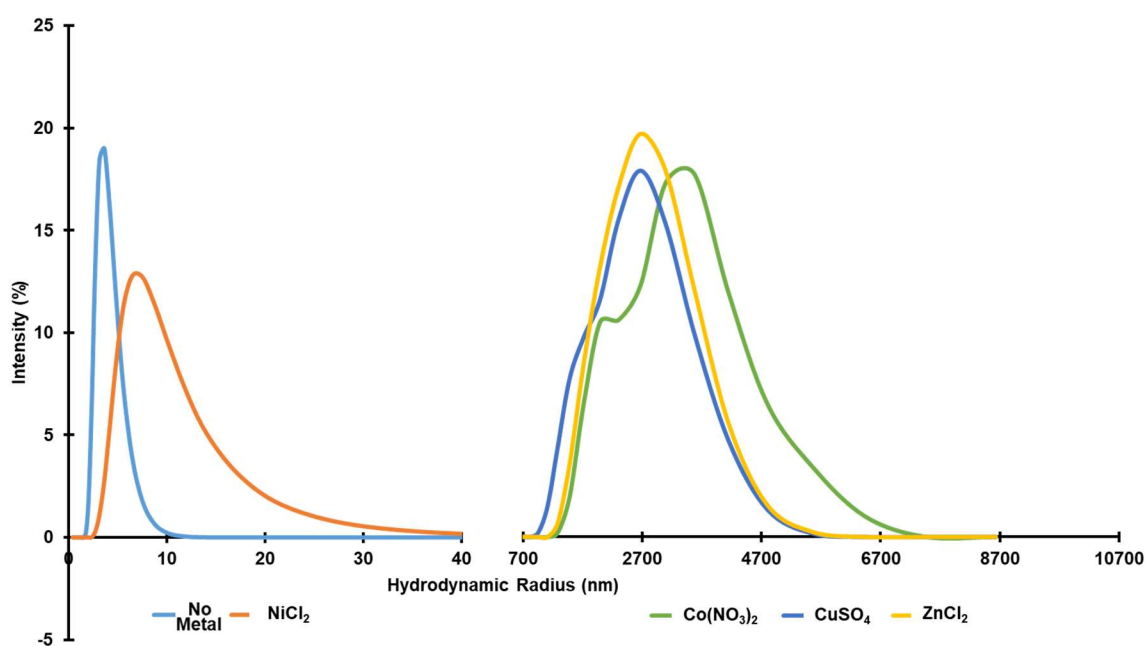


Figure 2.11. Dynamic Light Scattering of NCoH-FOGER (1 mM) with metal ions (300  $\mu$ M) in 20 mM MOPS overnight.

Scanning electron microscopy (SEM) was used to observe the morphology of precipitated assemblies. These precipitates were centrifuged, washed to remove buffer, and dried onto coverslips for analysis. SEM revealed that the precipitates consisted of petal-like or fibrillar particles, regardless of whether Zn(II), Co(II) or Cu(II) was used (Fig. 2.12). These structures can be characterized as being elongated with tapered ends.

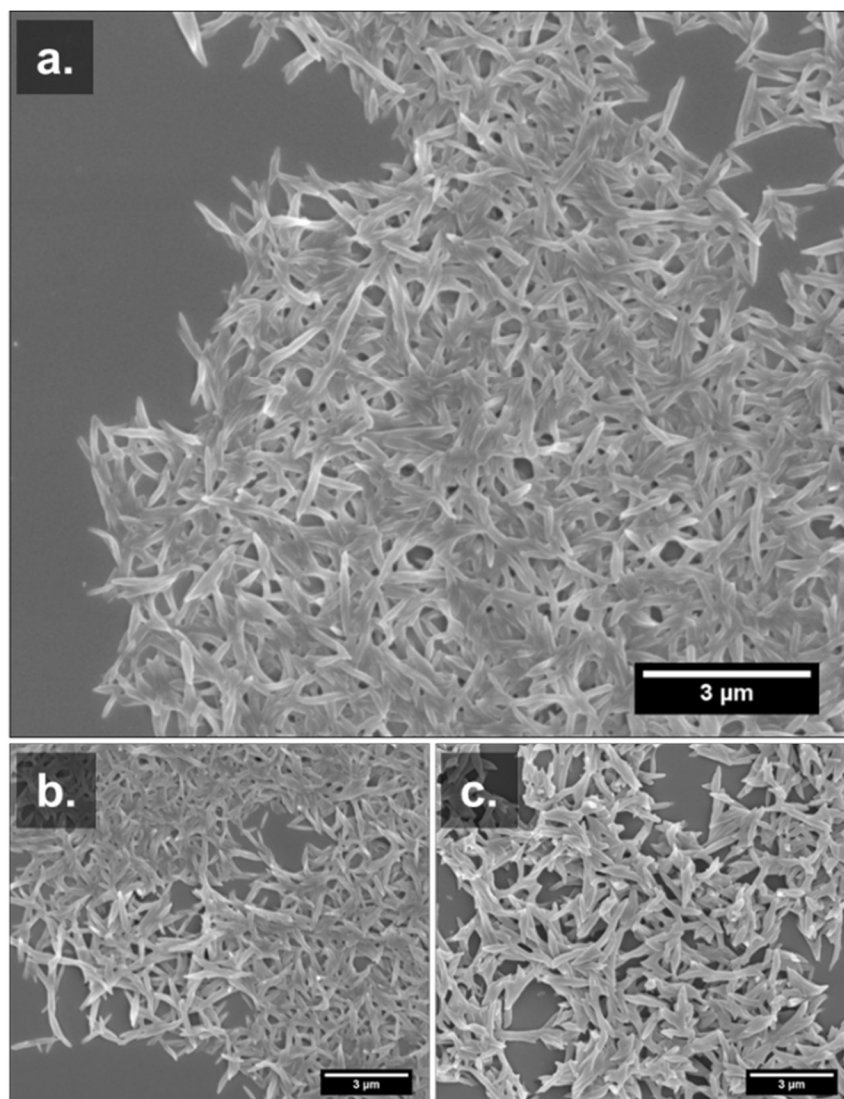


Figure 2.12. SEM Images of Assemblies formed from NCoH-FOGER (1 mM) in 20 mM MOPS Buffer (pH 7.4) overnight with 300  $\mu$ M (a)  $\text{Co}(\text{NO}_3)_2$ , (b)  $\text{CuSO}_4$ , and (c)  $\text{ZnCl}_2$ .

To further observe the fine structure of the particles, transmission electron microscopy (TEM) was employed (Fig. 2.13). Negative staining with uranyl acetate revealed that the assemblies display a banding pattern occurring with a periodicity of 9-10 nm. This pattern was thought to be a result of the linear arrangement of triple helices, each having a length between 9 and 10 nm. This length is similar to that observed for other collagen mimetic peptides with the same number of residues.<sup>13</sup> This possible linear arrangement of peptides also suggests that cell adhesive motifs will be displayed in 10 nm intervals at the surface of the particles.

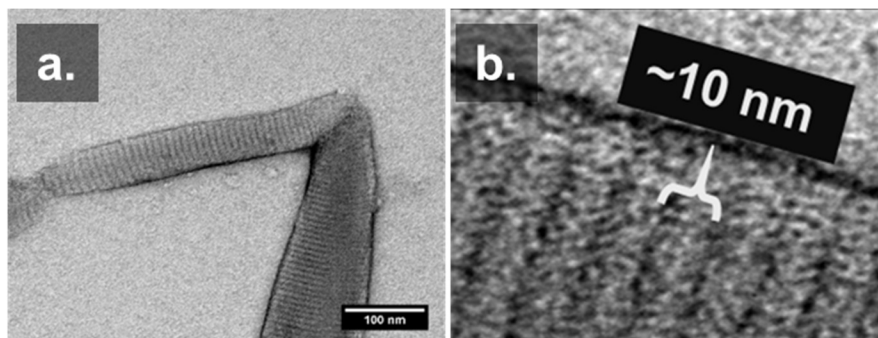


Figure 2.13. TEM Images of Assemblies formed from NCoH-FOGER (1 mM) with  $\text{ZnCl}_2$  (300  $\mu\text{M}$ ) in 20 mM MOPS Buffer overnight.

To get a better understanding of the self-assembly process, the morphology of assemblies was determined as a function of metal ion and peptide concentrations. These studies were done with  $\text{Zn(II)}$  and  $\text{Co(II)}$  ions. Some general trends were observed in each case. When very low concentrations (lesser than or equal to 300  $\mu\text{M}$ ) of both NCoH-FOGER and metal ions were used, no assembly occurred. This results indicate threshold concentrations below which defined particles do not seem to form. With  $\text{Zn(II)}$  ions, peptide concentrations had to be higher than metal ion concentrations in order to get defined particles. When the opposite was true, only amorphous precipitates were observed. In a phase diagram of NCoH-FOGER concentration and  $\text{Zn(II)}$  concentration, a region was observed where fibrillar particles were formed (Fig. 2.14 and Fig. 2.15). Within this region, increasing metal ion concentration seemed to decrease the length of the observed particles, although a large polydispersity was observed with this metal ion. At very high peptide concentrations, different particles, with blunt ends and multiple layers, were observed instead of fibrillar particles. We called entities with this morphology layered particles. With  $\text{Co(II)}$  ions, only amorphous and fibrillar morphologies were observed (Fig. 2.16. and Fig. 2.17). In general, increasing  $\text{Co(II)}$  or NCoH-FOGER concentrations seemed to decrease particle length (Tables 2-1 and 2-2).

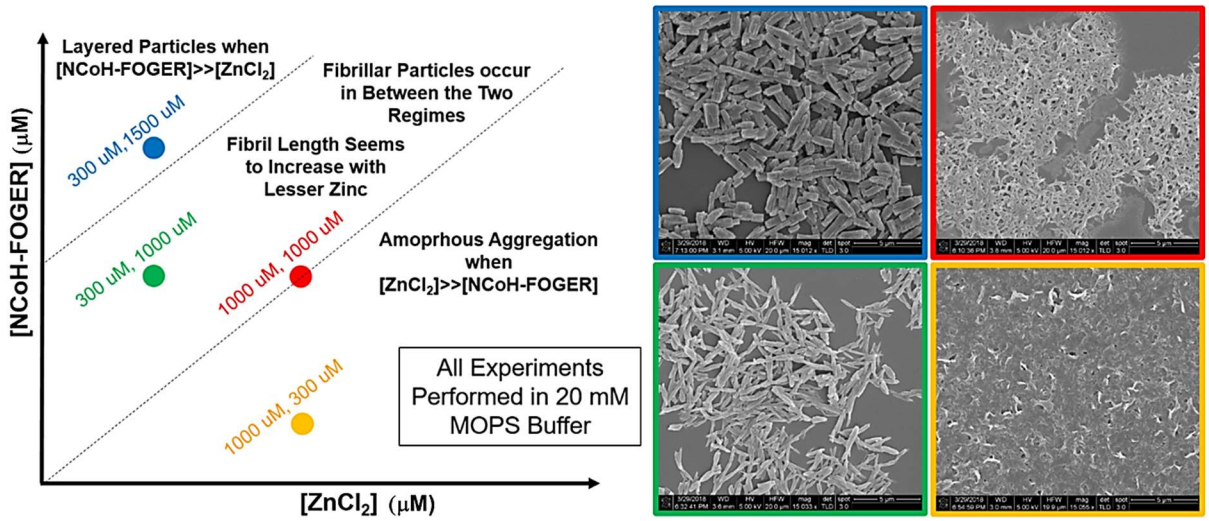


Figure 2.14. Phase diagram of NCoH-FOGER concentration and zinc chloride concentration showing morphologies achieved at different conditions.

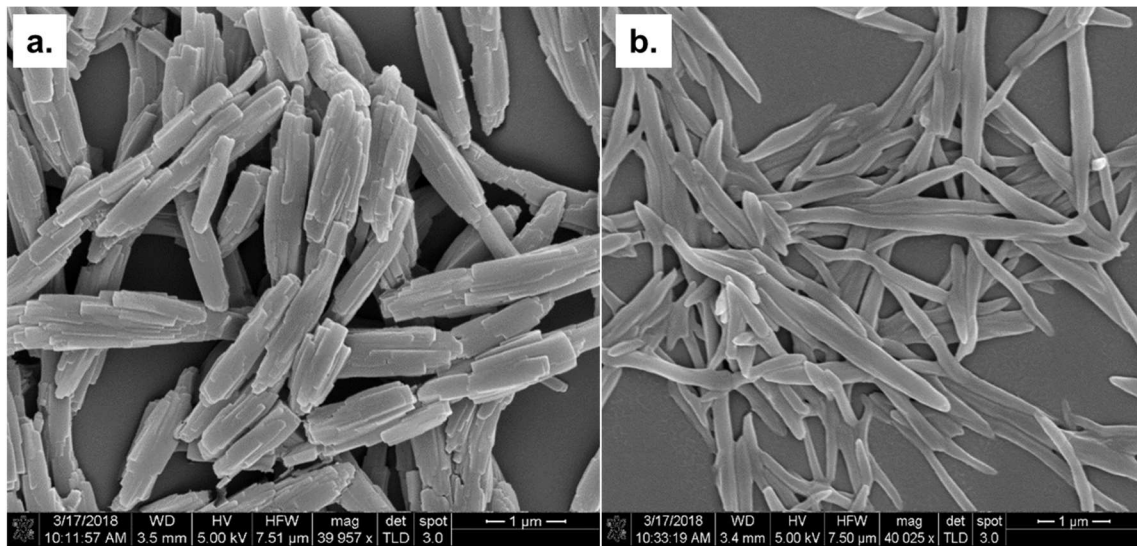


Figure 2.15. (a.) Layered particles from the assembly of 1.5 mM NCoH-FOGER and 300  $\mu\text{M}$   $\text{ZnCl}_2$  in MOPS buffer; (b.) Fibrillar particles from the assembly of 1 mM NCoH-FOGER and 300  $\mu\text{M}$   $\text{ZnCl}_2$  in 20 mM MOPS.

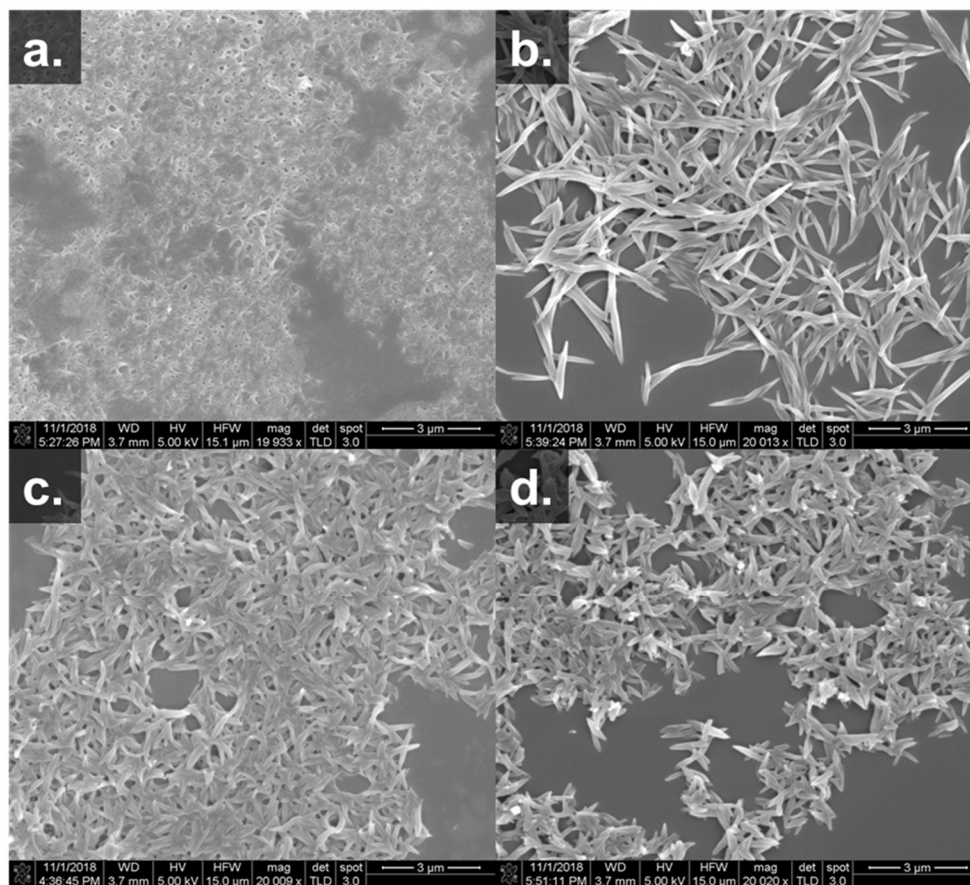


Figure 2.16. For all assemblies, 300  $\mu\text{M}$   $\text{Co}(\text{NO}_3)_2$  and 20 mM MOPS was used. NCoH-FOGER was varied: (a.) 300  $\mu\text{M}$ , (b.) 600  $\mu\text{M}$ , (c.) 1 mM, (d.) 1.2 mM

NCoH-FOGER Concentration ( $\mu\text{M}$ )	Length ( $\mu\text{m}$ ); Standard Deviation ( $\mu\text{m}$ )	Width ( $\mu\text{m}$ ); Standard Deviation ( $\mu\text{m}$ )
600	1.91; 0.78 *; ***	0.21; 0.05 +; +++
1000	1.03; 0.30 *; **	0.20; 0.04 +; ++
1200	0.83; 0.26 **; ***	0.21; 0.07 ++; +++

\*  $p = 2.2 \times 10^{-6}$ ;  $\alpha = 0.05$     +  $p = 0.21$ ;  $\alpha = 0.05$   
 \*\*  $p = 0.008$ ;  $\alpha = 0.05$     ++  $p = 0.38$ ;  $\alpha = 0.05$   
 \*\*\*  $p = 1.5 \times 10^{-8}$ ;  $\alpha = 0.05$     +++  $p = 0.90$ ;  $\alpha = 0.05$

Table 2-1. Measurements of particle lengths and widths of assemblies made from 300  $\mu\text{M}$   $\text{Co}(\text{NO}_3)_2$  and different NCoH-FOGER concentrations in 20 mM MOPS buffer overnight.

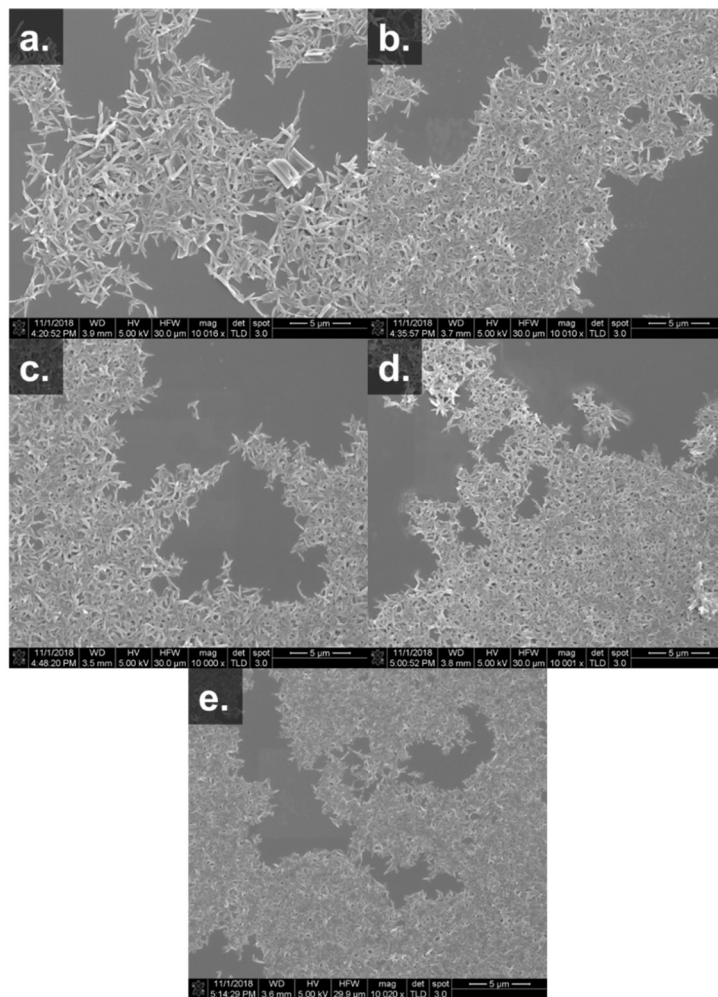


Figure 2.17. For all assemblies, 1 mM NCoH-FOGER and 20 mM MOPS was used.  $\text{Co}(\text{NO}_3)_2$  was varied: a) 200  $\mu\text{M}$ , b) 300  $\mu\text{M}$ , c) 600  $\mu\text{M}$ , d) 1 mM, e) 1.5 mM.

$\text{Co}(\text{NO}_3)_2$ Concentration ( $\mu\text{M}$ )	Length ( $\mu\text{m}$ ); Standard Deviation ( $\mu\text{m}$ )	Width ( $\mu\text{m}$ ); Standard Deviation ( $\mu\text{m}$ )
200	1.11; 0.25	0.21; 0.04
300	1.03; 0.29	0.20; 0.04
600	0.74; 0.25	0.16; 0.03
1000	0.49; 0.16	0.17; 0.04
1500	0.47; 0.14	0.16; 0.03

<sup>a</sup>  $p = 0.28$ ;  $\alpha = 0.05$       <sup>1</sup>  $p = 0.39$ ;  $\alpha = 0.05$   
<sup>b</sup>  $p = 1.8 \times 10^{-4}$ ;  $\alpha = 0.05$     <sup>2</sup>  $p = 0.003$ ;  $\alpha = 0.05$   
<sup>c</sup>  $p = 5.8 \times 10^{-5}$ ;  $\alpha = 0.05$     <sup>3</sup>  $p = 0.55$ ;  $\alpha = 0.05$   
<sup>d</sup>  $p = 0.58$ ;  $\alpha = 0.05$             <sup>4</sup>  $p = 0.18$ ;  $\alpha = 0.05$

Table 2-2. Measurements of particle lengths and widths of assemblies made from 1 mM NCoH-FOGER and different  $\text{Co}(\text{NO}_3)_2$  peptide concentrations in 20 mM MOPS buffer overnight.

### 2.3.5 Stabilization of NCoH-FOGER-Co(II) Particles

In preparing the petal shaped assemblies for biological experiments, we found that they were disrupted and dissolved in Dulbecco's minimal eagle medium (DMEM), which is commonly used in cell culture. Regardless of the divalent metal ion used, full solubilization was observed visually in DMEM within 30 seconds. Stabilizing the assemblies against dissolution was required to test their activity in cell-based assays. As such, we hypothesized that the Co(II) ions within an assembly could be oxidized to the exchange-inert Co(III) ions. Previous work has shown that chelation with Co(II) and subsequent oxidation of the complexes to Co(III) can be used to permanently immobilize hexahistidine-tagged proteins on surfaces.<sup>27</sup> Once assemblies from 1 mM NCoH-FOGER and 1 mM Co(NO<sub>3</sub>)<sub>2</sub> were formed in 20 mM MOPS buffer, 20 μL of 100 mM hydrogen peroxide was added. After incubation overnight, the assemblies were isolated by centrifugation and washing. To our delight, the oxidation resulted in particles that retained their morphological characteristics and were stable when suspended in DMEM (Fig. 2.18). Furthermore, the particles could be fluorescently tagged with His<sub>6</sub>Rhodamine and 1 mM zinc ion in MOPS buffer, allowing them to be tracked via fluorescence microscopy. With increased stability and fluorescent tagging achieved, we next began experiments with endothelial cells.

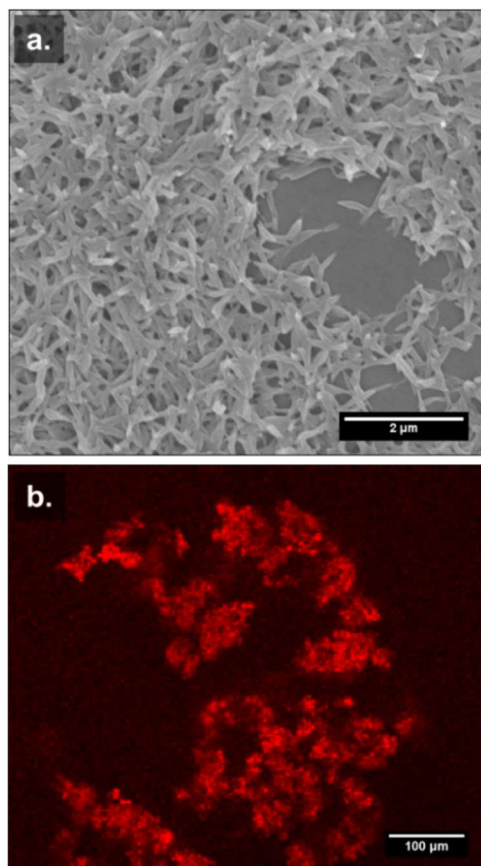


Figure 2.18. H<sub>2</sub>O<sub>2</sub> oxidized and His<sub>6</sub>-rhodamine tagged Cobalt(III)-NCoH-FOGER (Each 1 mM during preparation) imaged by (a) SEM after being resuspended in DMEM media for 24 h. (b) Fluorescence Microscopy of His<sub>6</sub>-rhodamine tagged Cobalt(III)-NCoH-FOGER particles resuspended in DMEM media for 24h.

### 2.3.6 Adherence of Cobalt(III)-NCoH-FOGER Particles to Endothelial Cells

Primary human umbilical vein endothelial cells (HUVEC, ATCC-PCS-100-013) were used in all cell-based experiments. The adherence of self-assembled particles to HUVEC was tested in media supplemented with 10% fetal bovine serum. When HUVEC cells were incubated with NCoH-FOGER cobalt assemblies in serum supplemented DMEM media, we observed that the cells interacted and bound to the His<sub>6</sub>Rhodamine labelled particles. The cells had been stained for viability with calcein AM (Fig. 2.19).

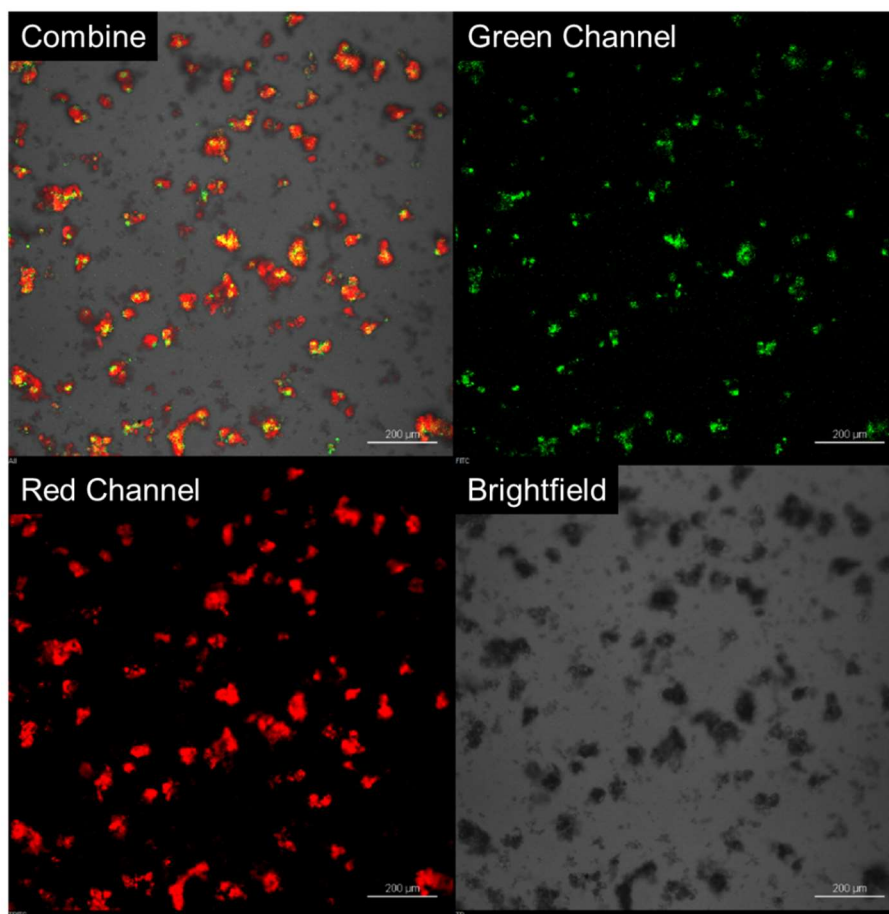


Figure 2.19. His<sub>6</sub>Rhodamine tagged NCoH-FOGER Co(III) Assembly (red channel) adhered to 200,000 Calcein AM stained HUVEC Cells (Green Channel) in DMEM with 10% FBS.

### 2.3.7 HUVEC Network Formation Induced By Cobalt(III)-NCoH-FOGER Particles

When fetal bovine serum was included in the culture media, endothelial cell network formation did not occur and instead cells appeared to simply interact with the cobalt(III)-NCoH-FOGER materials. It is notable that Whelan and Senger excluded serum in their experiments of type collagen induced endothelial cell morphogenesis.<sup>8</sup> In Boyden chamber assays, fetal bovine serum is often used as a positive control to indicate cell migration.<sup>28</sup> We hypothesized that the serum may be acting to enhance the migration of the cells to a degree that abrogates network formation. To test the possibility of endothelial cell tube formation, serum was excluded in our next experiments.

When HUVEC were incubated with the assemblies in serum free DMEM media, we observed the formation of networks of elongated cells within 4h (Fig. 2.20). This morphology resembled previously reported tube-like structures that formed when a monolayer of cells was treated with

collagen I in similar serum free conditions.<sup>8</sup> Senger and coworkers have suggested that such structures are formed as a result of integrin clustering and signaling.<sup>8</sup> The network formation did not occur in the absence of the peptide assemblies. The observation of this behavior with our materials suggests that a similar morphogenetic process could be occurring. When conducted with rhodamine tagged assemblies, the tubes seemed to have lower quality suggesting the rhodamine might be sterically blocking the integrin binding sites. Nevertheless, tube-like structures did form and the fluorophore allowed us to confirm that the cells were, in fact, bound to the material. Control experiments showed that the morphogenesis was not induced by non-oxidized assembly, soluble peptide, or  $\text{Co}(\text{NO}_3)_2$  alone (Fig. 2.21). As observed qualitatively through calcein staining, there was not any apparent loss of viability. As such, this study may be a true demonstration of endothelial network formation by polyvalent presentation of GFOGER sequences. This adds support to the hypothesis that collagen, through polyvalent GFOGER sequences, induces integrin clustering during endothelial morphogenesis.

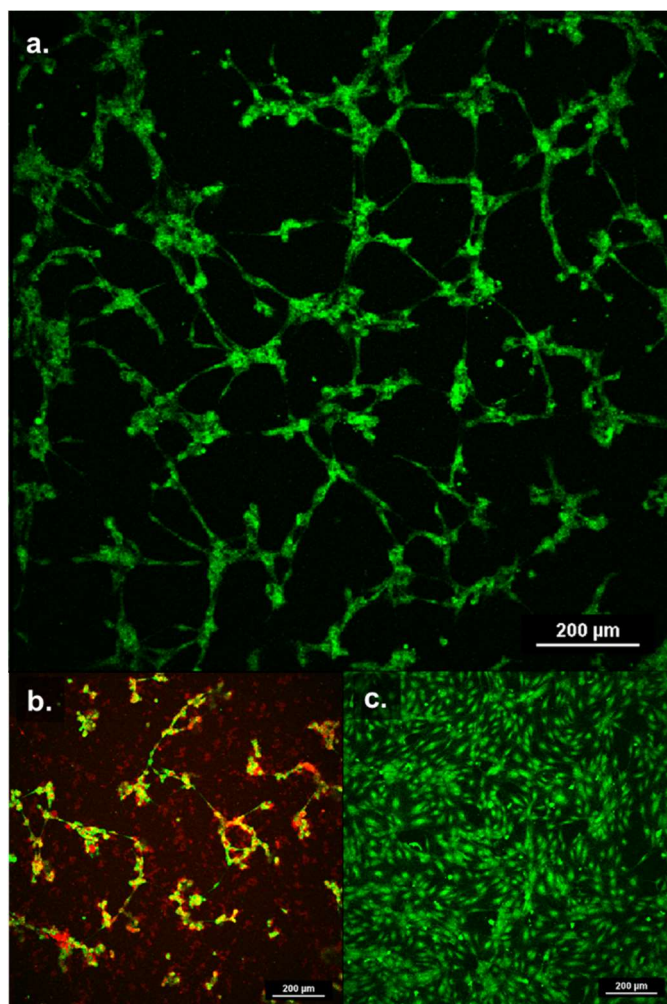


Figure 2.20. HUVEC network formation in serum free DMEM induced by a.) NCoH-FOGER-Co(III) assemblies and (b.) His<sub>6</sub>-rhodamine labelled assemblies; A sample without any material, (c.), did not form networks.

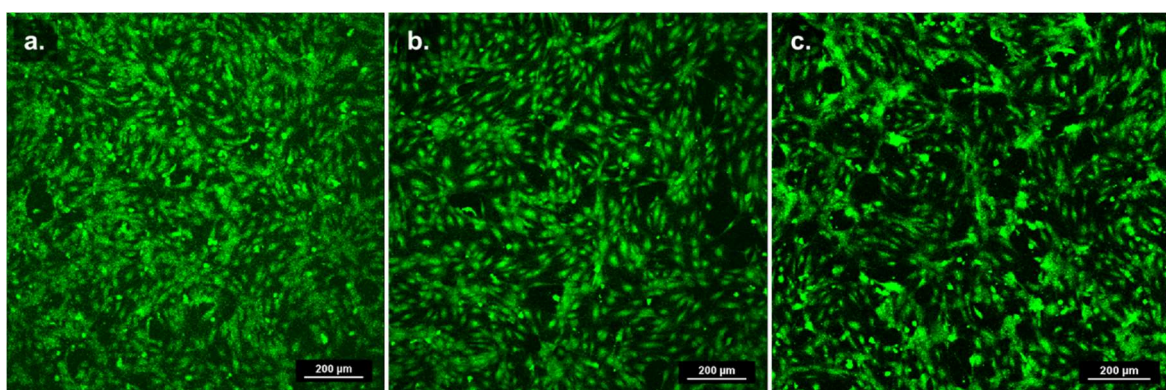


Figure 2.21. HUVEC network formation in serum free DMEM was not induced by controls: a.) 200  $\mu$ M NCoH-FOGER, (b.) 200  $\mu$ M Co(NO<sub>3</sub>)<sub>2</sub>, c.) non-oxidized NCoH-FOGER-Co(II) assemblies

### **2.3.8 Actin Staining in Endothelial Cells**

In previous studies, the early stages of endothelial tube formation was shown to be correlated with actin polymerization.<sup>8</sup> To interrogate this, we fixed and stained cells undergoing morphogenesis with FITC-phalloidin, which is selective for F-actin. Fluorescence microscopy revealed that the cells treated with NCoH-FOGER-Cobalt(III) assemblies displayed long actin fibers. In untreated cells, the green fluorescence seemed to localize near the nuclei of cells (Fig. 2.22). This data is similar to that observed previous for untreated cells and those treated with type I collagen.<sup>8</sup> Taken together, this suggests that the shape changes observed are perhaps driven by actin polymerization. This lends support to establishing that the morphogenesis observed here may be similar to that seen by Senger and Coworkers.

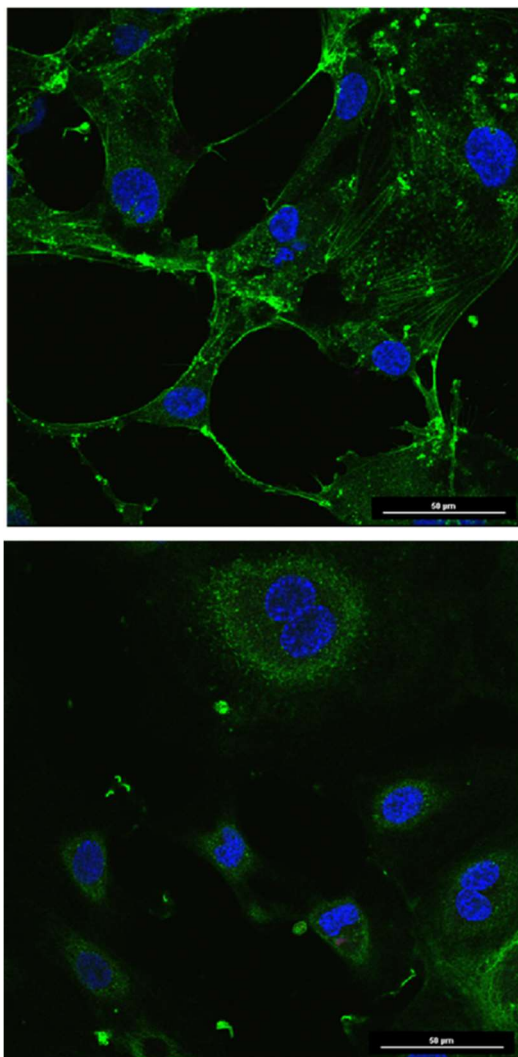


Figure 2.22. Cells stained with actin stained with FITC Phalloidin (Green) and nuclei stained with Hoescht 33342 dye (blue). (a.) Cells treated with NCoH-FOGER-Cobalt(III) assemblies in serum free DMEM show actin networks stained green with FITC-phalloidin. (b.) Untreated cells in serum free DMEM show green fluorescence only around nuclei.

### 2.3.9 Experiments with a More Stable Peptide, NCoH-FOGER-8

Because NCoH-FOGER was not a very stable triple helix in aqueous buffer, we decided to design and synthesize a more stable analog, NCoH-FOGER-8 (Fig. 2.23). To achieve higher stability, NCoH-FOGER was designed with one more Pro-Hyp-Gly unit, in accordance with previous literature showing that longer collagen peptides are more stable.<sup>29</sup>

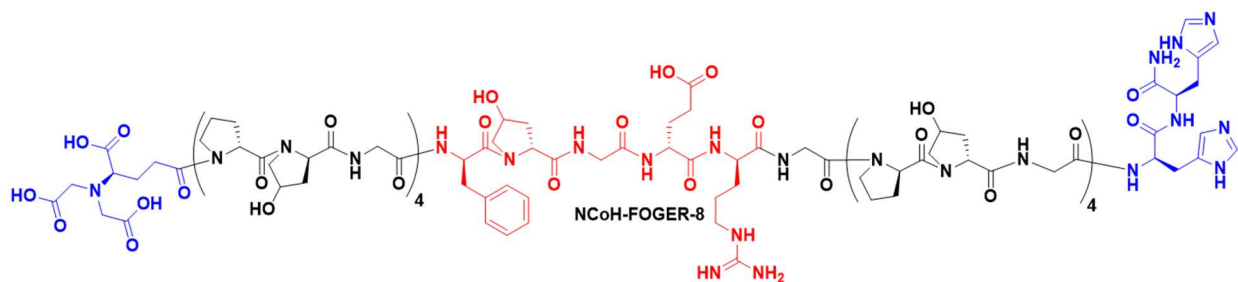


Figure 2.23. NCoH-FOGER-8, a longer analog of NCoH-FOGER

After solid phase peptide synthesis, NCoH-FOGER-8 was studied by circular dichroism spectroscopy and showed the spectral characteristics of a polyproline type II helix (2.24). In temperature dependent circular dichroism experiments, sigmoidal behavior was observed and a  $T_m$  of 35 °C (Fig. 2.24). This indicated the possible triple helical behavior of NCoH-FOGER-8.

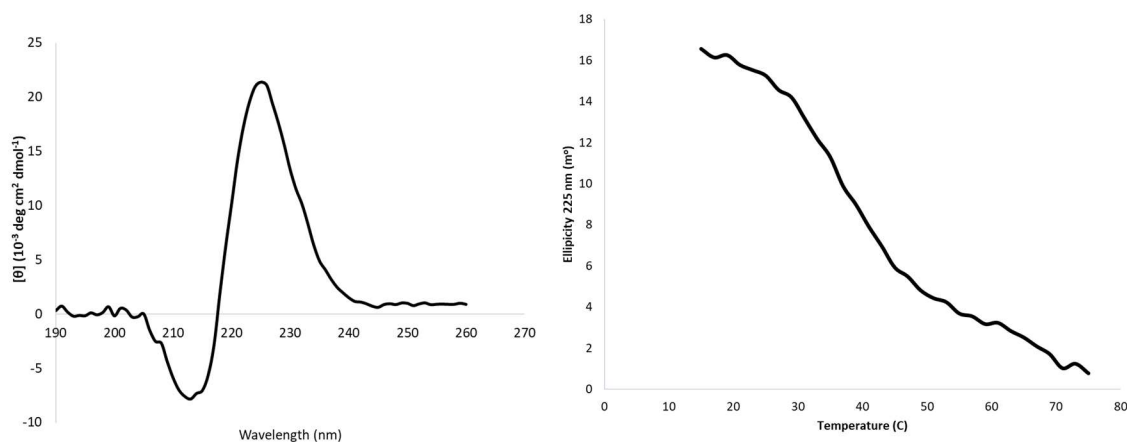


Figure 2.24. CD spectrum and melting curve for 100 uM NCoH-FOGER-8 in 20 mM MOPS buffer shows a  $T_m$  of 35 °C.

Metal triggered self-assembly of NCoH-FOGER-8 resulted in fibrillar particles (Fig. 2.25). NCoH-FOGER-8-Co(II) particles could be oxidized with hydrogen peroxide and retained their morphology after incubation in DMEM media overnight. Transmission electron microscopy revealed that NCoH-FOGER-8 displayed a periodic banding pattern (Fig. 2.26).

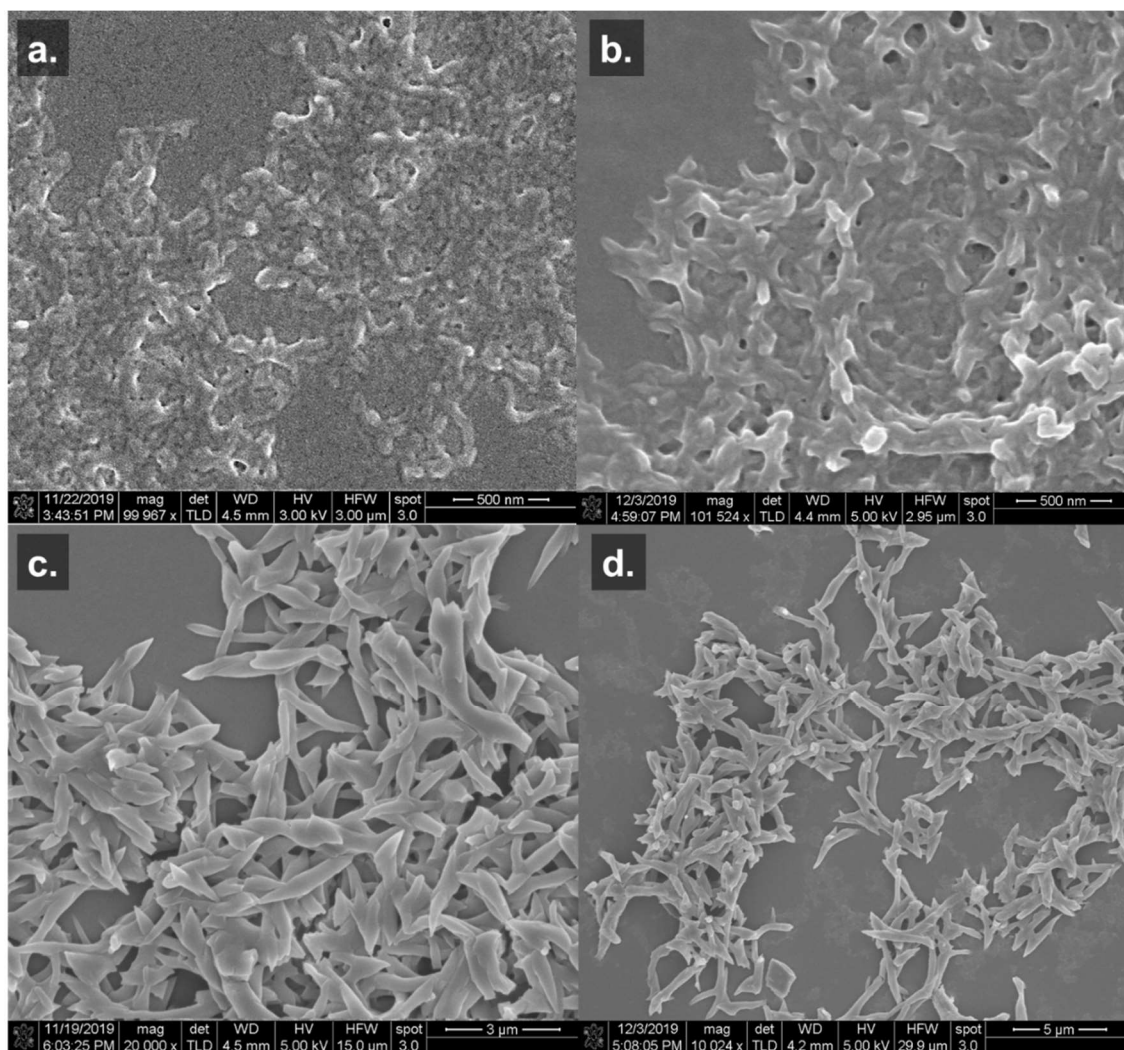


Figure 2.25. NCoH-FOGER-8 (1 mM) assembled with 1 mM (a)  $\text{ZnCl}_2$ , (b)  $\text{CuSO}_4$ , and (c)  $\text{Co}(\text{NO}_3)_2$  in 20 mM MOPS buffer. The cobalt (II) assemblies were oxidized with  $\text{H}_2\text{O}_2$  to cobalt (III), resuspended in DMEM media overnight, and then imaged (d.).

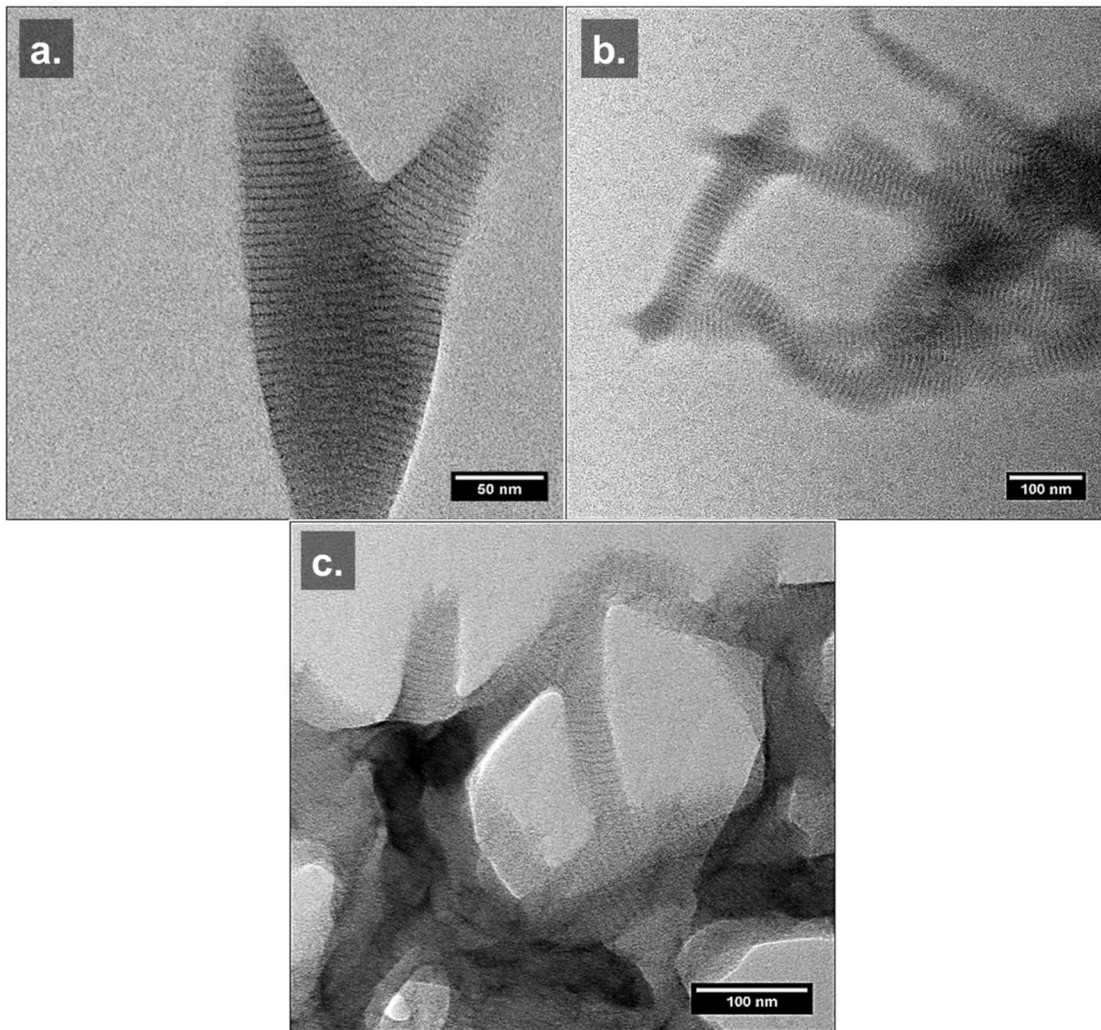


Figure 2.26. TEM of NCoH-FOGER-8 (1 mM) assembled with 1 mM (a)  $\text{Co}(\text{NO}_3)_2$ , (b)  $\text{CuSO}_4$ , and (c)  $\text{ZnCl}_2$  in 20 mM MOPS Buffer.

In endothelial network formation assays, NCoH-FOGER-8 seemed to form networks but they were of lower quality than those formed with NCoH-FOGER (Fig. 2.27).

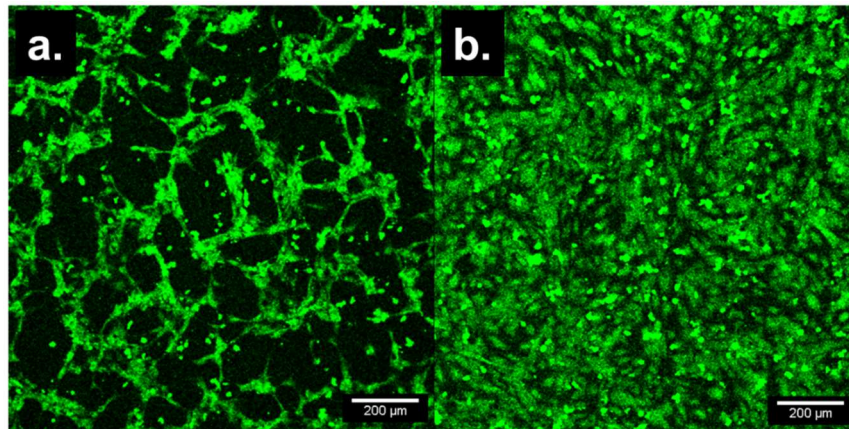


Figure 2.27. Endothelial Cells in serum free DMEM treated with a.) NCoH-FOGER-8 Cobalt(III) assemblies and b) not treated.

## 2.4 Conclusion

The peptide, NCoH-FOGER, can self-assemble into fibrillar particles, layered particles, and amorphous morphologies when triggered by metal ions. With fibrillar particles, a periodic banding pattern was observed by TEM. With cobalt ions, these particles can be stabilized against dissolution through oxidation from Co(II) to Co(III). These stabilized particles can be labelled with His-tagged dyes and visualized by fluorescence microscopy. These particles display the GFOGER sequence in a polyvalent manner. When added to a monolayer of serum starved endothelial cells, capillary-like networks are formed. With a cobalt(III) assemblies of a longer peptide, NCoH-FOGER-8, formed networks of lesser quality than NCoH-FOGER. In literature, the polyvalent presentation of GFOGER by collagen fibers is thought to cause integrin clustering and subsequent network formation in endothelial cells. The demonstration of a similar process in a synthetic polyvalent biomaterial adds support to this hypothesis. Future experiments will focus on immobilizing these particles on surfaces. This may allow for the fabrication of scaffolds for vascular tissue engineering.

## 2.5 Materials and Methods

**Materials** Fluorenylmethyloxycarbonyl (Fmoc) protected amino acids were purchased from ChemPep Inc. Hexafluorophosphate azabenzotriazole tetramethyl uranium (HATU), 1-hydroxyazabenzotriazole (HOAt), and N,N'-diisopropylethylamine (DIEA) were purchased from Chem Impex International Inc. ChemMatrix Rink Amide resin was purchased from PCAS

Biomatrix Inc. Trifluoroacetic acid (TFA), triisopropylsilane (TIPS), diethyl ether, and piperidine were purchased from Sigma Aldrich. Dichloromethane (DCM), methanol (MeOH), and N,N'-Dimethylformamide (DMF) were purchased from Fisher. His<sub>6</sub>Rhodamine was procured as a gift from Dr. Monessa Nambiar. Primary HUVEC, vascular cell media, and endothelial growth kit-VEGF were purchased from the ATCC. FITC-phalloidin was purchased from Abcam. DMEM media and fetal bovine serum was purchased from Thermo Fisher Scientific.

**Synthesis of Nitrilotriacetate Intermediate 2.** Compound **2** (650 mg, 92% yield) was obtained as a yellowish oil using a reported procedure.<sup>14</sup> <sup>1</sup>H NMR (300 MHz, CDCl<sub>3</sub>): δ3.44 (s, 4H), δ3.35(J = 12 Hz, d, 1H), δ2.67 (m, 2H), δ1.97 (m, 2H), δ1.46 (s, 27H).

**Synthesis of Nitrilotriacetate 3.** Compound **3** (650 mg, 92% yield) was obtained as a yellowish oil using a reported procedure.<sup>14</sup> <sup>1</sup>H NMR (300 MHz, CDCl<sub>3</sub>): δ3.44 (s, 4H), δ3.35(J = 12 Hz, d, 1H), δ2.67 (m, 2H), δ1.97 (m, 2H), δ1.46 (s, 27H).

**General Peptide Synthesis** Peptides were prepared using standard Fmoc-based synthesis techniques utilizing ChemMatrix Rink Amide resin. Four equivalents of Fmoc protected amino acids were coupled to 1 equivalent of resin (200 mg, 0.22 mmol/g) using HATU (4 eq), HOAt (4 eq.) and DIEA (8 eq) dissolved in DMF (20 mL). The amino acid and reagents were dissolved in DMF and the resulting yellow solution was added to the resin and agitated for 2 hours at room temperature. Afterwards, the resin was washed thrice with 15 mL each of DMF, DCM, MeOH, and then re-swollen with DCM. To deprotect the Fmoc group, the resin was suspended in 25% piperidine in DMF (20 mL) and agitated for 25 minutes. Following this reaction, the resin was washed give details. The ninhydrin-Kaiser test was used to detect free primary amines and the chloranil test was used to detect free secondary amines. Upon completion of the amino acid sequence, NTA (4 eq.) was coupled to the N-terminus using HATU (4 eq.), HOAt (4 eq.), and DIEA (8 eq.) in 20 mL DMF for 2 hours. Afterwards, the resin-bound peptide was washed with 15 mL each of DMF, DCM, and MeOH and dried under reduced pressure. The peptide was cleaved from resin using 15 mL of a cocktail of TFA/TIPS/H<sub>2</sub>O (95: 2.5: 2.5) for 1 hour. The reaction mixture was filtered through a frit. The filtrate was concentrated under reduced pressure and the crude peptide was precipitated by addition of cold diethyl ether (20 mL). The precipitate was

collected via centrifugation and the pellet was dried under reduced pressure. The crude product was dissolved in water and purified by semi-preparative RP HPLC using a Luna C18 (250 x 21.20 mm, 100 Å pore size, 10 micron, Phenomenex) column. NCoH-FOGER was purified using a 60 min. gradient of 5-50% solvent A (0.01% TFA in acetonitrile) in solvent B (0.01% TFA in water) at a flow rate of 12 mL per minute ( $R_t = 23.2$  min.,  $R_f = 0.39$ ). NCoH-FOGER-8 was purified using a 60 min. gradient of 5-80% solvent A in solvent B at a flow rate of 12 mL per minute ( $R_t = 16.5$  min.,  $R_f = 0.29$ ). The products were detected by absorbance at 214 nm. Peptide containing fractions were identified using MALDI-TOF mass spectrometry (NCoH-FOGER: calculated: 3066.37, experimental: 3066.4; NCoH-FOGER-8: calculated: 3333.46, experimental: 3331). Product containing fractions were combined, concentrated under reduced pressure and lyophilized to provide NCoH-FOGER in 99% purity (HPLC, 30 min. gradient of 5-50% solvent A in solvent B, 1.2 mL/min.,  $R_t = 15.8$  min.,  $R_f = 0.53$ ) and NCoH-FOGER-8 in 98% purity (HPLC, 30 min. gradient of 5-80% solvent A in solvent B, 1.2 mL/min.,  $R_t = 13.2$  min.,  $R_f = 0.44$ ).

**Circular Dichroism** All circular dichroism (CD) experiments were conducted using a JASCO J-810 spectropolarimeter, equipped with a PFD-425S Peltier temperature control unit. Peptide Stocks (10 mM in filtered water) were thermally annealed by heating at 90°C for 1h followed by slow cooling to room temperature. After overnight incubation in a fridge (~4°C), samples were prepared to contain 250 µM of each peptide in 20 mM MOPS. These buffered samples were incubated for another 24 h at 4°C and placed in a 0.1 cm path-length quartz cuvette for CD experiments. Spectra were collected, at room temperature, as an average of 3 scans between 190-260 nm (0.1 nm data pitch, 1 nm bandwidth, 100 nm/min scan rate, and 1 second response time). For temperature dependent experiments, spectra were collected similarly after 5 minute equilibration periods at different temperatures. The signal at 225 nm was plotted as a function of temperature to discern melting behavior. The transition melting temperature ( $T_m$ ) was found using from analysis of the first derivative plots (Change in signal vs. temperature).

**Metal-Ion Promoted Self-Assembly** To a 1.5 mL polypropylene centrifuge tube was added, in the given order, 3-(*N*-morpholino)propanesulfonic acid (MOPS) buffer stock (20 µL, 100 mM, pH=7.4), filtered milliQ water, peptide stock (10 mM in water), and metal salt solutions (10 mM in water). Upon mixing, the tube was capped and incubated at room temperature for 16 h. For all

experiments, the final concentration of MOPS buffer was 20 mM. The amount of water, peptide, and metal ion solutions were varied to give the desired final concentrations in a total volume of 100  $\mu\text{L}$ . If oxidation was needed, 20  $\mu\text{L}$  of  $\text{H}_2\text{O}_2$  (100 mM in water) was added, after the 16 h incubation period, directly to the suspension, containing cobalt-peptide assemblies, to give a total volume of 120  $\mu\text{L}$ . These samples were incubated at room temperature for another 24 h. After incubation, the precipitate-containing samples were centrifuged at  $10,000\times g$  for three minutes at 4  $^\circ\text{C}$ , and the supernatant was removed. Solids were re-suspended in water (100  $\mu\text{L}$ ), and this process was repeated two more times. The solids were then prepared as needed for use in further experiments.

**Turbidity Measurements** Assemblies were prepared as described above in a polystyrene 96 well plate instead of centrifuge tubes. For the non-assembled sample, NCoH-FOGER was diluted to the desired concentration without addition of any metal salts. EDTA was added to a final concentration of 10 mM in the relevant sample. After incubation at room temperature for 16 h, the absorbance was measured at 360 nm using a Tecan Infinite F-Plex plate reader. Samples with high absorbance indicated the presence of suspended solid, which caused the observed turbidity.

**Dynamic Light Scattering** Assemblies were prepared in centrifuge tubes as described above. For the non-assembled sample, NCoH-FOGER was diluted to the desired concentration without addition of any metal salts. After the 16 h incubation period, the solutions were moved into plastic cuvettes and placed into the sample holder of a ZetaSizer Nano ZS instrument with temperature set to 25  $^\circ\text{C}$ . Dynamic light scattering (DLS) was measured and the volume size distributions were obtained by analyzing correlation functions with the multiple spherical modes algorithm.

**Scanning Electron Microscopy** Assemblies were prepared as described and re-suspended in 100  $\mu\text{L}$  of DI water. Glass coverslips were affixed to stainless steel stubs using double sided copper tape. Five microliters of assembly suspension (in water) was placed on top of the affixed coverslips and allowed to air dry. Prior to imaging, these samples were sputter coated with platinum for 60 seconds. An FEI-Nova NanoSEM field emission microscope was used to analyze samples. Images were collected using a spot size of 3, accelerating voltage of 5 kV and 30  $\mu\text{m}$  aperture.

**Transmission Electron Microscopy** After preparation, assemblies were suspended in 100  $\mu\text{L}$  of water. Three microliters of these samples were placed onto carbon/formvar coated 400-mesh copper grids, which had been glow discharged. These were allowed to stand for 3 minutes and then blotted using filter paper. The sample grids were then passed through a drop of water 16 times followed by passage through a drop of 1% uranyl acetate 16 times. These were then blotted with filter paper and allowed to dry under ambient conditions. The sample containing grids were imaged using a Tecnai T20 Transmission Electron Microscope using a 100 kV accelerating voltage and 70  $\mu\text{m}$  objective aperture. Measurements in images were done using ImageJ.

**Preparation of Rhodamine-tagged Assemblies**  $\text{H}_2\text{O}_2$ -oxidized particles were prepared as described as above using 1 mM NCoH-FOGER and 1 mM  $\text{Co}(\text{NO}_3)_2$ . Afterwards, the particles were resuspended in 100  $\mu\text{L}$  of 20 mM MOPS buffer containing 1 mM  $\text{ZnCl}_2$ . This mixture was allowed to sit at room temperature for 15 minutes and then 2  $\mu\text{L}$  of His<sub>6</sub>Rhodamine (10 mM in water) was added. The mixture was incubated at room temperature in the dark for 30 minutes. Afterwards, the solid was isolated by centrifugation and washing with water similarly to that for metal ion promoted assembly.

**Stability of Oxidized Particles** Particles were prepared as described and re-suspended in 500  $\mu\text{L}$  of serum free DMEM media. This mixture was incubated at 37  $^\circ\text{C}$  for 24 h in a 1.5 mL centrifuge tube. Afterwards, the particles were isolated by centrifugation and washing with water. After resuspension in 100  $\mu\text{L}$  water, these samples were analyzed by SEM.

**Cell Culture** Primary HUVEC (ATCC PCS-100-013) were cultured in complete vascular cell basal media supplemented with endothelial growth kit-VEGF using protocols described in ATCC product sheets.<sup>30</sup>

**Endothelial Cell Experiments** Cold Geltrex (1:100 dilution in serum free DMEM) was added to each well of a 4-well imaging chamber (700  $\mu\text{L}$  per well). The chamber was incubated at 37  $^\circ\text{C}$  in an incubator for 1 hour and then allowed to cool to room temperature for 30 min. Wells were aspirated to remove all traces of solution and then 500  $\mu\text{L}$  of vascular cell basal media, supplemented with endothelial growth kit -VEGF and penicillin-streptomycin, was added to each

well. 200,000 HUVEC were added to each well and cells were allowed to settle and adhere for 16 h. Media was aspirated and cells in each well were washed three times with phosphate buffered saline (PBS). Once washed, 450 of serum free or complete DMEM was added as needed to wells. NCoH-FOGER-Cobalt(III) particles or other desired treatments, diluted in 50  $\mu$ L of identical media, were added to the cells. After incubation for 4h, 2  $\mu$ L of calcein-AM solution (500 nM diluted in serum-free DMEM) was added to each well. These samples were imaged using a Nikon A1R multiphoton confocal fluorescence microscope (488 nm laser for green fluorescence, 561 nm laser for red).

**Actin Staining** HUVEC were prepared and treated with particles or other desired condition in DMEM similarly to that described above. After 2h of treatment, 500  $\mu$ L of 8% paraformaldehyde in PBS was added directly to cells in media. The cells were fixed for 10 minutes and then all wells were aspirated. Wells were washed once with 500  $\mu$ L PBS to remove residual paraformaldehyde and 500  $\mu$ L of 1X Phalloidin FITC working solution (1:1000 dilution of AbCam 1000X Phalloidin-FITC in PBS containing 1% bovine serum albumin, 0.1% Triton-X-1000, and 1  $\mu$ M Hoescht 33342 dye was added. Samples were stained for 1 hour. Afterwards, all solutions were aspirated and wells were washed twice with 500  $\mu$ L of PBS. 500  $\mu$ L of fresh PBS was used as a mounting media for imaging using a Nikon A1R multiphoton confocal fluorescence microscope (405 nm laser for blue fluorescence; 488 nm laser for green fluorescence).

## 2.6 References

- [1] Krüger-Genge, Anne, Anna Blocki, Ralf-Peter Franke, and Friedrich Jung. "Vascular endothelial cell biology: An update." *International journal of molecular sciences* 20.18 (2019): 4411.
- [2] Mongiat, Maurizio, Eva Andreuzzi, Giulia Tarticchio, and Alice Paulitti. "Extracellular matrix, a hard player in angiogenesis." *International journal of molecular sciences* 17.11 (2016): 1822.
- [3] Kubota, Yasuo, Hynda K. Kleinman, George R. Martin, and Thomas J. Lawley. "Role of laminin and basement membrane in the morphological differentiation of human endothelial cells into capillary-like structures." *The Journal of cell biology* 107.4 (1988): 1589-1598.
- [4] Buranawat, B., P. Kalia, and L. Di Silvio. "Vascularisation of tissue-engineered constructs." *Standardisation in Cell and Tissue Engineering*. Woodhead Publishing, 2013. 77-103a.

- [5] Bauer, Stephen M., Richard J. Bauer, Zhao-Jun Liu, Haiying Chen, Lee Goldstein, and Omaid C. Velazquez. "Vascular endothelial growth factor-C promotes vasculogenesis, angiogenesis, and collagen constriction in three-dimensional collagen gels." *Journal of vascular surgery* 41.4 (2005): 699-707.
- [6] Senger, Donald R., Kevin P. Claffey, Julie E. Benes, Carole A. Perruzzi, Ageliki P. Sergiou, and Michael Detmar. "Angiogenesis promoted by vascular endothelial growth factor: regulation through  $\alpha 1\beta 1$  and  $\alpha 2\beta 1$  integrins." *Proceedings of the National Academy of Sciences* 94.25 (1997): 13612-13617.
- [7] Senger, D. R., Perruzzi, C. A., Streit, M., Koteliansky, V. E., de Fougerolles, A. R., & Detmar, M. (2002). "The  $\alpha 1\beta 1$  and  $\alpha 2\beta 1$  integrins provide critical support for vascular endothelial growth factor signaling, endothelial cell migration, and tumor angiogenesis." *The American journal of pathology* 160.1 (2002): 195-204.
- [8] Whelan, Mary C., and Donald R. Senger. "Collagen I initiates endothelial cell morphogenesis by inducing actin polymerization through suppression of cyclic AMP and protein kinase A." *Journal of Biological Chemistry* 278.1 (2003): 327-334.
- [9] Sweeney, Shawn M., Gloria DiLullo, Simon J. Slater, José Martinez, Renato V. Iozzo, Janelle L. Lauer-Fields, Gregg B. Fields, and James D. San Antonio. "Angiogenesis in collagen I requires  $\alpha 2\beta 1$  ligation of a GFP\* GER sequence and possibly p38 MAPK activation and focal adhesion disassembly." *Journal of Biological Chemistry* 278.33 (2003): 30516-30524.
- [10] Turner, Kevin R., Christopher Adams, Stephanie Staelens, Hans Deckmyn, and James San Antonio. "Crucial Role for Endothelial Cell  $\alpha 2\beta 1$  Integrin Receptor Clustering in Collagen-Induced Angiogenesis." *The Anatomical Record* (2019).
- [11] Pires, Marcos M., and Jean Chmielewski. "Self-assembly of collagen peptides into microflorettes via metal coordination." *Journal of the American Chemical Society* 131.7 (2009): 2706-2712.
- [12] Pires, Marcos M., Dawn Ernenwein, and Jean Chmielewski. "Selective decoration and release of His-tagged proteins from metal-assembled collagen peptide microflorettes." *Biomacromolecules* 12.7 (2011): 2429-2433.
- [13] Pires, M. M., Przybyla, D. E., Rubert Pérez, C. M., & Chmielewski, J. "Metal-mediated tandem coassembly of collagen peptides into banded microstructures." *Journal of the American Chemical Society* 133.37 (2011): 14469-14471.
- [14] Strauss, Kevin. "Metal-promoted self-assembly of collagen mimetic peptides into biofunctional scaffolds for stem cell delivery with the aim of tissue regeneration." (2016).
- [15] Behrendt, Raymond, Peter White, and John Offer. "Advances in Fmoc solid-phase peptide synthesis." *Journal of Peptide Science* 22.1 (2016): 4-27.
- [16] García-Martín, Fayna, Peter White, René Steinauer, Simon Côté, Judit Tulla-Puche, and Fernando Albericio. "The synergy of ChemMatrix resin® and pseudoproline building blocks renders Rantes, a complex aggregated chemokine." *Peptide Science: Original Research on Biomolecules* 84.6 (2006): 566-575.
- [17] Christensen, T., A. Eriksson, and L. E. Thornell. "A qualitative test for monitoring coupling completeness in solid phase peptide synthesis using chloranil." *Acta Chem Scand Ser B* 33 (1979).
- [18] Sarin, Virender K., Stephen BH Kent, James P. Tam, and Robert B. Merrifield. "Quantitative monitoring of solid-phase peptide synthesis by the ninhydrin reaction." *Analytical biochemistry* 117.1 (1981): 147-157.

- [19] Brodsky, B.; Li, M.; Long, C. G.; Apigo, J.; Baum, J. NMR and CD Studies of Triple-Helical Peptides. *Biopolymers: Original Research on Biomolecules*. 1992, 32, 447.
- [20] Kotch, F. W.; Raines, R. T. Self-assembly of Synthetic Collagen Triple Helices. *Proceedings of the National Academy of Sciences*. 2006. 103. 3028.
- [21] Hwang, S.; Shao, Q.; Williams, H.; Hilty, C.; Yao, Q. G. Methanol strengthens hydrogen bonds and weakens hydrophobic interactions in proteins—a combined molecular dynamics and NMR study. *The Journal of Physical Chemistry B*. 2011. 115. 6653.
- [22] Cole, J. L.; Lary, J. W.; Moody, T. P.; Laue, T. M. Analytical ultracentrifugation: sedimentation velocity and sedimentation equilibrium. *Methods in cell biology*. 2008. 84. 143.
- [23] Egli, J.; Siebler, C.; Köhler, M; Zenobi, R.; Wennemers, H. Hydrophobic Moieties Bestow Fast-Folding and Hyperstability on Collagen Triple Helices. *J. Am. Chem. Soc.* 2019, 141, 5607.
- [24] Lalande, M.; Comby-Zerbino, C.; Bouakil, M.; Dougard, P.; Chirot, F.; Pouilly, J.C. Isolated Collagen Mimetic Peptide Assemblies Have Stable Triple-Helix Structures. *Chemistry—A European Journal*. 2018. 24. 13728.
- [25] Baum, J.; Brodsky, B. Real-time NMR investigations of triple-helix folding and collagen folding diseases. *Folding and Design*. 1997. 2.4. R53.
- [26] Tanrikulu, I. Caglar, William M. Westler, Aubrey J. Ellison, John L. Markley, and Ronald T. Raines. "Templated Collagen “Double Helices” Maintain Their Structure." *Journal of the American Chemical Society* (2020).
- [27] Wegener, S. V.; Spatz, J. P. Cobalt(III) as a stable and inert mediator ion between NTA and His6-tagged proteins. *Angew. Chem. Int. Ed.* 2013, 52, 7593.
- [28] Campochiaro, Peter A., Janice A. Jerdan, and Bert M. Glaser. "Serum contains chemoattractants for human retinal pigment epithelial cells." *Archives of ophthalmology* 102.12 (1984): 1830-1833.
- [29] Pires, Marcos M., Jeeyeon Lee, Dawn Ernenwein, and Jean Chmielewski. "Controlling the morphology of metal-promoted higher ordered assemblies of collagen peptides with varied core lengths." *Langmuir* 28.4 (2012): 1993-1997.
- [30] ATCC Product Sheet (PCS-100-041). [www.atcc.org/~ps/PCS-100-041.ashx](http://www.atcc.org/~ps/PCS-100-041.ashx).

## CHAPTER 3. THE SELF ASSEMBLY OF A FLUORINATED COLLAGEN MIMETIC PEPTIDE

### 3.1 Introduction

Fluorine substitution is an established method to stabilize triple helical peptides against thermal unfolding.<sup>1</sup> Most collagen mimetic peptides have a core made up of a three-residue repeat, Gly-Xaa-Yaa.<sup>2</sup> The most common residue in the Xaa position is trans-4-hydroxyproline (Hyp). When the hydroxyl group in this residue is replaced with fluorine, peptide triple helices become ultra-stable.<sup>1</sup> The usage of the resulting fluorine substituted amino acid, trans-4-fluoroproline (Flp), in the Xaa position has been used to stabilize collagen mimetic peptides (CMPs) that modulate cancer cell adhesion.<sup>3</sup>

Fluorine induced ultrastability in collagen mimetic peptides relies on stereo-electronic effects in proline rings.<sup>4</sup> Proline rings adopt either an exo or endo ring puckering conformation within peptide chains. Both Flp and Hyp residues preferably adopt the exo conformation (Fig. 3.1). The antibonding node of C-O and C-F orbitals are good electron acceptors due to the high electronegativity of the heteroatoms.<sup>5</sup> As such, electron density in nearby C-H bonding orbitals is donated into these antibonding nodes. This  $\sigma(\text{C-H}) \rightarrow \sigma^*$  interaction enforces the exo conformation in these substituted proline derivatives.

Exo-puckering proline rings pre-organize peptide chains to form a collagen-like triple helix. Within a triple helix, each individual chain takes on a polyproline type II conformation, a structure held together by  $n \rightarrow \pi^*$  interactions between adjacent carbonyl groups.<sup>6</sup> When proline rings adopt an exo-pucker, adjacent carbonyl groups are brought closer together than in the endo conformation (Fig. 3.1). As such,  $n \rightarrow \pi^*$  interactions between amide carbonyl moieties become more favorable in this conformation. This enforces a polyproline type II helix in collagen peptide chains.<sup>7</sup> With the chains pre-organized in the correct conformation, inter-chain hydrogen bonds, originating in glycine residues, can lock in the triple helix.<sup>8</sup>

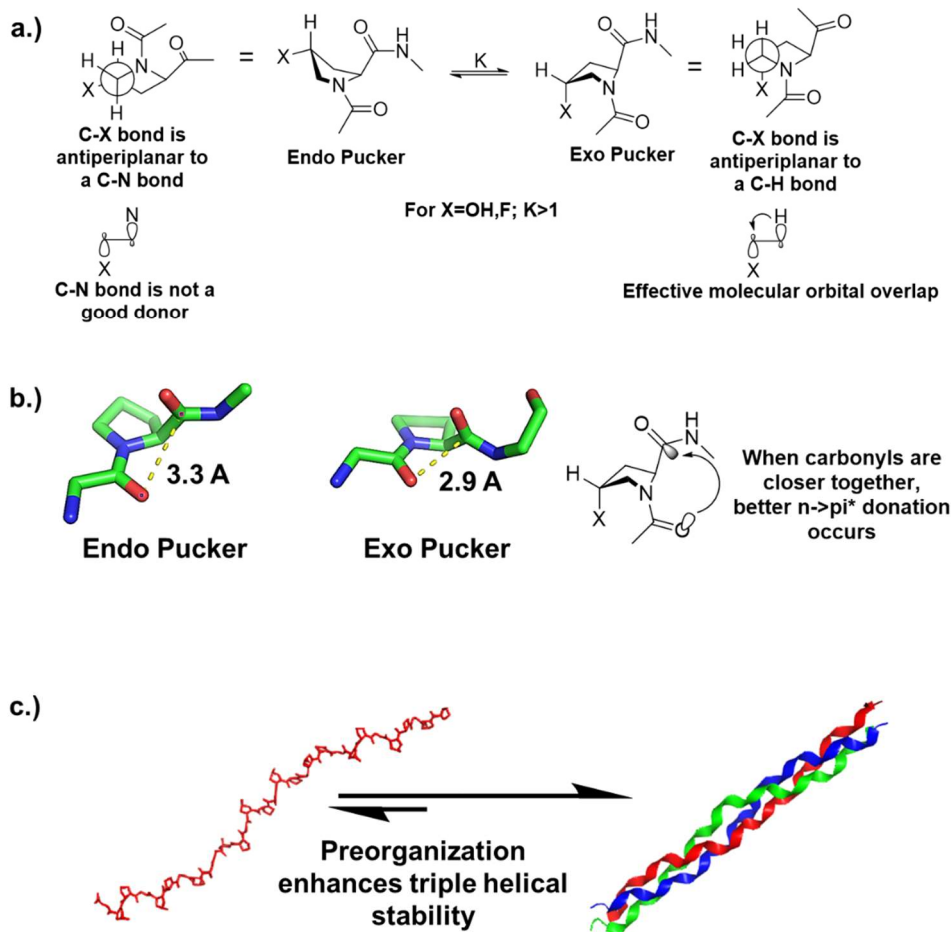


Figure 3.1. Stability of Collagen Triple Helix

The experiments detailed in this chapter will explore the effect of fluorine-induced triple helix stabilization on the metal-triggered self-assembly of CMPs. Previously, the effect of triple helical stability on metal ion-promoted self assembly was explored through varying the number of Pro-Hyp-Gly repeats.<sup>9</sup> Increasing the triplet copy number added more glycine hydrogen bonds and bolstered triple helical thermostability. When too few triplets were used, the resulting CMPs didn't assemble in the presence of metal ions. With 9 repeats or greater, assembly did occur and two types of morphologies were seen: microflorettes and saddle-like particles. This study pointed out the importance of triple helical stability for self-assembly. Fluorine substitution offers a second method to explore this trend. The resulting data can guide future designs towards functional biomaterials.

## 3.2 NCoH7 and NCoH7F

To explore the effect of fluorination, we used NCoH7 as a control CMP to make modifications with (Fig. 3.2). NCoH7 has a core of 7 Pro-Hyp-Gly repeats, a di-histidine moiety at the C-terminus, and an N-terminal nitrilotriacetate.<sup>9</sup> The transition melting temperature ( $T_m$ ) of NCoH7 was found to be 25 °C. Previously, this peptide was found to be incapable of self-assembly under conditions used for NCoH, a peptide with 9 Pro-Hyp-Gly repeats. Herein, we designed the peptide, NCoH7F, in which all Hyp residues were changed to Flp. We hypothesized that the resulting triple helix would be significantly more stable and allow the peptide to self-assemble at room temperature.

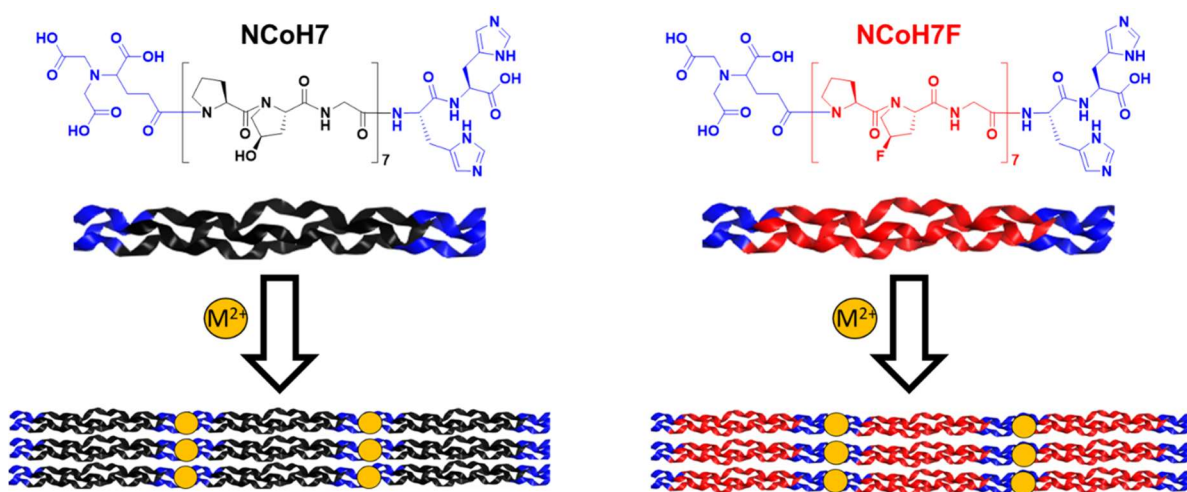


Figure 3.2. The design of NCoH7 and NCoH7F; yellow circles represent metal ions.

## 3.3 Results and Discussion

### 3.3.1 Synthesis of Fmoc-Seg-OH

We found that fmoc-trans-4-fluoropyrillidine carboxylic acid performs poorly when used in solid phase peptide synthesis (SPPS). To circumvent this, we synthesized an Fmoc-protected tripeptide segment, Fmoc-Pro-Flp-Gly-OH (abbreviated as Fmoc-Seg-OH), which can be used to synthesize NCoH7F by SPPS using trimeric segments. Fmoc-Seg-OH was prepared in 5 steps from the commercially available material, N-benzyloxycarbonyl-trans-4-hydroxyproline (Cbz-Hyp) (Fig. 3.3). An intramolecular Mitsunobu reaction was used to invert the stereochemistry of the hydroxyl group. The resulting lactone, **4**, was obtained in moderate yields due to a difficult purification by

flash chromatography. Lactone **4** was opened using the tert-butyl ester of glycine to yield compound **5**. Following this, the cis hydroxyproline residue in dipeptide, **5** was converted to trans fluoroproline using diethylamino sulfur trifluoride (DAST). In two steps, the Cbz protecting group was removed under hydrogenation conditions to reveal the free amine that was coupled to Fmoc-Proline to give **7**. In the final step, the tert-butyl protecting group was removed from **7** to give Fmoc-Seg-OH. This trimeric building block was used in solid phase synthesis to produce NCoH7F.

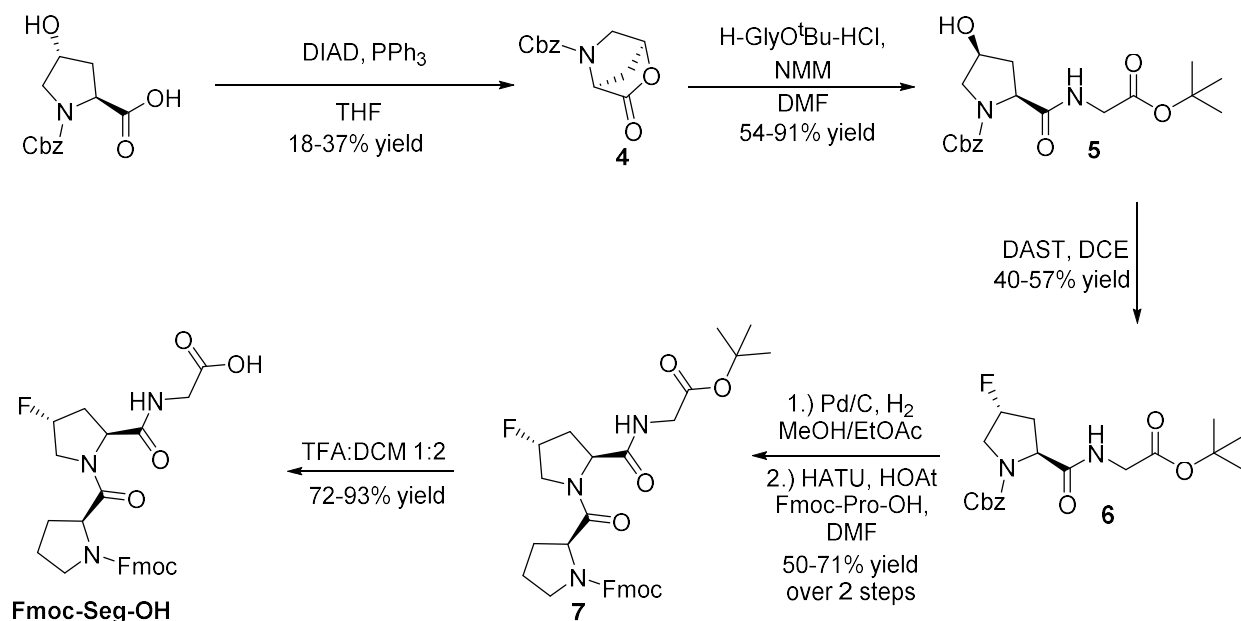


Figure 3.3. The Synthesis of Fmoc-Seg-OH

### 3.3.2 Solid Phase Synthesis of NCoH7F

Fmoc-based solid phase peptide synthesis (SPPS) methods were used to prepare NCoH7F<sup>10</sup> on the Rink Amide Chem-matrix resin.<sup>11</sup> Amino acids or Fmoc-Seg-OH were coupled using HATU, HOAt, and DIEA in DMF. Either the Kaiser-Ninhydrin test, for primary amino acid, or the chloranil method, for proline residues, was used to validate the occurrence of amino acid coupling.<sup>12, 13</sup> Fmoc groups were removed by agitation of the resin in 25% piperidine in DMF for 30 minutes. Coupling and deprotection reactions were repeated until all of the amino acids in the sequence were coupled. To cap the final free amine in the sequence, the protected nitrilotriacetate, **3**, was coupled in a similar manner using HATU, HoAt, and DIEA in DMF. NCoH7F was cleaved from resin using trifluoroacetic acid, TIPS, and water. Reversed Phase High Performance Liquid

Chromatography (RP-HPLC) was used to purify the molecule. For NCoH7F, peaks with complex shapes were seen when the purified compound was injected onto the HPLC instrument. Each of these peaks were identified as the peptide by mass spectrometry and if isolated peaks were re-analyzed, complex shapes were still observed. When a solution of purified NCoH7F, with ethylene diamine tetra-acetic acid (EDTA) added, was boiled, cooled, and then analyzed, two peaks were observed (Fig. 3.4). These were interpreted as the triple helix and the random coil conformations of the NCoH7F peptide. The complex shapes observed before boiling with EDTA are perhaps a result of peptide aggregation during the analysis. Each of these cases would be possible with a stabilized triple helical peptide. Matrix assisted laser desorption/ionization mass spectrometry (MALDI MS) was used to identify the peptide (Fig. 3.4).

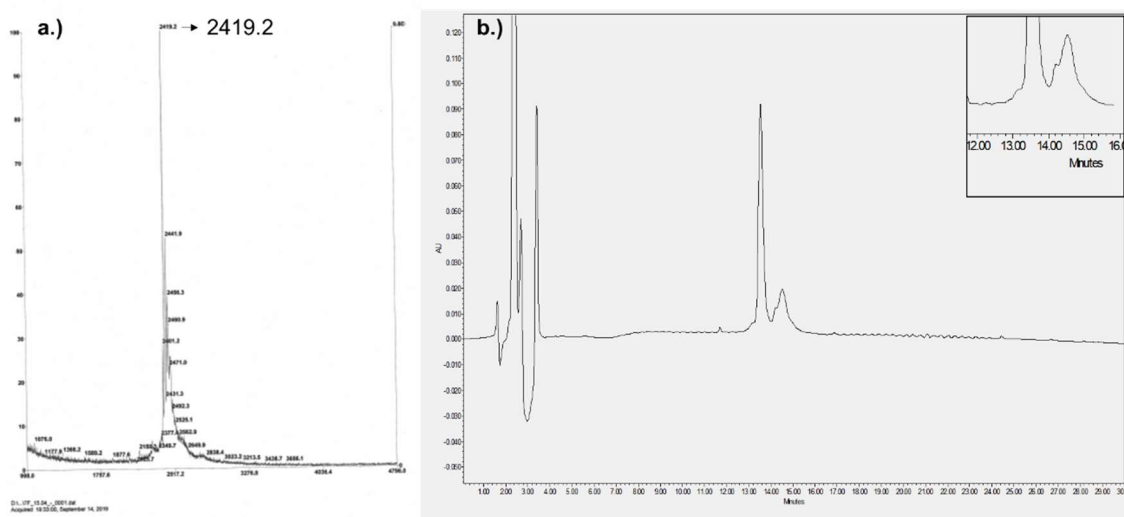


Figure 3.4. a.) MALDI-TOF spectrum showing NCoH7F as well as sodium and potassium adducts. b.) Purified NCoH7F boiled with EDTA prior to HPLC analysis shows 2 peaks, tentatively a random coil and a triple helix.

The hydroxylated peptide, NCoH7, was procured as a gift from Dr. Marcos Pires. This had been prepared as reported previously.<sup>9</sup>

### 3.3.3 Confirming the Triple Helicity of NCoH7 and NCoH7F

Circular dichroism spectroscopy was used to study the secondary structure of the peptides. Both had maximum ellipticities at 225 nm, a characteristic of the type II polyproline helix which each chain in a triple helix adopts (Fig. 3.5). Thermal stabilities of each was measured by monitoring

ellipticity at 225 nm at increasing temperatures. The melting curves observed for each were shown to be sigmoidal, as expected for the cooperative unfolding of a collagen triple helix, and the transition melting temperatures were 25 °C and 46 °C for NCoH7 and NCoH7F, respectively. These studies showed the possibility of triple helix formation. As expected, the folded fluoroproline containing peptide was shown to be significantly more thermally stable as expected.

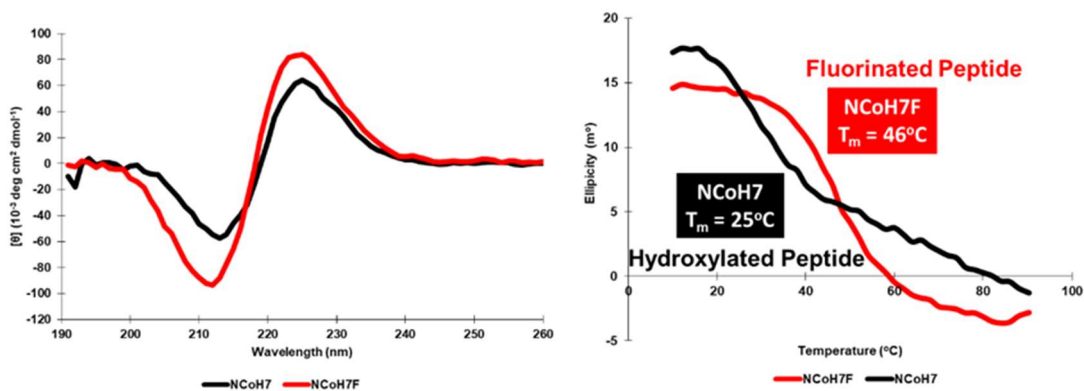


Figure 3.5. Circular Dichroism of 100  $\mu\text{M}$  NCoH7 and 100  $\mu\text{M}$  NCoH7F in 20 mM MOPS.

### 3.3.4 Metal-Triggered Self Assembly

Previously, 1 mM NCoH7 did not assemble and form a precipitate with 400  $\mu\text{M}$   $\text{ZnCl}_2$ , the same conditions used for a different peptide, NCoH.<sup>9</sup> However, it was shown to assemble into an amorphous morphology at 1 mM concentration in the presence of 1 mM  $\text{ZnCl}_2$ . We explored various conditions for assembly to get a better of this peptide's assembly properties. Most metal ions and conditions either gave no assembly or amorphous aggregates (Fig 3.6). With 1 mM NCoH7 and 700  $\mu\text{M}$  cobalt nitrate, however, we achieved the formation of fibrillar elongated particles (Fig 3.6). Considering that both NCoH7 and NCoH-FOGER, from the previous chapter, have a similar cylindroid shape when folded as triple helices, they both should have the ability to assemble into similar structure, albeit under different conditions. The formation of fibrillar particles from NCoH7 and cobalt ions was a validation of this hypothesis. We used these conditions to make direct comparisons of morphology between NCoH7 and NCoH7F assemblies.

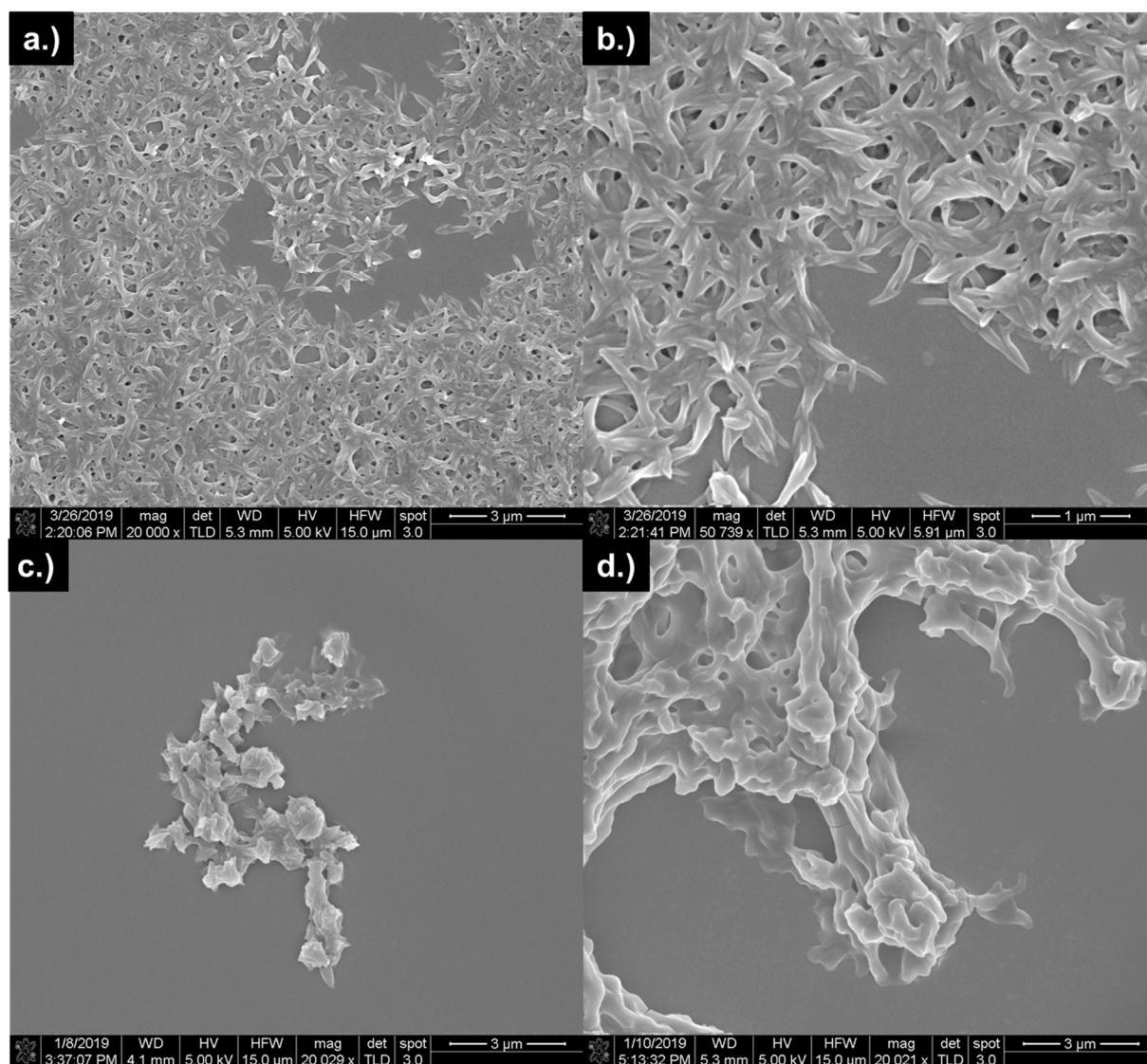


Figure 3.6. Structures formed with 1 mM NCoH7 and 700  $\mu\text{M}$   $\text{Co}(\text{NO}_3)_2$  (a. and b.), 700  $\mu\text{M}$   $\text{ZnCl}_2$  (c.), and  $\text{CuSO}_4$  (d.) in 20 mM MOPS overnight

Treatment of NCoH7F (1 mM) with 700  $\mu\text{M}$  cobalt nitrate also formed fibrillar particles in 20 mM MOPS overnight (Fig. 3.7). These particles were significantly smaller than those formed with NCoH7, however. While NCoH7 formed microparticles, NCoH7F formed nanoparticles. Unlike NCoH7, NCoH7F was capable of self-assembling at lower concentrations and with smaller amounts of metal ions as well. In all cases, metal-ion induced self-assembly of NCoH7F yielded similar elongated tapered particles. In addition, NCoH7F was capable of self-assembling without metal as well but over a much longer period of time. Metal-free self-assembly occurred over the duration of 2 hours while metal-induced self-assembly happened in seconds. The precipitate that

resulted from the metal-free self-assembly of NCoH7 had a flattened extended morphology. These peptide “flakes” were notably different from the fibrillar particles that were formed in the presence of metal. The ability of NCoH7F to self-assemble at lower concentrations than NCoH7 may be a result of its triple helical stability. Clearly, formation of a triple helix is important for metal-triggered self-assembly. A second relevant factor for self-assembly may be hydrophobicity. The decoration of a peptide triple helix with fluorine, instead of hydroxyl groups, may render it relatively hydrophobic. This hydrophobicity may explain NCoH7F’s additional ability to self-assemble without the trigger of a metal ion.

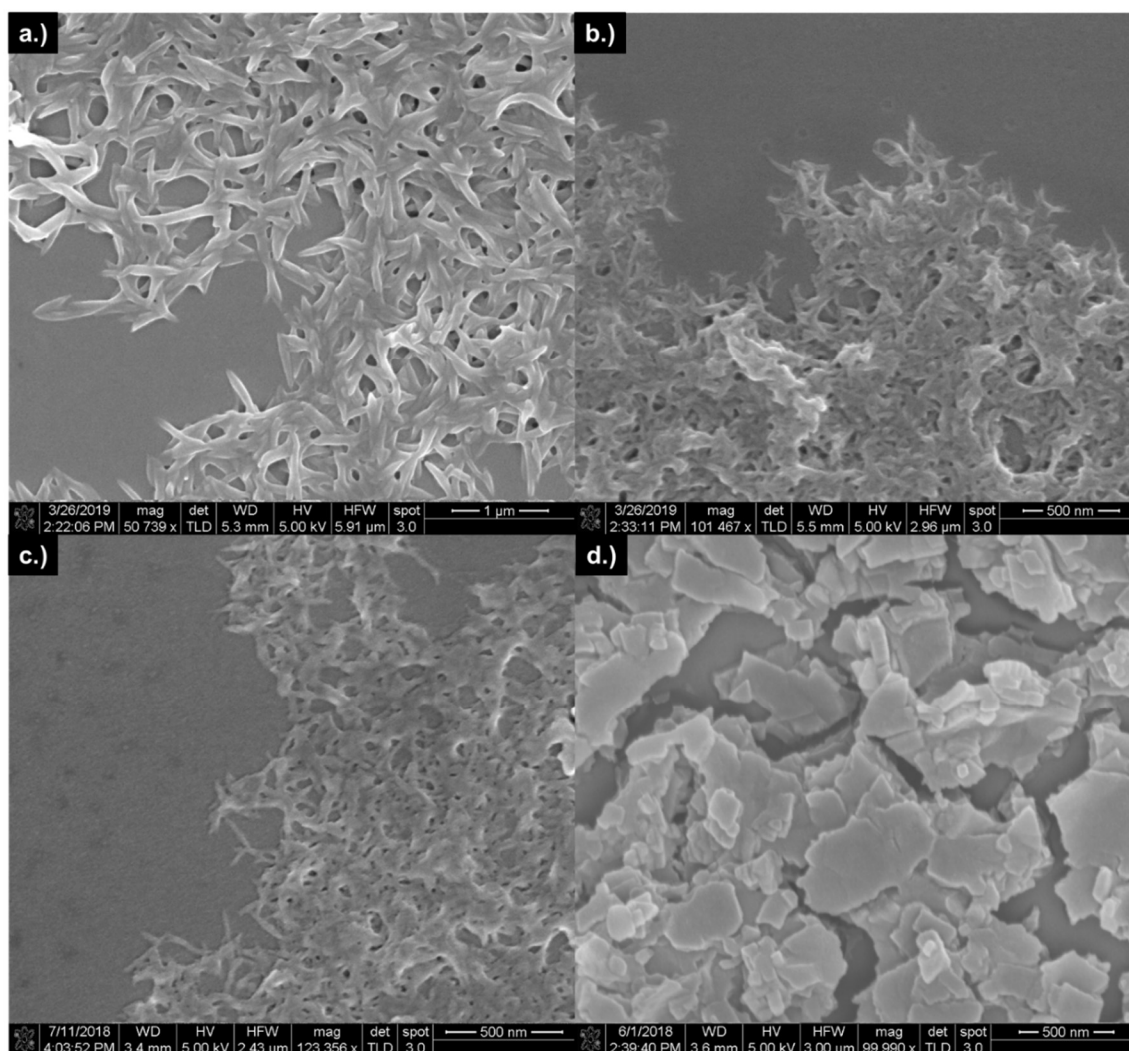


Figure 3.7. Side by side comparison of 1 mM NCoH7 and 1 mM NCoH7F assembly with 700  $\mu\text{M}$   $\text{Co}(\text{NO}_3)_2$  (a. and b., respectively); c.) Assembly of 500  $\mu\text{M}$  NCoH7F and 500  $\mu\text{M}$   $\text{Co}(\text{NO}_3)_2$ ; d.) assembly of 1 mM NCoH7F without any metal over 2h. All assemblies done overnight in 20 mM MOPS.

TEM allowed us to observe the self-assembled particles with much higher resolution (Fig. 3.8). With NCoH7-Co(II) particles, we observed a periodic banding across the surface of the particles perpendicular to the long axis (Fig. 3.9). The pattern could be explained by a linear arrangement of triple helices. TEM revealed the shape of NCoH7F particles in much higher resolution; however, banding was not observed as in NCoH7. The lack of banding is perhaps due to inability to fully resolve particles of such a small size using the chosen instrumental setup.

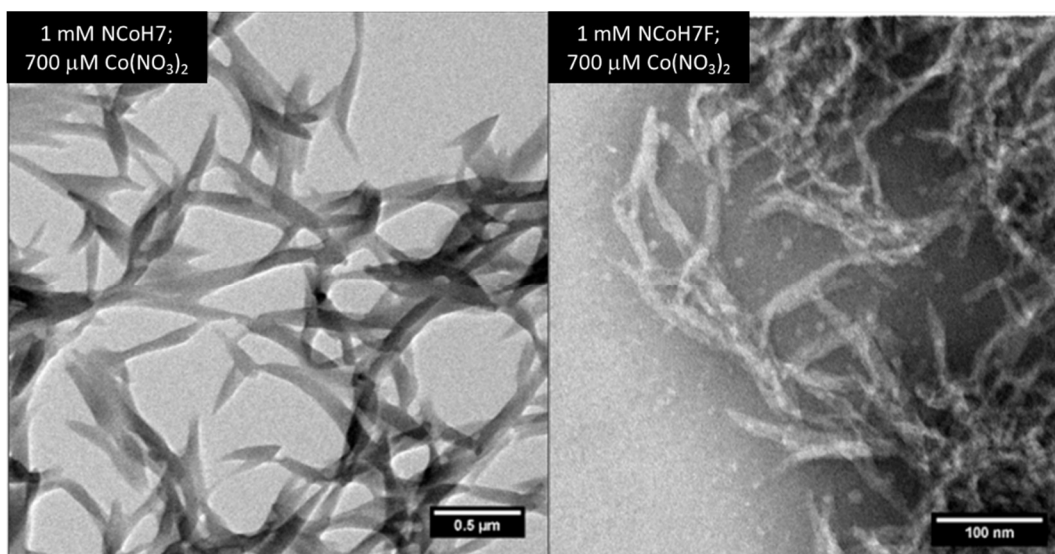


Figure 3.8. Side-by-side comparison of NCoH7 and NCoH7F cobalt(II) assemblies using TEM. Samples are stained with 1% uranyl acetate. All assemblies were prepared in 20 mM MOPS overnight.

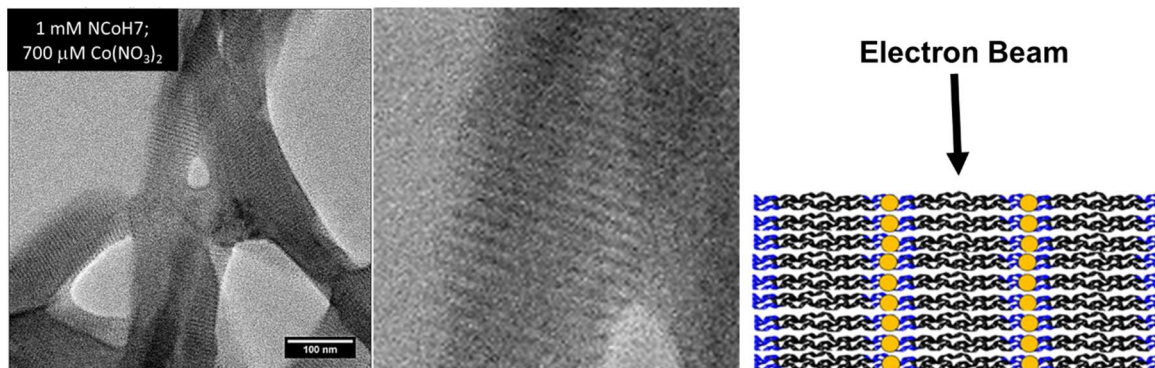


Figure 3.9. Close up of TEM images of NCoH7 assemblies reveals a banding pattern which could be the result of a linear assembly of triple helices.

### 3.3.5 A Discussion of Nucleation and Growth

Nucleation and growth is a two-step mechanism used to describe the formation of crystals, the self-assembly of metal-organic frameworks, the solidification of metal melts, and other materials.<sup>14, 15, 16, 17, 18, 19</sup> Nucleation, the first step, involves the formation of small regions of a solid phase within the continuous liquid phase. These nuclei are often unstable and will tend to dissolve back into solution due to their small size. The second step, growth, occurs when nuclei lasts long enough to become larger and extend into a full domain of the new solid phase. Both nucleation and growth will deplete the soluble species which is forming the new solid phase.<sup>17</sup> Crystallization is a classic example of the interplay of nucleation and growth. When a supersaturated solution begins to crystallize, discrete nuclei form within the continuous liquid phase. If these nuclei are formed too quickly, the concentration of the soluble phase diminishes and there is little driving force for growth to occur. The resulting crystals will be very small.<sup>17</sup> This principle underlies the formation of quantum dot nanocrystals, whose small size is achieved by selecting conditions to favor nucleation and minimize growth.<sup>15</sup> If very few nuclei are formed and further nucleation is hindered, however, the supersaturation of the solution will allow the nuclei to grow into large well-formed crystals.<sup>17</sup> This method is useful in the formation of metal organic frameworks and metallic solids, where large crystals are often desirable.<sup>18, 19</sup> Metal organic frameworks, usually grown at higher temperatures, are formed under conditions where nuclei and crystal defects are rendered soluble. As such, very few nuclei survive long enough to allow for growth to occur. The growth of a small number of nuclei results in large well-formed MOF crystals. Considering the conceptual similarity of our metal-peptide assemblies to metal organic frameworks, we hypothesized that a similar theory could explain our observed results.

The differences of particle size observed between NCoH7 and NCoH7F may be a result of different nucleation rates (Fig. 3.10). We hypothesize a scenario in which peptide triple helices with metal ions would reversibly self-assemble into a nucleus that could then grow into a full particle if it survived long enough. Unfolded random coil chains, at least within this scheme, do not contribute to nucleation and growth of assemblies. With NCoH7F, the stability of the triple helix allows for rapid nucleation. This rapid nucleation would result in very small particle size, in agreement with what is observed. With NCoH7, the triple helix is relatively unstable. As a result, the nucleation is slow and much larger particles are formed. This is also in agreement with experimental

observations. The inability of NCoH7 to self-assemble at lower concentrations, in comparison to NCoH7F, may be explained by the lower rate of nucleation as well. After all, if nucleation does not occur, self-assembly would become impossible. While still just a hypothesis, the nucleation-growth mechanism explains many experimental observables.

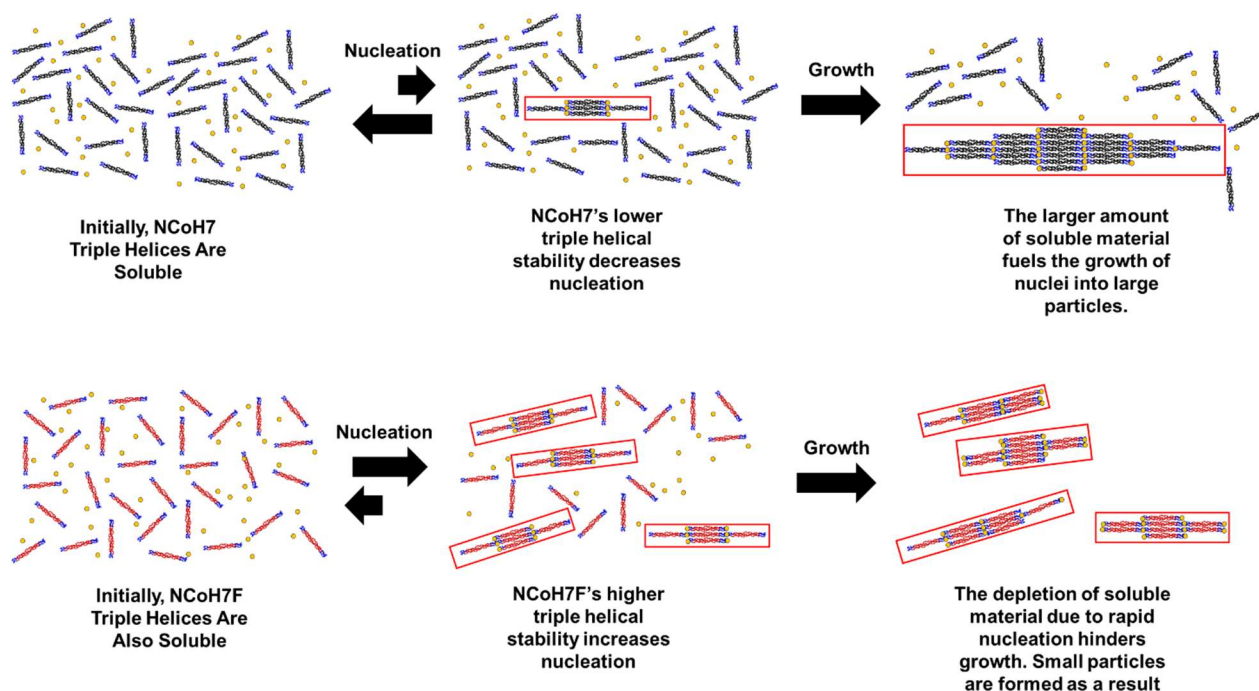


Figure 3.10. A Nucleation and Growth Mechanism May Explain the Particle Sizes Observed in NCoH7 and NCoH7F assemblies

### 3.3.6 Oxidation and Stabilization of Peptide-Cobalt Particles

Having studied the self-assembly of NCoH7 and NCoH7F, we next gauged the stability of assembled particles in phosphate buffered saline, a biologically relevant medium. While NCoH7F-cobalt assemblies remained insoluble in PBS, assemblies from NCoH7 were seen to immediately dissolve. This may be a consequence of NCoH7's lower triple helix stability. As such, we explored the oxidation of these particles by hydrogen peroxide. This would potentially oxidize cobalt (II) to the exchange inert cobalt (III) and render the resulting assemblies stable to dissolution.<sup>20</sup> An oxidation procedure similar to that used for NCoH-FOGER was employed with NCoH7- and NCoH7F-Co(II) assemblies. After assembly overnight, 20  $\mu$ L of 100 mM  $H_2O_2$  was added directly to assembly buffers. The suspensions were incubated for another night and then the solids were

isolated by centrifugation and washing. These oxidized assemblies were then suspended in PBS. Dissolution was not observed visually, indicating that the assemblies were now stabilized. The solids were re-isolated from PBS solution after 24 h and observed using electron microscopy. Expected morphologies were observed were both NCoH7 and NCoH7F assemblies (Fig. 3.11). This indicated that the structures of the particles were resistant to PBS.

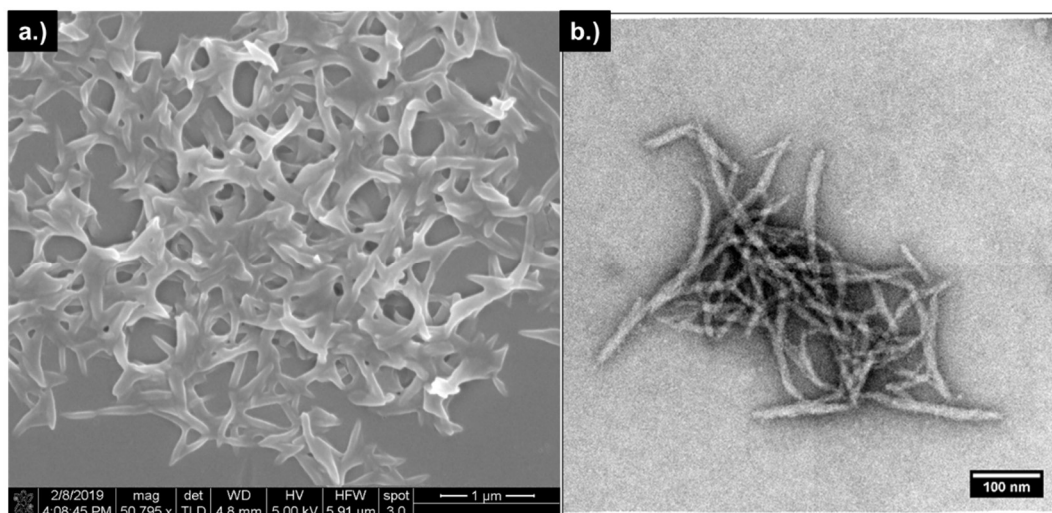


Figure 3.11. Oxidized cobalt assemblies of NCoH7 (a.) and NCoH7F (b.) after suspension in PBS for 24 h.

### 3.4 Conclusion

The substitution of Flp in place of Hyp within a collagen mimetic peptide core increased triple helix stability. In the context of metal triggered self-assembly, fluorination increased the ability of a peptide to self-assemble at lower concentrations. Furthermore, NCoH7, a hydroxylated peptide, self-assembled into large particles while NCoH7F, a fluorinated peptide, formed much smaller particles of a similar morphology. These observations allowed us to postulate that metal triggered self-assembly can be considered a nucleation-growth process.

### 3.5 Materials and Methods

**Materials** Fluorenylmethyloxycarbonyl (Fmoc) protected amino acids were purchased from ChemPep Inc. Hexafluorophosphate azabenzotriazole tetramethyl uronium (HATU), 1-hydroxyazabenzotriazole (HOAt), and N,N'-diisopropylethylamine (DIEA) were purchased from

Chem Impex International Inc. ChemMatrix Rink Amide resin was purchased from PCAS Biomatrix Inc. Trifluoroacetic acid (TFA), triisopropylsilane (TIPS), diethyl ether, piperidine, DAST, triphenylphosphine, DIAD, 10% Pd/C were purchased from Sigma Aldrich. Tert-butyl Glycinate Hydrochloride was purchased from Chem Impex International. Dichloromethane (DCM), methanol (MeOH), N,N'-Dimethylformamide (DMF), tetrahydrofuran (THF), dichloroethane (DCE), and other solvents were purchased from Fisher.

**Synthesis of 4** Cbz-Hyp (1.8 g, 6.6 mmol) and triphenylphosphine (2.1 g, 7.9 mmol) were weighed into a 250 mL roundbottom flask. A stir bar was placed in this flask and the system was sealed with a rubber septum. A nitrogen line was integrated through a syringe needle that pierced through the rubber septum. While stirring, tetrahydrofuran (40 mL) was added using a 50 mL glass syringe. Once the solids had dissolved, the reaction was moved into an ice bath and allowed to cool while stirring for 30 min. After this, di-isopropyl azodicarboxylate (1.6 mL, 7.9 mmol) was added dropwise. The solution first turned yellow when the addition was started and once most of the reagent was added, a white precipitate was observed. The reaction was allowed to stir as the ice bath melted and came to room temperature. After stirring at room temperature overnight, the solvent was removed in vacuo. Afterwards, the yellow oily crude was dried further under higher vacuum. Once dried, a small amount of diethyl ether was added and the crude was sonicated. More diethyl ether was added and the crude was further sonicated as need until dissolution was achieved. Once the yellow oil had dissolved, a white precipitate, triphenylphosphine oxide, formed. The suspension was filtered to remove this solid and the filtrate was dried in vacuo. A minimal amount of DCM was used to transfer the crude product onto a column. The product was purified using flash chromatography (75 mm column diameter, silica packed to a 5 in. height, 7% diethyl ether in DCM was used as an eluent, 100 mL fractions were collected, product was observed starting at fraction 11). The product containing fractions were mixed and concentrated. 900 mg of product **4** was obtained in 57% yield as a white puffy solid.  $^1\text{H}$  NMR (300 MHz,  $\text{CDCl}_3$ ):  $\delta$ 7.36 (m, 5H),  $\delta$ 5.15 (m, 2H),  $\delta$ 5.10 (br. s, 1H),  $\delta$ 3.58 (J = 12 Hz, t, 2H),  $\delta$ 2.24 (J = 12Hz, d, 1H),  $\delta$ 2.04 (J = 12 Hz, d, 1H).

**Synthesis of 5** Tert-butyl Glycinate Hydrochloride (475 mg, 2.83 mmol) was weighed into a 50 mL round bottom flask. A stir bar and DMF (8 mL) was added. The suspension was stirred and trimethylamine (1.97 mL, 14.16 mmol) was added dropwise. As the base was added, the stirring

mixture became even cloudier. This was stirred for 2 hours. The lactone **4** (700 mg, 2.83 mmol) was weighed into a separate flask and dissolved in DMF (7 mL). The solution of **4** was added dropwise into the stirring suspension of tert-butyl glycinate and trimethylamine. The reaction was further stirred for 24 hours. After this, it was poured into deionized water. This aqueous layer was extracted thrice with EtOAc. The organic layers were mixed and extracted twice with 5% citric acid, once with DI water, twice with 5% sodium bicarbonate, and once again with DI water in this order. The organic layer was dried with sodium sulfate, filtered, and concentrated in vacuo to yield the product in 65% yield as a yellowish oil (700 mg). <sup>1</sup>H NMR (300 MHz, CDCl<sub>3</sub>): δ7.34 (m, 5H), δ5.10 (m, 3H), δ4.38 (m, 2H), δ3.92 (J = 18 Hz, qd, 1H), δ3.76 (m, 1H), δ3.59 (m, 2H), δ2.24 (m, 2H), δ1.71 (br. s, 2H), δ1.47 (s, 7H).

**Synthesis of 6** Dipeptide **5** (700 mg, 1.85 mmol) was dissolved in DCE (10 mL) in a 250 mL round bottom flask. The solution was stirred in an ice bath for 20 min. under nitrogen. Diethylamino sulfur trifluoride (293.3 μL, 2.22 mmol) was then added dropwise using a glass syringe. As this reagent was added, the solution began to turn to a cream color and a very small amount of white gas evolved. The gas dissipated within a minute of stirring further. The syringe used to add DAST was washed with DCM and the washings were collected in a beaker. After this, methanol was added to the beaker and used to rinse the syringe in order to neutralize any remaining DAST. The reaction was stirred further in the ice bath for between 30 min. and an hour and monitored by thin layer chromatography (1:4 DCM:Ether, Starting material remains near the baseline, a side product will be observed at the front line, and the desired product will have R<sub>f</sub>=0.6). Once the reaction was completed, methanol was added to quench any remaining DAST and the solvent was removed in vacuo. A minimal amount of DCM was used to load the crude product onto a column. The crude was purified using flash chromatography (60 mm diameter, 5 in. silica height, 1:4 DCM:Diethyl Ether was the eluent, 30 mL fractions were collected; the product eluted at fraction 22). The product containing fractions were mixed and concentrated to give dipeptide **6** (430 mg, 66% yield) as a clear oil, which foamed under high vacuum if any residual solvent was present. <sup>1</sup>H NMR (300 MHz, CDCl<sub>3</sub>): δ7.34 (m, 5H), δ5.14 (m, 3H), δ4.53 (m, 1H), δ3.95 (m, 2H), δ3.65 (m, 1H), δ2.42 (m, 2H), δ1.67 (br. s, 1H), δ1.46 (s, 8H). <sup>19</sup>F NMR (300 MHz, CDCl<sub>3</sub>): δ-178.53 (m, 0.67F), δ-179.64 (m, 0.33F).

**Synthesis of 7** To a flask containing **6** (430 mg, 1.13 mmol), EtOAc (5 mL) and a stir bar were added. The flask was swirled to dissolve the gel-like compound. With the solution stirring, 10% Pd/C (130 mg, 30 wt%) was added portion-wise. Methanol (5 mL) was added along the sides of the flask to wash down the carbonaceous residue. The flask was sealed with a septum, an outlet needle was added, and hydrogen gas, from a balloon, was allowed to flush the flask and move out through the outlet for 20 seconds. After this, the outlet needle was removed and two balloons of hydrogen were affixed. The reaction was monitored by thin layer chromatography (diethyl ether was used as the eluent, the starting material  $R_f=0.7$ , the product was not UV active but could be stained using ninhydrin with heating, the product did not move above the baseline, streaking was observed after ninhydrin treatment). After completion, the solution was filtered through celite to remove Pd/C and the filtrate was concentrated in vacuo. The product was taken forward without any further purification. To the round bottom flask containing this product, DMF (5 mL) and a stir bar were added. The flask was swirled to dissolve the residue. While stirring, reagents were added in the following order allowing 5 min. in between each: N-methylmorpholine (373  $\mu$ L, 3.39 mmol), Fmoc-Pro-OH (381 mg, 1.13 mmol), HOAt (153 mg, 1.13 mmol), and HATU (429 mg, 1.13 mmol). The reaction was stirred for 4h and deionized water was added. This mixture was poured into a separatory funnel and the aqueous layer was extracted thrice with EtOAc. The organic layers were mixed and extracted twice with 5% citric acid, once with DI water, twice with 5% sodium bicarbonate, and once again with DI water in this order. The organic layers were further dried with sodium sulfate and concentrated in vacuo. Flash chromatography was performed (25 mm diameter, 5 in. silica height, 4:1 EtOAc:Hexanes as the eluent, collecting 20 mL fractions, product began to elute at fraction 6). The product containing fractions were mixed and concentrated to give **7** as an oily residue. 1:1 Diethyl ether:hexanes was added and the flask was swirled. The oily residue turned white. The solvents were again removed in vacuo to give **7** as a white puffy solid (400 mg, 63% yield).  $^1\text{H}$  NMR (300 MHz,  $\text{CDCl}_3$ ):  $\delta$ 7.78 (J = 9 Hz, d, 2H),  $\delta$ 7.66 (m, 2H),  $\delta$ 7.42 (J = 6 Hz, t, 2H),  $\delta$ 7.31 (J = 6 Hz, t, 2H),  $\delta$ 5.25 (m, 1H),  $\delta$ 4.73 (m, 1H),  $\delta$ 4.42 (m, 3H),  $\delta$ 4.23 (m, 1H),  $\delta$ 3.81 (m, 2H),  $\delta$ 3.62 (m, 3H),  $\delta$ 2.18 (m, 2H),  $\delta$ 1.96 (m, 2H),  $\delta$ 1.60 (br s, 3H),  $\delta$ 1.44 (s, 4H),  $\delta$ 1.36 (s, 2H).

**Synthesis of Fmoc-Seg-OH** Tripeptide **7** (400 mg, 0.7 mmol) was dissolved in DCM (4 mL). Trifluoroacetic acid was added dropwise (2 mL). The solution was stirred for 3h. The solvents

were removed in vacuo and DCM was added. The solvents were once again removed in vacuo. The repeated addition of DCM and removal of solvents helps to remove residual trifluoroacetic acid. After three rounds of solvent removal, a minimal amount of DCM was used to dissolve the semi-solid residue. Diethyl ether was added and a white precipitate was formed. The solvent was decanted away. Diethyl ether was thrice used to triturate the white solid. The solid product, Fmoc-Seg-OH (330 mg, 92% yield) was then dried under high vacuum. <sup>1</sup>H NMR (300 MHz, CDCl<sub>3</sub>): δ7.77 (J = 9 Hz, d, 2H), δ7.62 (m, 2H), δ7.42 (J = 6 Hz, t, 2H), δ7.31 (J = 6 Hz, t, 2H), δ5.38 (m, 1H), δ4.77 (m, 1H), δ4.44 (m, 3H), δ4.22 (m, 1H), δ3.81 (m, 2H), δ3.52 (m, 3H), δ2.19 (m, 2H), δ1.94 (m, 2H).

**General Peptide Synthesis** Peptides were prepared using standard Fmoc-based synthesis techniques utilizing ChemMatrix Rink Amide resin (100 mg, 0.22 mmol/g). Four equivalents of Fmoc protected amino acids were coupled to equivalent of resin (based on loading) using HATU (4 eq), HOAt (4 eq.) and DIEA (8 eq) dissolved in DMF (10 mL). The amino acid and reagents were mixed and dissolved in DMF (10 mL) and the resulting yellow solution was added to the resin and agitated for 2 hours at room temperature. Afterwards, the resin was washed thrice with 10 mL DMF, thrice with 10 mL DCM, thrice with 10 mL MeOH, and then re-swollen with 10 mL DCM. To deprotect the Fmoc group, the resin was suspended in 10 mL of 25% piperidine in DMF and agitated for 25 minutes. Following this reaction, the resin was washed thrice with 10 mL DMF, thrice with 10 mL DCM, thrice with 10 mL MeOH, and then re-swollen with 10 mL DCM. The ninhydrin-Kaiser test was used to detect free primary amines and the chloranil test was used to detect free secondary amines.<sup>12, 13</sup> Upon completion of the amino acid sequence, nitrilotriacetate **3** (4 eq.) was coupled to the N-terminus of this peptide using HATU (4 eq.), HOAt (4 eq.), and DIEA (8 eq.) in 10 mL DMF for 2 hours. Afterwards, the resin-bound peptide was washed as described previously and dried under reduced pressure. Peptides were cleaved from resin using a cocktail of 10 mL TFA/TIPS/H<sub>2</sub>O (95: 2.5: 2.5) for 1 hour. The reaction mixture was filtered through a frit filter. The filtrates were concentrated under reduced pressure and crude peptide was precipitated by addition of cold diethyl ether (10 mL). The precipitate was collected via centrifugation and the pellet was dried under reduced pressure. The crude product was dissolved in water (3 mL) and purified by semi-preparative RP-HPLC using a Luna C18 (250 x 21.20 mm, 100 Å pore size, 10 micron, Phenomenex) column. The mobile consisted of a linear gradient of 12 mL/min 10 to 80%

solvent A (0.1% trifluoroacetic acid in acetonitrile) in solvent B (0.1% trifluoroacetic acid in water). Fractions were collected based on optical absorption at 214 nm. Product containing fractions were identified using MALDI-TOF mass spectrometry (Calculated: 2422.45; Experimental: 2419.2). These were mixed, concentrated under reduced pressure to remove organic solvents, and lyophilized to yield NCoH7F at 97% purity.

**Circular Dichroism** All circular dichroism (CD) experiments were conducted using a JASCO J-810 spectropolarimeter, equipped with a PFD-425S Peltier temperature control unit. Peptide Stocks (10 mM in filtered water) were thermally annealed by heating at 90°C for 1h followed by slow cooling to room temperature. After overnight incubation in a fridge (~4°C), samples were prepared by dilution of stocks in desired buffers. These buffered samples were placed in a 0.1 cm path-length quartz cuvette and used for CD experiments. Spectra were collected, at room temperature, as an average of 3 scans between 190-260 nm (0.1 nm data pitch, 1 nm bandwidth, 100 nm/min scan rate, and 1 second response time). For temperature dependent experiments, spectra were collected similarly after 5 minute equilibration periods at different temperatures. The signal at 225 nm was plotted as a function of temperature to discern melting behavior. The transition melting temperature ( $T_m$ ) was found using from analysis of the first derivative plots (Change in signal vs. temperature).

**Metal-Ion Promoted Self-Assembly** To a 1.5 mL polypropylene centrifuge tube was added, in the given order, 3-(*N*-morpholino)propanesulfonic acid (MOPS) buffer stock (20  $\mu$ L, 100 mM, pH=7.4), filtered milliQ water, peptide stock (10 mM in water), and metal salt solutions (10 mM in water). Upon mixing, the tube was capped and incubated at room temperature for 16 h. For all experiments, the final concentration of MOPS buffer was 20 mM. The amount of water, peptide, and metal ion solutions were varied to give the desired final concentrations in a total volume of 100  $\mu$ L. If oxidation was needed, 20  $\mu$ L of H<sub>2</sub>O<sub>2</sub> (100 mM in water) was added, after the 16 h incubation period, directly to the suspension, containing cobalt-peptide assemblies, to give a total volume of 120  $\mu$ L. These samples were incubated at room temperature for another 24 h. After incubation, the precipitate-containing samples were centrifuged at 10,000 $\times$  g for three minutes at 4 °C, and the supernatant was removed. Solids were resuspended in water (100  $\mu$ L), and this process was repeated two more times. The solids were then prepared as needed for use in further experiments.

**Scanning Electron Microscopy** Assemblies were prepared as described and re-suspended in 100  $\mu\text{L}$  of DI water. Glass coverslips were affixed to stainless steel stubs using double sided copper tape. Five microliters of assembly suspension (in water) was placed on top of the affixed coverslips and allowed to air dry. Prior to imaging, these samples were sputter coated with platinum for 60 seconds. An FEI-Nova NanoSEM field emission microscope was used to analyze samples. Images were collected using a spot size of 3, accelerating voltage of 5 kV and 30  $\mu\text{m}$  aperture.

**Transmission Electron Microscopy** After preparation, assemblies were suspended in 100  $\mu\text{L}$  of water. Three microliters of these samples were placed onto carbon/formvar coated 400-mesh copper grids, which had been glow discharged prior. These were allowed to stand for 3 minutes and then blotted using filter paper. The sample grids were then passed through a drop of water 16 times followed by passage through a drop of 1% uranyl acetate or 2% phosphotungstic acid for 16 times. These were then blotted on filter paper and allowed to dry under ambient conditions. The sample containing grids were imaged using a Tecnai T20 Transmission Electron Microscope using a 100 kV accelerating voltage and 70  $\mu\text{m}$  objective aperture. Measurements in images were done using ImageJ.

### 3.6 References

- [1] Holmgren, Steven K., et al. "A hyperstable collagen mimic." *Chemistry & biology* 6.2 (1999): 63-70.
- [2] Shoulders, Matthew D., and Ronald T. Raines. "Collagen structure and stability." *Annual review of biochemistry* 78 (2009): 929-958.
- [3] Malkar, Navdeep B., et al. "Modulation of triple-helical stability and subsequent melanoma cellular responses by single-site substitution of fluoroproline derivatives." *Biochemistry* 41.19 (2002): 6054-6064.
- [4] Shoulders, Matthew D., Kimberli J. Kamer, and Ronald T. Raines. "Origin of the stability conferred upon collagen by fluorination." *Bioorganic & medicinal chemistry letters* 19.14 (2009): 3859-3862.
- [5] Hodges, Jonathan A., and Ronald T. Raines. "Stereochemical effects on collagen stability: the dichotomy of 4-fluoroproline diastereomers." *Journal of the American Chemical Society* 125.31 (2003): 9262-9263.
- [6] Newberry, Robert W., and Ronald T. Raines. "The  $n \rightarrow \pi^*$  Interaction." *Accounts of chemical research* 50.8 (2017): 1838-1846.
- [7] Etzkorn, Felicia A., et al. "Conformational Analysis of  $n \rightarrow \pi^*$  Interactions in Collagen Triple Helix Models." *The Journal of Physical Chemistry B* 123.2 (2018): 496-503.

- [8] Erdmann, Roman S., and Helma Wennemers. "Importance of ring puckering versus interstrand hydrogen bonds for the conformational stability of collagen." *Angewandte Chemie International Edition* 50.30 (2011): 6835-6838.
- [9] Pires, Marcos M., et al. "Controlling the morphology of metal-promoted higher ordered assemblies of collagen peptides with varied core lengths." *Langmuir* 28.4 (2012): 1993-1997.
- [10] Behrendt, Raymond, Peter White, and John Offer. "Advances in Fmoc solid-phase peptide synthesis." *Journal of Peptide Science* 22.1 (2016): 4-27.
- [11] García-Martín, Fayna, et al. "The synergy of ChemMatrix resin® and pseudoproline building blocks renders Rantes, a complex aggregated chemokine." *Peptide Science: Original Research on Biomolecules* 84.6 (2006): 566-575.
- [12] Christensen, T., A. Eriksson, and L. E. Thornell. "A qualitative test for monitoring coupling completeness in solid phase peptide synthesis using chloranil." *Acta Chem Scand Ser B* 33 (1979).
- [13] Sarin, Virender K., et al. "Quantitative monitoring of solid-phase peptide synthesis by the ninhydrin reaction." *Analytical biochemistry* 117.1 (1981): 147-157.
- [14] Avrami, Melvin. "Kinetics of phase change. I General theory." *The Journal of chemical physics* 7.12 (1939): 1103-1112.
- [15] Thanh, Nguyen TK, N. Maclean, and S. Mahiddine. "Mechanisms of nucleation and growth of nanoparticles in solution." *Chemical reviews* 114.15 (2014): 7610-7630.
- [16] Bagherzadeh, Elham, et al. "Preparation, optimization and evolution of the kinetic mechanism of an Fe-MIL-88A metal–organic framework." *CrystEngComm* 21.3 (2019): 544-553.
- [17] Vekilov, Peter G. "Nucleation." *Crystal growth & design* 10.12 (2010): 5007-5019.
- [18] Van Vleet, Mary J., et al. "In Situ, time-resolved, and mechanistic studies of metal–organic framework nucleation and growth." *Chemical reviews* 118.7 (2018): 3681-3721.
- [19] Han, K., et al. "Effects of vanadium addition on nucleation and growth of pearlite in high carbon steel." *Materials science and technology* 10.11 (1994): 955-963.
- [20] Wegner, Seraphine V., Franziska C. Schenk, and Joachim P. Spatz. "Cobalt (III)-Mediated Permanent and Stable Immobilization of Histidine-Tagged Proteins on NTA-Functionalized Surfaces." *Chemistry–A European Journal* 22.9 (2016): 3156-3162.
- [21] Pires, Marcos M., Dawn Ernenwein, and Jean Chmielewski. "Selective decoration and release of His-tagged proteins from metal-assembled collagen peptide microflorettes." *Biomacromolecules* 12.7 (2011): 2429-2433.

# PUBLICATION

## Self-Assembled Metal-Collagen Peptide Particles Promote Endothelial Cell Morphogenesis

Vallabh Suresh, Ryan W. Curtis, Courtney D. Rupert, Julia Beck, Jean Chmielewski

**ABSTRACT:** Here, we report a study on the properties of NCoH-FOGER, a collagen mimetic peptide incorporating an integrin-binding cell adhesive sequence. This peptide demonstrated the ability to form particles resembling fibers upon addition of divalent metal cations, as observed by electron microscopy. Upon negative staining, a regular banding pattern is observed on the surface of these particles, a property exhibited by natural collagen. Based on our observations, we propose a structure of linearly arranged triple helices. The peptide demonstrated the ability to cause endothelial cells to form network-like structures.

### Introduction

The fiber forming protein, collagen, directs many cell behaviors through a bioactive sequence, phenylalanine-hydroxyproline-glycine-glutamate-arginine (FOGER).<sup>1,2,3</sup> This sequence has been shown to be important for tube formation by endothelial cells, a process relevant for angiogenesis.<sup>4,5</sup> Collagen-mimetic peptide models bearing the FOGER sequence were found to inhibit the tube formation of cells encapsulated in collagen gels.<sup>5</sup> The peptides are thought to function by binding and blocking integrins, the receptors that interact with the FOGER sequence.<sup>5,6</sup> Similarly, antibodies blocking the relevant integrins also inhibited tube formation.<sup>4</sup> However, when these integrins were clustered with a system of two antibodies, intracellular actin polymerization, a process associated with tube formation, was observed. It is therefore conceivable that collagen presents the FOGER sequence in a polyvalent manner that leads to integrin clustering and not just simple binding.<sup>7</sup>

The higher order self-assembly of collagen-mimetic peptides has yielded a variety of different biomaterials that

mimic natural collagen matrices.<sup>8,9,10,11,12,13,14,15,16</sup> In many cases, cell adhesive sequences, like FOGER and RGD, are included within these materials in an effort to confer bioactivity.<sup>17,18,19,20</sup> Well plate surfaces treated with FOGER displaying collagen peptide amphiphile nanofibers or peptide-lanthanide frameworks displayed enhanced potential for cell adhesion.<sup>17,20</sup> Adsorption of FOGER containing peptides on titanium and polycaprolactone surfaces lead to enhanced implant osseointegration.<sup>21,22</sup> Adsorbed FOGER peptides also showed strong activity in the induction of thrombus formation.<sup>23</sup> Polyethylene glycol gels incorporating the sequence, like natural collagen gels, direct the formation of human umbilical vein endothelial cell (HUVEC) networks.<sup>24</sup> Herein, we describe fibrillar particles prepared from the transition metal dependent self-assembly of a collagen mimetic peptide, NCoH-FOGER. These cell adhesive particles are able to direct the morphogenesis and network formation of HUVEC cells in an actin-associated process.

### Results and Discussion

**Peptide Design.** The core of the NCoH-FOGER peptide is made up of the cell-adhesive FOGER sequence, flanked by repeat POG sections for promoting triple helix formation. At the C- and N-termini, respectively, NCoH-FOGER was constructed with dihistidine and nitrilotriacetic acid (NTA) motifs. These would enable metal-dependent self-assembly in a linear head-to-tail manner (Figure 1). Based on this, we hypothesized that the resulting assembled materials would exhibit a regular polyvalent pattern of cell adhesive ligands to promote integrin clustering. The linear self-assembly based design is similar to a previously reported peptide, NCoH.<sup>16</sup>

triple helix consists of a trimer of polyproline type II helices. This type of a structure is known to display cooperative unfolding.<sup>25</sup> We monitored the ellipticity at 225 nm as a function of temperature. The resulting curve showed sigmoid character, indicating cooperativity, with a transition melting temperature ( $T_m$ ) at 30°C (Supporting Information). Similar studies were performed with peptide dissolved in buffered aqueous methanol. The triple helix is known to be highly stable in aqueous methanol.<sup>26</sup> This may be due to the lower competition from the solvent for the hydrogen bonds that hold the structure together.<sup>27</sup> The CD spectrum in aqueous methanol was nearly identical to that

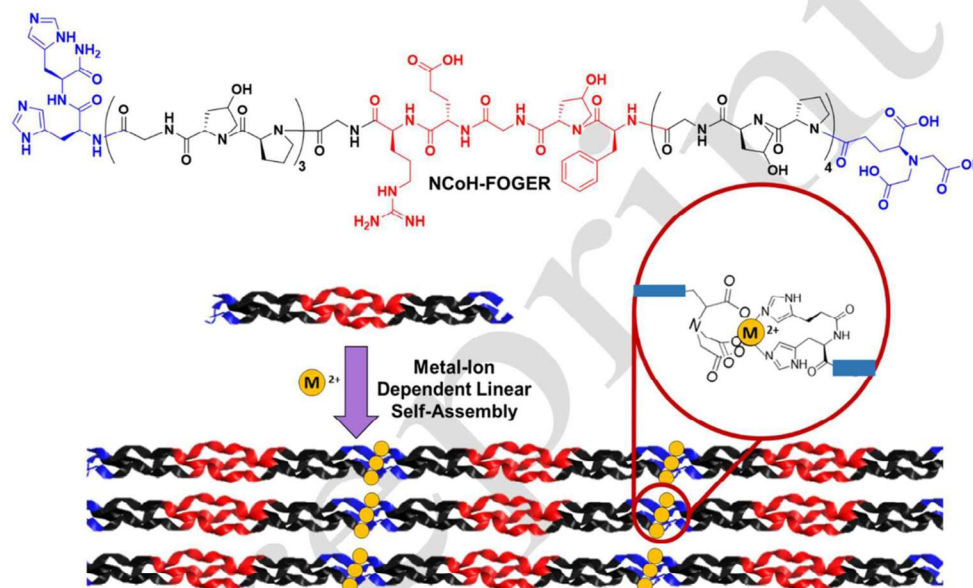


FIGURE 1. The Structure of the peptide, NCoH-FOGER, and a schematic of its metal-ion dependent self-assembly

**Synthesis and Identification of NCoH-FOGER.** NCoH-FOGER was synthesized using Fmoc-based solid phase techniques on Rink Amide ChemMatrix resin. A tert-butyl protected NTA unit was synthesized by known and coupled to the N-terminus of the peptide.<sup>16</sup> Once the sequence and modifications were completed, the peptide was cleaved from resin using a trifluoroacetic acid cocktail, purified to homogeneity using reversed phase high performance liquid chromatography, and identified using Matrix Assisted Laser Desorption/Ionization (MALDI) mass spectrometry.

**Solution State Structural Characterization of NCoH-FOGER.** The circular dichroism spectrum of NCoH-FOGER was determined in 3-N-morpholinopropane sulfonic acid (MOPS) buffer at pH 7.4. A strong positive ellipticity was observed at 225 nm, indicating a polyproline type II helix (Supporting Information).<sup>25</sup> A collagen-like

triple helix structure was observed in totally aqueous solution. Temperature dependent CD spectroscopy showed a cooperative transition with a  $T_m$  of 52°C, indicating significant stabilization of the folded structure in methanol. These CD spectral characteristics and the thermal stabilization of NCoH-FOGER in aqueous methanol are consistent with a triple helical structure.

We next interrogated the tentative triple helical structure by a combination of analytical ultracentrifugation (AUC) and native ion-mobility spectrometry (IMS) to measure the oligomerization states of NCoH-FOGER. AUC, a technique previously used for other triple helices, revealed solution state species with masses of 9.15 and 6 kDa.<sup>26</sup> These corresponded to the expected trimer and a dimer with a ratio of about 2 to 1 in solution. At lower concentrations of peptide, however, only larger masses (>10 kDa) were observed and given that these could not be assigned, optical artefacts in the AUC data were suspected.<sup>28</sup> Native IMS, used by the groups of Wennemers and Pouilly

previously, was therefore also employed and confirmed the presence of a dimer and trimer across a range of concentrations.<sup>29,30</sup> Isotopic abundance calculations agreed with the 2 to 1 ratio of trimer to dimer. Put together, CD, AUC, and IMS suggest that NCoH-FOGER is capable of forming a triple helical structure but also to lesser extent, a dimeric species. Dimeric species have been detected previously by real-time NMR investigations of collagen peptide folding.<sup>31</sup>

**Characterizing the Metal Dependent Self-Assembly of NCoH-FOGER in Buffered Solution.** Transition metal salt solutions were added to buffered solutions of NCoH-FOGER. Upon addition of Zn(II), Cu(II), or Co(II) ions, turbidity was observed within 1 min. This behavior was not observed with the addition Ni(II) ions. Monitoring of the absorbance of the solutions at 360 nm confirmed the observed turbidity and showed that it did not occur with Ni(II) or when metal ions were not added (Supporting Information). To further confirm that metal ions were involved in the self-assembly process, ethylenediaminetetraacetic acid (EDTA), a competing metal chelator, was added to the solution. This removed any turbidity observed in the solution indicating that metal chelation is important in this self-assembly process.

Dynamic light scattering analysis showed that under conditions where turbidity was observed, hydrodynamic radii were found to be greater than a micron with a high polydispersity (Supporting Information). The sizes observed are outside the range in which this technique can be considered accurate so this data was used to qualitatively confirm that a large precipitate had, in fact, formed within the solution. The hydrodynamic radius of the unassembled peptide in solution was found to be about 4 nm, which is in agreement with previously reported peptides.<sup>16, 29</sup> Upon addition of Ni(II), we observed that the hydrodynamic radius increased to about 13 nm. This is perhaps due to a much lower level of self-assembly in solution that does not yield an isolable precipitate.

**Morphology of the Precipitated Materials.** Scanning electron microscopy (SEM) was used to observe the morphology of precipitated assemblies. These precipitates were centrifuged, washed to remove buffer, and dried onto coverslips for analysis. SEM revealed that the precipitate consisted of petal-like or fibrillar particles, regardless of whether Zn(II), Co(II) or Cu(II) was used (Figure 2). These structures can be characterized as being elongated with tapered ends, a morphology reminiscent of natural collagen fibrils.<sup>32</sup> To get a better understanding of the self-assembly process, the morphology of Co(II) assemblies was determined as a function of metal ion and peptide concentrations (Supporting Information). Increasing the metal ion concentration tended to decrease the length of the observed particles. Increasing the concentration of NCoH-FOGER generally tended to do the same above a threshold concentration of 300  $\mu$ M. At or below this value, particles looked to be damaged or not fully formed. The widths of particles measured were found to be close 0.2 microns in all cases.

To further observe the fine structure of the particles, transmission electron microscopy (TEM) was employed. Negative staining with uranyl acetate or phosphotungstic acid revealed that the assemblies display a banding pattern occurring with a periodicity of 9-10 nm (Figure 2). This pattern was thought to be a result of the linear arrangement of triple helices, each having a length between 9 and 10 nm. This length is similar to that observed for other collagen mimetic peptides with the same number of residues. This possible linear arrangement of peptides also suggests that cell adhesive motifs will be displayed in 10 nm intervals at the surface of the particles.

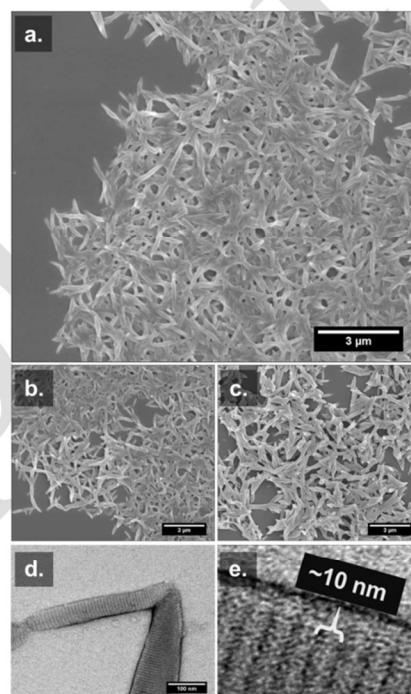


FIGURE 2. SEM Images of Assemblies formed from NCoH-FOGER (1 mM) in 20 mM MOPS Buffer (pH 7.4) with 300  $\mu$ M (a)  $\text{Co}(\text{NO}_3)_2$ , (b)  $\text{CuSO}_4$ , and (c)  $\text{ZnCl}_2$ . (d) TEM of uranyl acetate stained zinc assemblies showing a 10 nm regular banding pattern possibly due to linear organization of triple helices.

**Particle Stabilization and Fluorescent Tagging.** In preparing the petal shaped assemblies for biological experiments, we found that they were disrupted and dissolved by phosphate buffered saline (PBS) and Dulbecco's minimal eagle medium (DMEM), two solutions commonly used in cell culture. Regardless of the divalent metal ion used, full solubility was observed visually in PBS within 30 seconds. Stabilizing the assemblies against dissolution was required to test their activity in cell-based assays. As such,

we hypothesized that the Co(II) ions within an assembly with this metal could be oxidized to exchange-inert Co(III) ions. A previous work has shown that chelation with Co(II) and subsequent oxidation of the complexes to Co(III) can be used to permanently immobilize hexahistidine-tagged proteins on surfaces.<sup>33</sup> Assemblies formed from 1 mM NCoH-FOGER and 1 mM  $\text{Co}(\text{NO}_3)_2$  were resuspended with hydrogen peroxide. To our delight, the oxidation resulted in particles that retained their morphological characteristics and were stable when suspended in both PBS and DMEM (Figure 3.). Incubation in these media for 24 h did not disrupt the periodic banding as observed by TEM. Furthermore, the particles could be fluorescently tagged with His<sub>6</sub>Rhodamine after a light treatment with zinc ions, allowing them to be tracked via fluorescence microscopy. With increased stability and fluorescent tagging achieved, we next began experiments with endothelial cells.

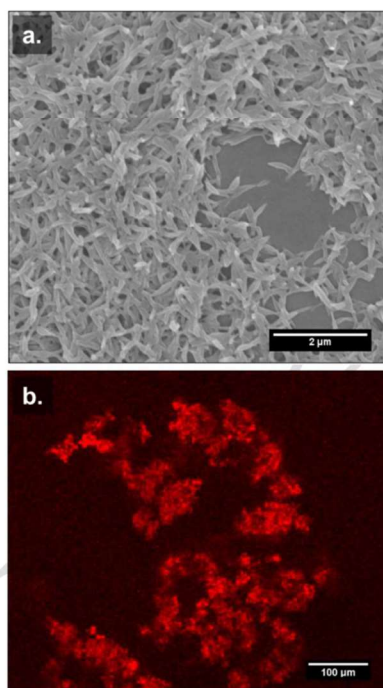


FIGURE 3.  $\text{H}_2\text{O}_2$  oxidized and His<sub>6</sub>Rhodamine tagged Cobalt-NCoH-FOGER (Each 1 mM during preparation) imaged by (a) SEM after being resuspended in DMEM media for 24 h. (b) Fluorescence Microscopy of same particles suspended in DMEM media.

#### Endothelial Cell Adhesion and Morphogenesis.

When HUVEC cells were incubated with NCoH-FOGER cobalt assemblies in complete DMEM media, we observed that clumps were formed between cells, stained for viability with calcein AM, and the red fluorescent material. The

morphology of the cells in the clumps was rounded, a characteristic of cells in 3-dimensional culture (Supporting Information).<sup>18</sup> This experiment showed that the particles and the cells could adhere to each other. However, when HUVEC were incubated with the assemblies in serum free DMEM media, we observed the formation of networks of elongated cells within 4h (Figure 4). These resembled previously reported tube-like structures that formed when a monolayer of cells were treated with collagen I in similar serum free conditions.<sup>4</sup> Senger and coworkers have suggested that such structures are formed as a result of integrin clustering and signaling.<sup>4</sup> The observation of this behavior with our materials suggests that a similar morphogenetic process could be occurring. A polyvalent presentation of integrin binding FOGER sequences, capable of clustering integrins, is perhaps important for morphogenesis as induced both type I collagen and for our assemblies. Control experiments showed that the morphogenesis was not induced by non-oxidized assembly, soluble peptide, or  $\text{Co}(\text{NO}_3)_2$  alone. When conducted with rhodamine tagged assemblies, the tubes seemed to have lower quality suggesting the rhodamine might be sterically blocking the integrin binding sites. Nevertheless, tube-like structures did form and the fluorophore allowed us to confirm that the cells were, in fact, bound to the material. As observed qualitatively through calcein staining, there was not any significant loss of viability.

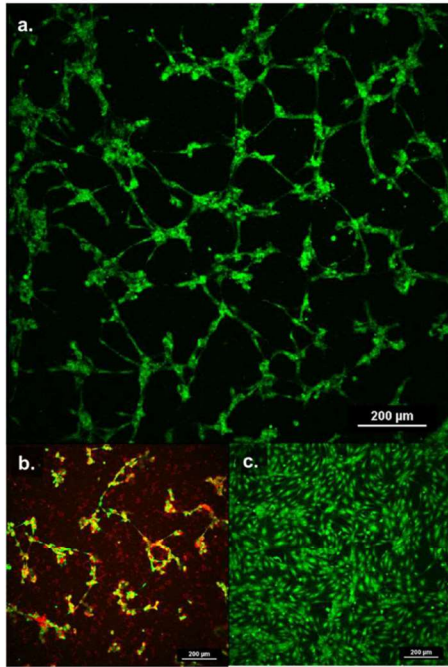


FIGURE 4. (a.) HUVEC cells (Stained Green with Calcein AM) treated with oxidized NCoH-FOGER cobalt assemblies change shape and form network-like structures. (b) Cells treated with His<sub>6</sub>Rhodamine tagged assemblies (Red). (c) Untreated Cells in serum free media.

In previous literature, the early stages of the shape change was shown to be correlated with actin polymerization.<sup>4</sup> To interrogate this, we fixed and stained cells undergoing morphogenesis with FITC-phalloidin, which is selective for F-actin. Fluorescence microscopy revealed that the cells treated with NCoH-FOGER-Cobalt assemblies displayed long actin fibers while in the negative control, the green fluorescence seemed to localize near the nuclei of cells (Figure 5). This data is similar to that observed previous for cells treated with type I collagen.<sup>4</sup> Taken together, this suggests that the shape changes observed are perhaps driven by actin polymerization. This lends support to establishing that the morphogenesis observed here may be similar to that seen by Senger and Coworkers.<sup>4</sup>

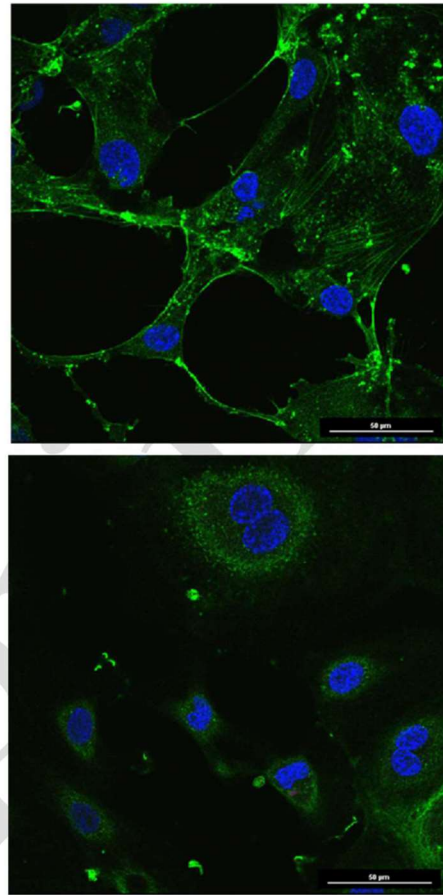


FIGURE 5. Fixed HUVEC cells stained with FITC-phalloidin (green) to show actin and Hoescht (blue) to show the nucleus. (a) Treated with oxidized NCoH-FOGER cobalt assemblies for 2h prior to fixing. (b) Untreated cells.

**Conclusion.** In summary, NCoH-FOGER, a collagen mimetic peptide containing an integrin binding sequence, is capable of forming a triple helix and self-assembling in a metal dependent manner into fibrillar particles. Oxidation stabilizes these to dissolution in biologically relevant. These particles were found to be capable of inducing endothelial cell to elongate and form connected networks in a similar way to type I collagen in a previous work. The periodic banding observed at their surfaces by TEM suggests that they likely display many copies of the integrin binding sequence. Thus, the observed bioactivity may be related to the particles' ability to cluster integrin receptors. Phalloidin staining showed that actin polymerization is involved in the material induced morphogenesis of endothelial cells, illustrating further its similarity with the type I collagen induced process. These studies may pave the way

for future cell-directing biomaterials with potential application in wound healing. Future studies will further unravel the nature of the morphogenetic process observed here and compare it to that seen with collagen I.

## REFERENCES

- (1) Hynes, R. O. Integrins: versatility, modulation, and signaling in cell adhesion. *Cell*. 1992, 69, 11.
- (2) Knight, C.G.; Morton, L.F.; Peachey, A.R.; Tuckwell, D.S.; Farndale, R.W.; Barnes, M.J. The collagen-binding A-domains of integrins  $\alpha(1)\beta(1)$  and  $\alpha(2)\beta(1)$  recognize the same specific amino acid sequence, GFOGER, in native (triple-helical) collagens. *J Biol Chem*. 2000; 275, 35.
- (3) Knight, C.G.; Morton, L.F.; Onley, D.J.; Peachey, A.R.; Messent, A.J.; Smethurst, P.A.; Tuckwell, D.S.; Farndale, R.W.; Barnes, M.J. Identification in collagen type I of an integrin  $\alpha(2)\beta(1)$ -binding site containing an essential GER sequence. *J Biol Chem*. 1998, 273, 33287.
- (4) Whelan, M. C.; Senger, D. R. Collagen I Initiates Endothelial Cell Morphogenesis by Inducing Actin Polymerization Through Suppression of Cyclic AMP and Protein Kinase A. *J. Biol. Chem*. 2003, 278, 327.
- (5) Sweeney, S. M.; DiLullo, G.; Slater, S. J.; Martinez, J.; Iozzo, R. V.; Lauer-Fields, J. L.; Fields, G. B.; San Antonio, J. D. Angiogenesis in Collagen I Requires  $\alpha(2)\beta(1)$  ligand of a GFP-GER Sequence and Possibly p38 MAPK Activation and Focal Adhesion Disassembly. *J. Biol. Chem*. 2003, 278, 30516.
- (6) Emsley, J.; Knight, C. G.; Farndale, R. W.; Barnes, M. J. Structure of the Integrin  $\alpha(2)\beta(1)$ -binding Collagen Peptide. *J. Mol. Bio*. 2004, 335, 1019.
- (7) Karimi, F.; O'Connor, A. J.; Qiao, G. G.; Heath, D. E. Integrin Clustering Matters: A Review of Biomaterials Functionalized with Multivalent Integrin-Binding Ligands to Improve Cell Adhesion, Migration, Differentiation, Angiogenesis, and Biomedical Device Integration. *Adv. Healthc. Mater*. 2018, 7, 1701324.
- (8) Paramonov, S.E.; Gauba, V.; Hartgerink, J.D. Synthesis of Collagen-like Peptide Polymers by Native Chemical Ligation. *Macromolecules*. 2005; 38, 7555.
- (9) Cejas, M. A.; Kinney, W. A.; Chen, C.; Vinter, J. G.; Almond, H. R. Jr; Balss, K. M.; Maryanoff, C. A.; Schmidt, U.; Breslav, M.; Mahan, A.; Lacy, E.; Maryanoff, B. E. *Proc. Natl. Acad. Sci. U S A*. 2008, 105, 8513.
- (10) Jiang, T.; Xu, C.; Liu, Y.; Liu, Z.; Wall, J. S.; Zuo, X.; Lian, T.; Salaita, K.; Ni, C.; Pochan, D.; Conticello, V. P. *J. Am. Chem. Soc*. 2014, 136, 4300.
- (11) Tanrikulu, I. C.; Forticaux, A.; Jin, S.; Raines, R. T. Peptide tessellation yields micrometre-scale collagen triple helices. *Nat. Chem*. 2016, 8, 1008.
- (12) Rele, S.; Song, Y.; Apkarian, R. P.; Qu, Z.; Conticello, V. P.; Chaikof, E. L. D-Periodic Collagen-Mimetic Microfibers. *J. Am. Chem. Soc*. 2007, 129, 14780.
- (13) Przybyla, D. E.; Rubert-Pérez, C. M.; Gleaton, J.; Nandwana, V.; Chmielewski, J. Hierarchical Assembly of Collagen Peptide Triple Helices into Curved Disks and Metal Ion-Promoted Hollow Spheres. *J. Am. Chem. Soc*. 2013, 135, 3418.
- (14) Pires, M. M.; Przybyla, D. E.; Chmielewski, J. A Metal-Collagen Peptide Framework for Three-Dimensional Cell Culture. *Angew. Chem. Int. Ed*. 2009, 48, 7813.
- (15) Pires, M. M.; Przybyla, D. E.; Rubert-Pérez, C. M.; Chmielewski, J. Metal-Mediated Tandem Coassembly of Collagen Peptides into Banded Microstructures. *J. Am. Chem. Soc*. 2011, 133, 14469.
- (16) Pires, M. M.; Chmielewski, J. Self Assembly of Collagen Peptides into Microfibrilles via Metal Coordination. *J. Am. Chem. Soc*. 2009, 131, 2706.
- (17) Sun, X.; Liu, Z.; Xu, X.; Wang, S.; Guo, C.; Xiao, J. A self-assembling collagen mimetic peptide system to simultaneously characterize the effects of osteogenesis imperfecta mutations on conformation, assembly and activity. *Journal of Materials Chemistry B*. 2019, 7, 3201.
- (18) Hernandez-Gordillo, V.; Chmielewski, J. Mimicking the extracellular matrix with functionalized, metal-assembled collagen peptide scaffolds. *Biomaterials*. 2014, 35, 7363.
- (19) Chen, J.; Zou, X. Self-assemble peptide biomaterials and their biomedical applications. *Bioactive Materials*. 2019, 4, 120.
- (20) Luo, J.; Tong, Y.W. Self-assembly of collagen-mimetic peptide amphiphiles into biofunctional nanofiber. *ACS Nano*. 2011, 5, 7739.
- (21) Wojtowicz, A. M.; Shekaran, A.; Oest, M.E.; Dupont, K.M.; Templemen, K.L.; Hutmacher, D.W.; Guldberg, R.E.; Garcia, A.J. Coating of biomaterial scaffolds with the collagen-mimetic peptide GFOGER for bone defect repair. *Biomaterials*. 2010, 31, 2574.
- (22) Reyes, C.D.; Petrie, T.A.; Burns, K.L.; Schwartz, Z.; Garcia, A.J. Biomolecular surface coating to enhance orthopaedic tissue healing and integration. *Biomaterials*. 2007, 28, 3228.
- (23) Munnix, I.C.A.; Gilio, K.; Siljander, P.R.M.; Raynal, N.; Feijge, M.A.H.; Hackeng, T.M.; Deckmyn, H.; Smethurst, P.A.; Farndale, R.W.; Heemskerk, J.W.M. Collagen-mimetic peptides mediate flow-dependent thrombus formation by high-or low-affinity binding of integrin  $\alpha(2)\beta(1)$  and glycoprotein VI. *Journal of Thrombosis and Haemostasis*. 2008, 6, 2132.
- (24) Garcia, J. R.; Clark, A. Y.; Garcia, A. J. Integrin-specific hydrogels functionalized with VEGF for vascularization and bone regeneration of critical-size bone defects. *Journal of biomedical materials research Part A*. 2016, 104, 889.
- (25) Brodsky, B.; Li, M.; Long, C. G.; Apigo, J.; Baum, J. NMR and CD Studies of Triple-Helical Peptides. *Biopolymers: Original Research on Biomolecules*. 1992, 32, 447.
- (26) Kotch, F. W.; Raines, R. T. Self-assembly of Synthetic Collagen Triple Helices. *Proceedings of the National Academy of Sciences*. 2006, 103, 3028.
- (27) Hwang, S.; Shao, Q.; Williams, H.; Hilty, C.; Yao, Q. G. Methanol strengthens hydrogen bonds and weakens hydrophobic interactions in proteins—a combined molecular dynamics and NMR study. *The Journal of Physical Chemistry B*. 2011, 115, 6653.
- (28) Cole, J. L.; Lary, J. W.; Moody, T. P.; Laue, T. M. Analytical ultracentrifugation: sedimentation velocity and sedimentation equilibrium. *Methods in cell biology*. 2008, 84, 143.
- (29) Egli, J.; Siebler, C.; Köhler, M.; Zenobi, R.; Wennemers, H. Hydrophobic Moieties Bestow Fast-Folding and Hyperstability on Collagen Triple Helices. *J. Am. Chem. Soc*. 2019, 141, 5607.
- (30) Lalonde, M.; Comby-Zerbino, C.; Bouakil, M.; Dougard, P.; Chirot, F.; Pouilly, J.C. Isolated Collagen Mimetic Peptide Assemblies Have Stable Triple-Helix Structures. *Chemistry—A European Journal*. 2018, 24, 13728.
- (31) Baum, J.; Brodsky, B. Real-time NMR investigations of triple-helix folding and collagen folding diseases. *Folding and Design*. 1997, 2.4, R53.
- (32) Graham, H. K.; Holmes, D. F.; Watson, R. B.; Zenobi, R.; Kadler, K. E. Identification of Collagen Fibril Fusion during Vertebrate Tendon Morphogenesis. The Process Relies on Unipolar Fibrils and is Regulated by Collagen-Proteoglycan Interaction. *J. Mol. Bio*. 2000, 295, 801.
- (33) Wegener, S. V.; Spatz, J. P. Cobalt(III) as a stable and inert mediator ion between NTA and His6-tagged proteins. *Angew. Chem. Int. Ed*. 2013, 52, 7593.